REPORT DOCUMENTATION PAGE

1. AGENCY USE ONLY (Leave blank)	2. REPORT DATE July 12, 1995	3. REPORT TYPE AND DATES COVERED Report

1951023 147

4. TITLE AND SUBTITLE

High-Speed Four-Color Infrared Digital Imaging for Studying In-Cylinder Processes in a DI Diesel Engine

5. FUNDING NUMBERS

DAAL03-92-G-0249

6. AUTHOR(S)

K. T. Rhee

7. PERFORMING ORGANIZATION NAME(S) AND ADDRESS(ES)

Rutgers, The State University of New Jersey
College of Engineering
Mechanical and Aerospace Engineering
Piscataway, NJ 08854

8. PERFORMING ORGANIZATION REPORT NUMBER

9. SPONSORING/MONITORING AGENCY NAME(S) AND ADDRESS(ES)

U. S. Army Research Office
P. O. Box 12211
Research Triangle Park, NC 27709-2211

10. SPONSORING/MONITORING AGENCY REPORT NUMBER

ARO 29696.15-EG

11. SUPPLEMENTARY NOTES

The view, opinions and/or findings contained in this report are those of the author(s) and should not be construed as an official Department of the Army position, policy, or decision, unless so designated by other documentation.

12a. DISTRIBUTION/AVAILABILITY STATEMENT

Approved for public release; distribution unlimited.

12b. DISTRIBUTION CODE

DTIC
SELECTED
OCT 2 4 1995
G

13. ABSTRACT (Maximum 200 words)

The study was to investigate in-cylinder events of a direct injection-type diesel engine by using a new high-speed infrared (IR) digital imaging systems for obtaining information that was difficult to achieve by the conventional devices.

For this, a new high-speed dual-spectra infrared digital imaging system was developed to simultaneously capture two geometrically identical (in respective spectral) sets of IR images having discrete digital information in a (64x64) matrix at rates as high as over 1,800 frames/sec each with exposure period as short as 20 μsec. At the same time, a new advanced four-color IR imaging system was constructed. The first two sets of spectral data were the radiation from water vapor emission bands to compute the distributions of temperature and specie in the gaseous mixture and the remaining two sets of data were to find the instantaneous temperature distribution over the cylinder surface.

More than eight reviewed publications have been produced to report many new findings including: Distributions of Water Vapor and Temperature in a Flame; End Gas Images Prior to Onset of Knock; Effect of MTBE on Diesel Combustion; Impact of Oxygen Enrichment on In-cylinder Reactions; Spectral IR Images of Spray Plume; Residual Gas Distribution; Preflame Reactions in Diesel Combustion; Preflame Reactions in the End Gas of an SI Engine; Postflame Oxidation; and Liquid Fuel Layers during Combustion in an SI Engine.

In addition, some computational analysis of diesel combustion was performed using KIVA-II program in order to compare results from the prediction and the measurements made using the new IR imaging diagnostic tool.

14. SUBJECT TERMS

High-speed, Infrared Spectral Images, Direct-injection, Diesel Combustion, New Discoveries

15. NUMBER OF PAGES

108

16. PRICE CODE

17. SECURITY CLASSIFICATION OF REPORT	18. SECURITY CLASSIFICATION OF THIS PAGE	19. SECURITY CLASSIFICATION OF ABSTRACT	20. LIMITATION OF ABSTRACT
UNCLASSIFIED	UNCLASSIFIED	UNCLASSIFIED	UL

Table of Content

High-Speed Four-Color Infrared Digital Imaging for Studying In-Cylinder Processes in a DI Diesel Engine

1. Introduction

Several main improvements in modern Diesel engines are implemented in order for increasing the thermal efficiency and at the same time reducing the emissions of both NOx and particulates. Because of the mutual exclusivity involved in achieving these goals for the existing Diesel systems, e.g. a design change for reducing the NOx emission generally results in an increase of particulate emission and vice versa, one may suggest that some radical changes will have to be made in the engine or fuel for achieving advancement of the Diesel engine technology. New measures presently studied for achieving the objectives are reflected in some recent literatures: injection rate shaping [1]*; ultra high fuel injection pressure [2]; sensor-electronic controlled engine [3]; low-heat rejection engine [4]; unconventional fuels and additives [5]; and even intake-air oxygen enrichment [6]. The use of exhaust gas treatment devices [7] is also a part of those changes being investigated for solving the problems.

A similarly important strategy being taken for improving modern Diesel engines is to achieve a better understanding of the events taking place in the combustion chamber, particularly when such new unconventional changes are made on the engines. While the computational modeling approach is an economical way of helping design a desirable Diesel engine, the modeling method itself implies imperfection and indicates the need for experimental verification in order to get more out of it. Realizing the limitations in producing useful in-cylinder measurements by means of the existing diagnostic tools, one may also suggest that some radically new methods will have to be employed for obtaining better pieces of in-cylinder information.

The approach taken for the present study was to employ a newly developed diagnostic tool, a high-speed spectral infrared imaging system [8-16]. In addition, the KIVA II computer code was used in an attempt to compare the results from the experiment with those from the predictions, which was performed under a separate sponsorship.

2. Methods

2-1. Engine

After searching for a CI engine apparatus which permits easy access to the combustion chamber and also maintains engine characteristics representing a large population of DI CI engines, it was decided to newly design and fabricate the system in our laboratory, under a sponsorship of the U.S. Department of Defence University Research Initiative. Among the key considerations taken for this goal was to employ the existing engine components as much as possible (that also reduced the cost of fabrication and maintenance) and to modify the engine cylinder head to facilitate the use of either intrusive or nonintrusive engine diagnostic tools.

Upon investigating what is available for the work and evaluating the basic layout of the engine, it was decided to use components of the Cummins 903 engine and the complete engine design was carried out in collaboration with Power Energy International and BKM, Inc. In taking such measures into consideration so as to preserve the representative engine characteristics, a section of the multicylinder 903 engine head was modified. The

1

modifications include: conversion of one of the intake valves to the optical access; a new rocker-arm mechanism; a measure to use either a Cummins unit injector or BKM's electronic controlled injector; and separate control of both coolant and oil flows in the cylinder head and the block, respectively; reserving a provisional large amount of space in the crankcase for facilitating installation of a linkage system that retains thermocouple wires from the piston-crown to the data system outside the engine crankcase.

In this engine when the mechanical injector was used, the start of fuel injection varied with load and the end of fuel injection stayed about the same, typically around 27 crank angle (CA) after the top-dead-center (aTDC), which is reflected on the subsequent combustion processes. Among more details of the engine are: borexstroke, 139x117mm; connecting rod length, 201mm; compression ratio, 13.5:1; injector hole diameter, 0.19mm; and number of holes, 7. Figure 1 shows a schematic presentation of the engine, which was mated either a mechanical fuel injector (PT type) or BKM's electronic injector as mentioned above.
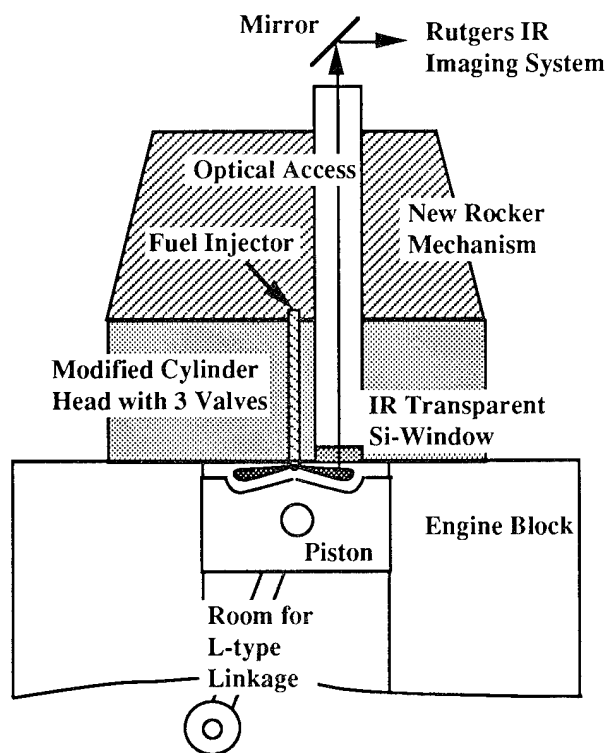
Fig. 1. Schematic Presentation of the Single Cylinder Engine Mounted by a
Cummins 903 Cylinder Head with Optical Access for
the SIS or Rutgers IR System.

2-2. Electonic-controlled Fuel Injector

The electronically controlled high-pressure injection (HPI) system which replaced the Cummins PT type injector in our 903 engine was basically a Servojet unit injector of the accumulator type [18]. Because of the crowded engine cylinder head due to new installation of an optical access and a pressure transducer (in addition to the existing

components such as the valve train), the relatively bulky Servojet unit was not usable in the apparatus. Keeping the original system design features, an entirely new injector unit was fabricated in our laboratory: Among the key considerations taken into account for this was to use original injector tips of the Cummins PT nozzle, which was to provide technical and economic flexibility in choosing different injector tip geometries. The operation of the injector was performed by using the same electronic package given with the original Servojet unit.

An extensive bench-top characterization of this new injector package was performed prior to in-cylinder measurement. This was necessary to determine several important pieces of information about the new HPI, including the relationships of the actual start of fuel injection and the amount of fuel injected per cycle to the input control by the electronic signals, i.e., the pulse width and timing, and the accumulator pressure, respectively. It is pointed out that the start of injection was defined as the time when the fuel plume tip reached a sensor located about 10mm away from the injector nozzle hole. The injection (sac) pressure-time history was not measured in the present characterization, but is inferred to be the same as the original unit [18], which resembles a spike-shape that collapses rapidly to have a very short residual period of low injection pressure.

2-3. High-speed Multispectral Infrared Imaging System

A new diagnostic device, called the Rutgers System or Super Imaging System (SIS) as referred to by others, was the key component permitting us to perform the present investigation. The system has four units of high-speed IR digital imaging cameras which are lined up to a single optical train. The basic idea of this SIS is to simultaneously obtain four geometrically identical images in respective spectral bands of the in-cylinder events at successive instants of time.

This device, which was made operational about a year ago, is a result of the progressive system development undertaken at the Internal Combustion Engines Laboratory of Rutgers University. Since the events in many thermal systems occur rapidly and some of important processes are invisible, at first a single-camera digital IR imaging system was developed having an imaging rate of as high as over 1,800 frames/sec and with an independently variable exposure period as short as $20\mu sec$. The experience gained from this work led us to the next development of a two-camera system, which was applied to the determination of temperature and water vapor distributions in a hydrogen flame [8]. An entirely new four-camera system was designed at the same time, which resulted in the present SIS.

The reason for simultaneously capturing four spectral images by the SIS is briefly explained next. It is basically to achieve quantitative imaging, i.e., determining distributions of temperature and species concentration in a combustion chamber.

Figure 2 is introduced here for describing the purpose of multispectral imaging. It represents a typical combustion chamber having a wall surface and combustion products in front. When the spectral bands are properly chosen, two sets of spectral images of a designated species are obtained (via λ_{g1} and λ_{g2}) and the same from the surface may be captured (via λ_{s1} and λ_{s2}) with a minimum mutual interference.

According to a spectral diagram generated by using our new data-base computer program, which employs the single-line-group model [10], as shown in Fig. 3, it seemed possible to attain a goal of spectrometric analysis. The analysis may be performed by either

3

dual-band method for studying the combustion product mixture [8]. Note that the support through the ARO's AASERT program has made possible to develop this new computer program.
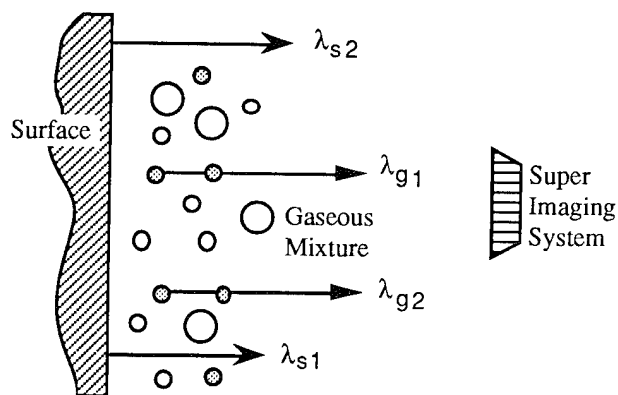
Fig. 2. Multispectral Imaging from a Combustion Chamber.

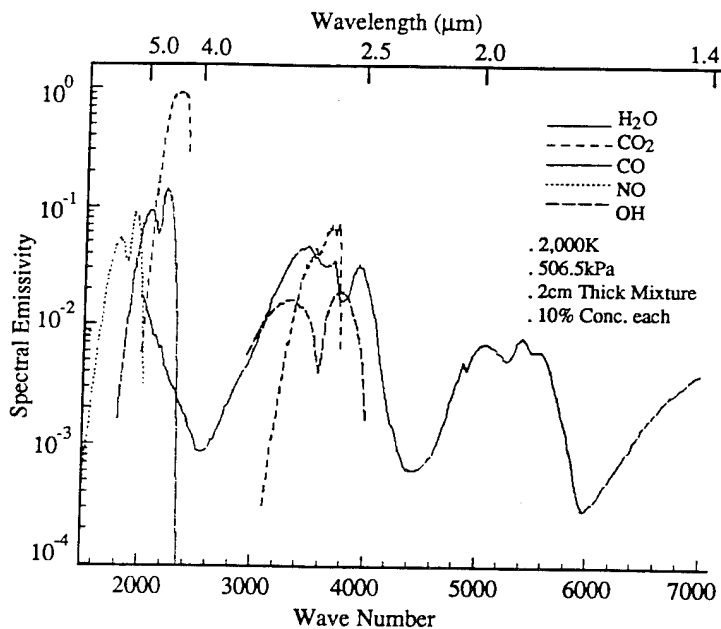

Fig. 3. Spectral Emissivity of a Gaseous Mixture having thickness of two centimeters at a uniform temperature of 2,000K and five atmospheric pressure.

In spite of this seemingly promising concept, contrary to previous reports suggesting otherwise [8,9], we discovered that there are measurable amounts of interference by radiation from some unknown species in the cylinder, particularly over

4

those in 2.2µm band. (A new imaging data correction method is presently being explored for eliminating the interference.) It is also noted that our laboratory propane-air flame exhibited interference by a similar radiation in the same band. While such interference delays our implementation of quantitative imaging, our exploratory study of the multispectral images from the SIS provided us with a new potential for investigating the in-cylinder processes, such as preflame reactions [16,17] and the post-flame oxidation (PFO) [17]. Thanks to its spectral discriminating ability, the SIS enables us to simultaneously capture (at least qualitatively for now) images of a specific gaseous species, and even soot formation, at successive instants of time.

Figure 4-(A) shows a new optical train of the SIS permitting the simultaneous multiple imaging in four spectral bands. The radiation coming through an IR optical access in the engine (Fig. 1) is collected by the cassegrain unit. Then, it is relayed to respective IR cameras after passing through three (custom-designed) spectral beam splitters. This manipulation of light rays results in four images in separate broad bands placed over the respective PtSi imagers housed in cryogenically cooled Dewars. A narrow band filter assigned to each Dewar finally leads to achieving the spectral digital image per camera (in 12-bit dynamic resolution). Since the present system was an application of existing components in an unconventional way, the entire circuits boards that drive the imagers and retrieve the output were newly designed in our laboratory. Figure 4-(B) is offered for illustrate the total imaging system, which include the optical unit representing Fig. 4-(A).
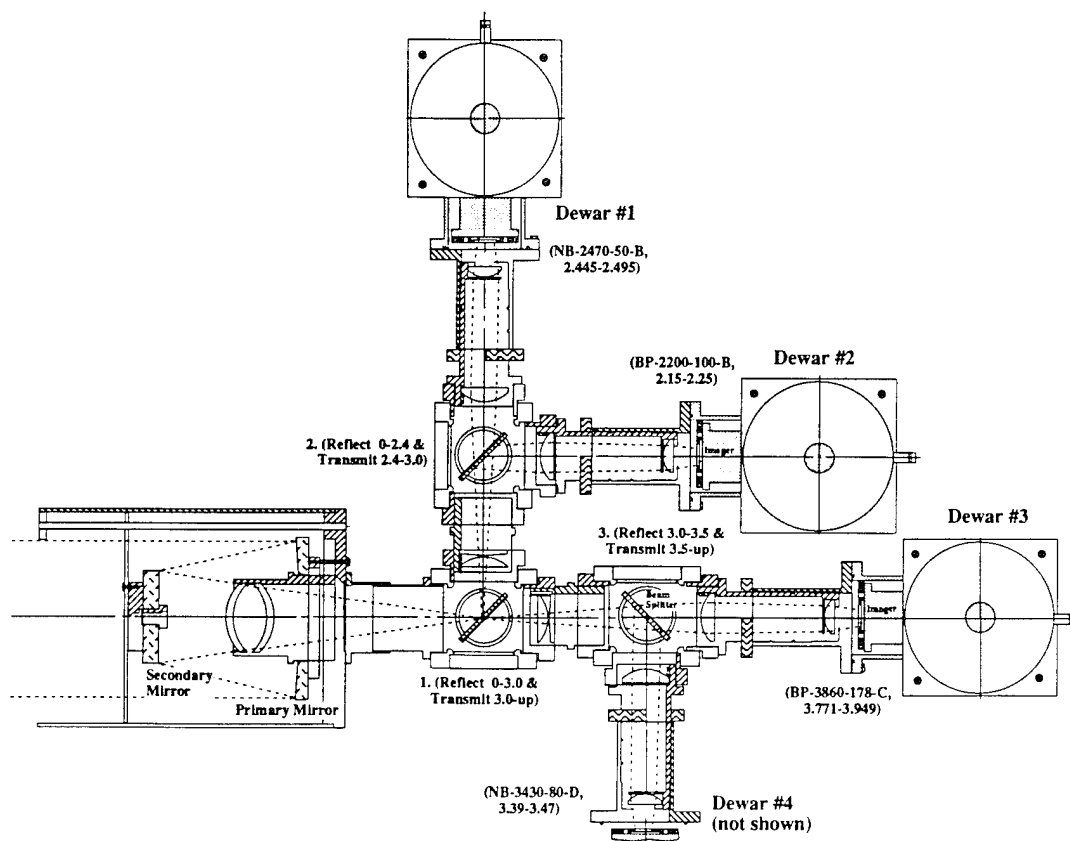

Fig. 4-(A). Optical Train of the Rutgers Super Imaging System.
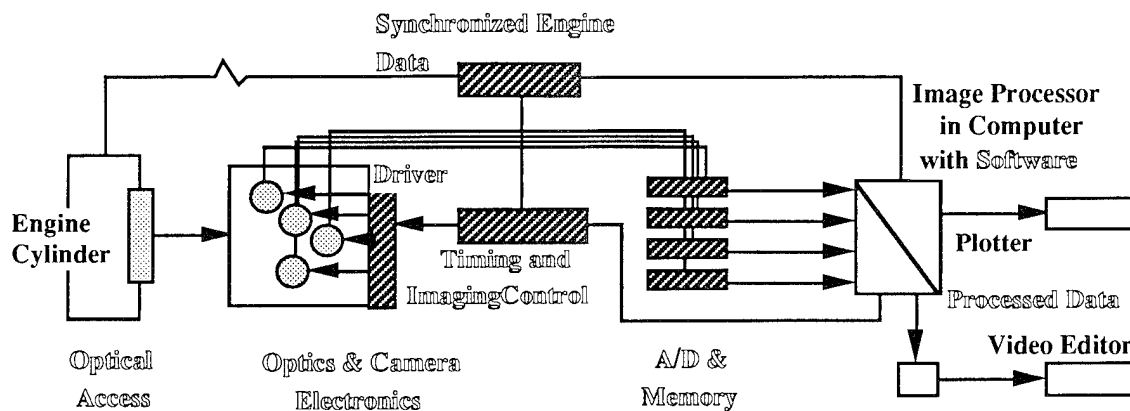
Fig. 4. (B) Optical Arrangement of the Rutgers Super Imaging System.

2-4. Prediction by KIVA-II

As mentioned earlier, expecting a meaningful comparison of predictions made by the KIVA II computer program of Diesel engine combustion with results from experiment, this three-dimensional finite difference method program was adjusted by including corresponding engine data as close as possible to those in the experiment. Some progressive steps were taken for this work in order to eliminate or minimize probable misuse of the code by consulting with KIVA-II user group members and by conducting a parametric analysis of the combustion processes. The values introduced for the key code parameters are listed in Table-I. Two different grids were employed in the study: case-(1) nx=26, ny=20 and nz=18; and case-(2) nx=14, ny=8 and nz=18. The typical CPU time in the Pittsburgh Super Computing Facility required per computation for the former and latter grids were 35.5 and 2.4 hours, respectively. Because of the limited amount of CPU time available for the present work, i.e., total about 250hrs at the Computing Facility, only a few computations were performed using the former grid and the main portion of parametric study was performed by using the latter.

Table-I

DTI, initial time step	2.0×10^{-5}
RPM, engine speed	500
STROKE	11.66
CONROD	20.66
THSECT, azimuthal dim. of mesh	51.4286
SWIPRO, initial swirl	3.11
TSPMASS, mass injected	0.0390
CALINJ, injection time	-11.0
CADINJ, injection duration	38.0
TILTXY, rotation of injector	25.714
TILTXZ, injector incline	84.0
DCONE, injector thickness	5.0
ANOZ, injector hole area	2.859×10^{-4}
TKESW, turbulence on	1.0
SGSL, k-ε model	

6

3. Results

New publications have been prepared under the present sponsorship of the ARO as listed next [10-17. The meaningful results are all explained in the detail in the papers as included in appendix. Brief explanations are given in the text to summarize the significance of the work achieved during the course of the work.

In addition, the technology know-how obtained under the present sponsorship was directly applied for engine studies with participation of industrial components as explained later. Many invited technical presentations were made in addition to the publications, which are also listed thereafter.

3-1. New Publications

1. Jiang, H., McComiskey, T., Qian, Y., Jeong, Y.I., Rhee, K.T., and J.C. Kent,"A New High-Speed Spectral Infrared Imaging Device Applied for Imaging Gaseous Mixtures from Combustion Devices," Combustion Science and Technology, 90, 5-6, p. 341, 1993.

2. McComiskey, T., Jiang, H., Qian, Y., Rhee, K.T., and Kent, J.C., "High-Speed Spectral Infrared Imaging of Spark Ignition Engine Combustion," SAE Paper-930865, 1993.

3. Jiang, H., Qian, Y. and Rhee, K.T., "High-Speed Dual-Spectra Infrared Imaging," Optical Engineering, 32 (6), pp. 1281-1289, 1993.

4. Kajitani, S., Clasen, E., Campbell, S. and Rhee, K.T., "Partial-load and Start-up Operations of Spark ignition Engine with Oxygen Enriched Air," SAE Paper-932802, 1993.

5. Jeong, Y.I., Qian, Y., Campbell, S. and Rhee, K.T., "Investigation of a Direct Injection Diesel Engine by High-Speed Spectral IR Imaging and KIVA-II," SAE Paper-941732, 1994.

6. Kajitani, S., Usisaki, H., Clasen, E., Campbell, S. and Rhee, K.T., "MTBE for Improved Diesel Combustion and Emissions?," SAE Paper-941688, 1994.

7. Clasen, E., Campbell, S., and Rhee, K.T., "Spectral IR Images of Direct Injection Diesel Engine Combustion with High Pressure Fuel Injection," SAE Paper-950605, 1995.

8. Song, K., Clasen, E., Chang, C., Campbell, S., and Rhee, K.T., "Post-flame Oxidation and Unburned Hydrocarbon in a Spark-ignition Engine," SAE Paper to be presented in International Fuels and Lubes Meeting, October, 1995.

3-2. Technology Transfer and Industrial Participation

The new diagnostic tool, the SIS developed under the present ARO support was used for investigating events in the engine cylinder in collaboration with several industrial concerns, including: (1) Ford Motor Company; (2) Texaco Research Center; and (3) Ethyl Corporation. The technology know-how was also applied to perform alternative fuels research under a separate sponsorship of the U.S. Department of Energy (through National Renewable Energy laboratory).

3-3. Invited Technical Presentations

The principal investigator, K. T. Rhee was invited to deliver technical presentations of the results obtained under the present sponsorship, including those listed below:

1. Rhee, K.T., Kent, J.C. and Studzinski, W. "High-Speed Spectral Infrared Imaging for IC Engine Research-Emission Reduction,"DOE, ASC and SAE Sponsored Symposium, The Mechanisms & Chemistry of Pollutant Formation in Internal Combustion Engines, University of California, San Diego, July 23, 1993.

2. Rhee, K.T., "High-Speed Four-Color Infrared Digital Imaging for Studying In-Cylinder Processes in a DI Diesel Engine," U.S. ARO Engine Workshop, Princeton University, March 14-15, 1994.

3. Rhee, K.T., "High-Speed Multispectral Infrared Imaging and Data Processing Method," (Expense paid) Invited Lecture at 21st Int'l Congress on High-Speed Photography and Photonics, August 30-31, 1994, Daejeon, Korea.

4. Rhee, K.T., "High-Speed Spectral Infrared Imaging Applied to Engine-Fuel Research," Ford Motor Company, March 3, 1995.

5. Rhee, K.T., "High-Speed Spectral Infrared Imaging Applied to Thermal Systems Research," Villanova University, March 17, 1995

6. Rhee, K.T., "Engine/Fuel Studies at Rutgers-Some Urgent Issues," U.S. Department of Energy, Alternative Fuels Utilization Program, March 23, 1995.

7. Rhee, K.T., "Engine/Fuel Studies using Rutgers IR System," Princeton University, U.S. Department of Energy Working Group, March 31, 1995.

8. Rhee, K.T., "Engine/Fuel Studies at Rutgers," Ethyl Petroleum Additives, Inc. Richmond, VA, May 24, 1995.

4. New Results and Discoveries

Although explained in the new publications, the following lists the entirely new results and discoveries obtained under the present sponsorship. The papers describing the individual results are included in brackets.

o. Distributions of Water Vapor and Temperature in a Flame
[Optical Engineering, 32 (6), pp. 1281-1289, 1993]

o. End Gas Images Prior to Onset of Knock
[SAE Paper- 930865, 1993]

o. Effect of MTBE on Diesel Combustion
[SAE Paper-941688, 1994]

o. Impact of Oxygen Enrichment on In-cylinder Reactions
[SAE Paper-932802, 1993]

o. Spectral IR Images of Spray Plume
[SAE Paper-941732, 1994]

o. Residual Gas Distribution
[SAE Paper for 1995 Fuels and Lub Meeting]

o. Preflame Reactions in Diesel Combustion
[SAE Paper-950605, 1995]

o. Preflame Reactions in the End Gas of an SI Engine
[SAE Paper for 1995 Fuels and Lub Meeting]

o. Postflame Oxidation
[SAE Paper for 1995 Fuels and Lub Meeting]

o. Liquid Fuel Layers during Combustion in an SI Engine
[SAE Paper for 1995 Fuels and Lub Meeting]

Individual topics are discussed in detail in the corresponding papers included in appendix. Among the most significant findings is the locally burning fuel-rich pockets over the cylinder head of an SI engine equipped with the conventional port injection fuel injection system. As explained in the paper, the late burning centers are considered to be a very significant (if the most) source of the unburned hydrocarbon emitted by the engine, and at the same time reducing the efficiency.

It may be rather too early to evaluate the impact of this discovery at the present, but if the automobile manufacturers rectify the problem soon, which has never been reported/known in the past, the emission improvement will be highly significant and the saving in fuel consumption will be many many millions of dollars in the U.S. alone.

5. Academic Degrees Awarded under the Present Study

The individuals graduated with degrees under the present study include:

T. McComiskey, MS degree
H. Jiang, Ph.D degree
Y.I., Jeong, Ph.D degree

6. References

1. Tow, T.C., Pierpoint, D.A. and Reitz, R.D., "Reducing Particulate and NOx Emissions by using Multiple Injections in a Heavy Duty D.I. Diesel Engine," SAE Paper-940897.

2. Kobayshi, s. et al., "Measurement of Flame Temperature Distribution in DI Diesel Engine with High Pressure Huel Injection," SAE Paper-920692, 1992.

3. Yang, Minggao, Sorenson, S.C., "Direct Digital Control of Diesel Engines, " SAE Paper-940372, 1994.

4. Wood, M.E., Bryzik, W. and Schwarz, E., "100 Hour Endurance Testing of a High Output Adiabatic Diesel Engine," SAE Paper-940951, 1994.
5. Kajitani, S., Usisaki, H., Clasen, E., Campbell, S. and Rhee, K.T., "MTBE for Improved Diesel Combustion and Emissions?," SAE Paper-941688, 1994.

6. Desai, R.R., Gaynor, E., and Watson, H.C., "Giving Standard Diesel Fuels Premium Performance Using Oxygen-Enriched Air in Diesel Engines," SAE Paper-932806, 1993.

7. Pataky, G., Baumgard, K.J., Gratz, L.D., Bagley, S.T., Leddy, D.G., Johnson, J.H., "Effect of an Oxidation Catalytic Converter on Regulated and Unregulated Diesel Emissions," SAE Paper-940243, 1994

8. Matsui, Y., Kamimoto, T. and Matsuoka, S., "A Study on the Application of the Two-color Method to the Measurement of Flame Temperature and Soot Concentration in Diesel Engines, " SAE Paper-800970, 1980.

9. Ferriso, C.C., Ludwif, C.B. and Boynton, F.P., "A Band-Ratio Technique for Determining Temperatures and Concentrations of Hot Combustion Gases from Infrared-Emission Spectra," 10th Symposium (Int'l) on Combustion, pp161-175, 1965.

10. Jiang, H., McComiskey, T., Qian, Y., Jeong, Y.I., Rhee, K.T., and J.C. Kent,"A New High-Speed Spectral Infrared Imaging Device Applied for Imaging Gaseous Mixtures from Combustion Devices," Combustion Science and Technology, 90, 5-6, p. 341, 1993.

11. McComiskey, T., Jiang, H., Qian, Y., Rhee, K.T., and Kent, J.C., "High-Speed Spectral Infrared Imaging of Spark Ignition Engine Combustion," SAE Paper-930865, 1993.

12. Jiang, H., Qian, Y. and Rhee, K.T., "High-Speed Dual-Spectra Infrared Imaging," Optical Engineering, 32 (6), pp. 1281-1289, 1993.

13. Kajitani, S., Clasen, E., Campbell, S. and Rhee, K.T., "Partial-load and Start-up Operations of Spark-ignition Engine with Oxygen Enriched Air," SAE Paper-932802, 1993.

14. Jeong, Y.I., Qian, Y., Campbell, S. and Rhee, K.T., "Investigation of a Direct Injection Diesel Engine by High-Speed Spectral IR Imaging and KIVA-II," SAE Paper-941732, 1994.

15. Kajitani, S., Usisaki, H., Clasen, E., Campbell, S. and Rhee, K.T., "MTBE for Improved Diesel Combustion and Emissions?," SAE Paper-941688, 1994.

16. Clasen, E., Campbell, S., and Rhee, K.T., "Spectral IR Images of Direct Injection Diesel Engine Combustion with High Pressure Fuel Injection," SAE Paper-950605, 1995.

17. Song, K., Clasen, E., Chang, C., Campbell, S., and Rhee, K.T., "Post-flame Oxidation and Unburned Hydrocarbon in a Spark-ignition Engine," SAE Paper to be presented in International Fuels and Lubes Meeting, October, 1995.

18. Abata, D., Stroia, B.J., Beck, N.J., and Roach, A.R., "Diesel Engine Flame Photographs with High Pressure Injection," SAE Paper-880298, 1988.

A New High-Speed Spectral Infrared Imaging Device Applied for Flame Studies

H. JIANG, T. McCOMISKEY, Y. QIAN, Y. I. JEONG, K. T. RHEE *Department of Mechanical and Aerospace Engineering Rutgers, The State University of New Jersey New Brunswick, New Jersey 08903*

J. C. KENT *Engine Research Department, Ford Motor Company, Dearborn, Michigan 48124*

Abstract—A high-speed spectral infrared imaging system has been developed for facilitating investigation of thermal processes, including those in combustion devices. The new system has several unique performance characteristics: variable and high speed frame rate; variable and short exposure period; independent control of imaging parameters; digital imaging in high dynamic resolution; spectral imaging, externally triggered individual images; and large number of frames per each data acquisition. Its design and performance verification was made by obtaining instantaneous thermal images that permit visualization of reaction fronts and subsequent mixing of combustion products of a Bunsen burner, a rectangular Poiseuille-flow burner, and a spark-ignition engine. Some results from this work are compared with those obtained using conventional methods reported in other literature. It is demonstrated that findings, otherwise difficult to obtain, are made possible by this newly developed tool.

INTRODUCTION

Imaging in the infrared (IR) range aids investigation of thermochemical processes in combustion devices in several unique ways. It complements the visible range imaging by capturing more extensive fingerprints from the spectrum of reacting species in a wide range of temperature. This spectral data may be used to obtain quantitative imaging, such as determination of instantaneous spatial distributions of temperature and species concentration by employing two-color method or other spectrometric analysis. Since IR imaging is capable of obtaining images of relatively low-temperature gaseous mixtures, which are generally invisible, some problems otherwise difficult to investigate can be examined by this method as explained in this paper.

There are several desirable characteristics expected from a versatile IR imaging system that are advantageous for investigating combustion problems: successive imaging at speeds fast enough to follow rapid combustion events; short exposure periods of imaging in order to freeze these procedures; digitized images in high dynamic resolution to ensure the accuracy of measurement; spectral imaging to achieve quantitative data reduction; and acquisition of large amounts of images at once. It is also desirable that those system parameters can be independently varied to obtain quality images under different experimental conditions. Of particular importance is the requirement of high dynamic-resolution in digitization and storage of analog video output. This is because the temperature range in combustion devices is wide and its radiation must be captured in accurate numeric values.

No existing IR imaging system was found to deliver those features for satisfying such research needs. Literature survey, however, suggested that rapidly advancing electro-optical technologies were so significant that development of a new device meeting those requirements may be feasible. motivating us to initiate design of a new high-speed IR imaging system several years ago. The basic methodology and a partial description of our new IR imaging system were explained when its initial applications were reported (Jiang and Rhee, 1990; Rhee, 1991). However, due to the need for extensive technology

know-how and resources involved in the system development, the construction of a prototype unit was carried out with interdisciplinary participations and collaboration with industrial concerns. In this paper, the system concept verification is presented by explaining important issues encountered in its development and by reporting results obtained from several combustion devices.

NEW DESIGN AND DEVELOPMENT

Among the main components in the new IR imaging system are (Fig. 1): (1) optical assembly; (2) imager (housed in a liquid-nitrogen Dewar); (3) electronic circuits package (for driving and reading-out the imager); (4) A/D converter circuits; (5) memory and its control circuits; (6) image grabber and processor; (7) data acquisition controller and (8) computer and data display. This prototype system which consisted of breadboard component packages was operated by using modified off-the-shelf software and a great amount of our own computer programs.
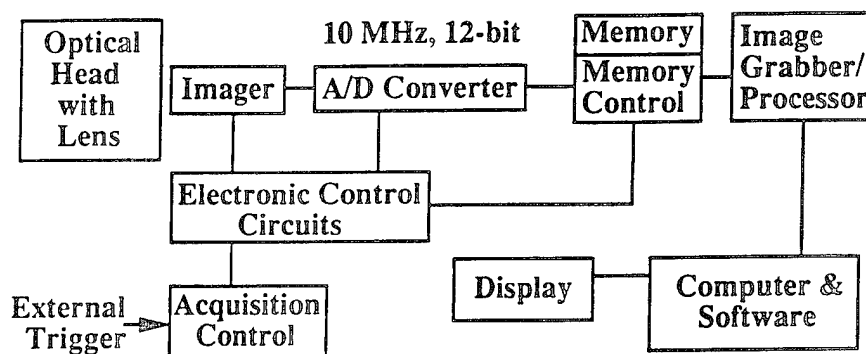
FIGURE 1.   Schematics of New IR Imaging System in 12-bit Data Acquisition.

Imager and Optical Assembly

Since high-speed imaging is easier to achieve when a focal plane array (FPA) is employed, as opposed to a single detector or line (detector array) imager (which needs scanning and limits the framing rate), only FPA is considered here. Literature study indicates that there are several types of advanced IR FPAs made of different materials (with respective operating temperature in K; spectral response in μm), namely InAsSb (100; 2-8); HgCdTe (often denoted by MCT) (40-77; 2-15); InSb (77;1-5.5); PtSi (77; 1-5.5) and Silicon (300; 0.3-1.1). In spite of the high responsivity by the MCT and InSb detectors in the low-temperature regime they have drawbacks. Their FPA imagers are made mostly in hybrid-forms by making the sensor matrix and the output readout portions separately. Two pieces are then combined mechanically, which results in high manufacturing cost which forces the number of pixels per imager to be small. They cannot be fabricated in economical monolithic devices (by making both portions in one piece in the same manufacturing-line silicon process) which includes an easy data readout scheme, such as charge-coupled device (CCD) architecture.

On the other hand, it is well-established that monolithic manufacturing technology allows the production of PtSi FPA, not only with minimum pixel-to-pixel variations in sensitivity but also at relatively low cost. Its yield rate, i.e., the portion of successful imagers out of a wafer lot, continues to improve. Further, its development was initiated

by Shepherd and Yang (1973) of Rome Air Development Center (RADC), Hanscom AFB, MA. The basic idea of the PtSi device is to eject the "hot" holes, strong enough to go over the "Schottky barrier," out of a thin layer of p-type silicon, according to radiation absorbed by the layer. The net negative charge remaining in the silicon electrode is read out via a CCD readout structure. At present, its manufacturing method is probably the most advanced technology for IR sensing arrays. There have been many imagers with different pixel numbers, size, fill factors and readout schemes introduced in the past (the larger the number of pixels, the more recently they have been introduced), e.g. 25x50; 32x64; 64x128; 160x244; 320x244; 512x512; and 620x480 (Kosonocky, 1991).

One of the main objectives initially set forth in our system development, as explained earlier, was to achieve the highest frame rate and at the same time maintaining a reasonable spatial resolution in the imager. Upon extensive analysis of this issue, it was decided to use FPAs having 64x128 pixels each (with a single video port). In practice, by taking a "noninterlacing" mode, we have achieved 64x64 pixel operation but with doubled intensity output and increased framing rates. Note that because of the output readout structure in a serial mode and the upper limit in the pixel readout speed in existing PtSi imagers, which is around 10 MHz at present (over 20 MHz in laboratory experiments), the top framing rate is basically inversely proportional to the number of pixels per imager. In the present system with the above mentioned imager, we are able to obtain frame rates of over 1,800 frames/sec for qualitative imaging and more than 1,600 frames/sec for meaningful quantitative data acquisition (in 12-bit dynamic resolution) with exposure period as short as 70 μsec, which can be reduced to 20 μsec for qualitative imaging.

Note that as indicated by Planck's equation, the useful response to the wavelength regime by the PtSi Schottky barrier detector (1-5.5 μm) makes it quite proper to image objects ranging from room temperature to very high (flame) temperatures. This permits investigating what is difficult to achieve by visible ray imaging. This spectral dependency obviously dictates the selection of materials in the optical assembly. In our study, two different optical assemblies have been designed and fabricated: One unit with four lens elements made of germanium having a transmission range of 2.1-5.5 μm (75 mm, f/2, 4.6°FOV) and the other employing a reflective optics layout with correction lenses and beam splitters made of calcium fluoride having an overall transmission range of 1.5-6.0 μm. Note that the latter assembly is employed in our new high-speed four-color imaging system. which will be separately reported.

Electronic Control Circuits

In a typical PtSi CCD-compatible imager, there are four main parts, namely the sensing area, A-, B- and C-registers. The (negative) charges built up in individual pixels of the sensing area according to receipt of radiation during the exposure period, by a transfer pulse to the imager, are immediately transferred to the B-register whose number of cells equal (half, if interlace type) the number of sensing pixels. The individual charges in B-register (line by line according to the line pulses) are sent to either the A- or C-register which have as many cells as those in each line of B-register. After each transfer of line charges to, C-register, for instance. they are then forwarded, out of C-register, through a charge amplifier to produce analog output through a video line (port) in series according to pixel pulses, which may be digitized for storage in the frame buffer. Note that the individual timing periods are dictated by the imager geometry, material and others.

The term, "interlace (IT) type", means that when the negative charge built up in the sensing area is sent to the corresponding register in each pixel, the following two modes can be taken: The transfer of charge is made by adding two adjacent sensing cells to

store the sum in an assigned register cell (because the register has cells, if an IT type, one-half the number of pixels in the imager), which is a noninterlace mode. Or the charges are transferred in two steps, first, one half of the sensing areas and the other. This operation is referred to as the IT mode, which doubles the spatial resolution.

The above brief description of signal readout from a CCD imager indicates a need for many carefully organized timing signals (each with a proper bias level in individual pulses) to be provided to the imager, typically having over 32 pins, so that analog video signals can be acquired for subsequent processing. The timing diagram for most imagers is available to the public but the detailed circuit diagrams remain as in-house information of the imager developer. Some generic circuit diagrams have been made available for PtSi CCD systems (Cochran, 1986) but fabrication of new sets of circuits for our PtSi imager was made with outside experts' support. In spite of the lengthy process of designing, constructing and testing this new prototype circuit package, we were able to compile data in an efficient and controlled manner even under severely demanding experimental conditions.

A/D Converter.

In order to rapidly convert analog video signal readouts in series from the imager register into digital data with high accuracy, a high-speed and high-dynamic resolution A/D converter is an important requirement. We employed a new digitizer unit equipped with A/D converter having 10 MHz in 12-bit into our system, which was the state-of-the-art when we started the initial design. Recently, an A/D converter with the maximum speed of 20 MHz in 12-bit was introduced into the market. Because of complexities in the A/D converter circuits stemming from high frequency signals controlling the data sampling and mutual interaction among components, the design and fabrication of the digitizer package required considerable expenditures of time. It should be noted that extensive control of the electronic circuit package mentioned above was essential for timely sampling in the A/D converter in order to accurately digitize the video signals issued from the imager for subsequent data storage in our new memory package.

Frame Grabber with Memory

Once the sensor data is transformed into the digital domain, digital techniques may be applied for processing and storage. The pipeline image processor in the digital domain has been well developed in the past to achieve operational speed of several hundred MHz in various ranges of dynamic resolution. According to our calibration conducted during the process of the system development, some of the image processors on the market were unable to deliver the nominal data handling in 12-bit resolution because of circuitry problems. Although such problems may not be noticed or pose serious consequences for most qualitative imaging purposes that make use of low dynamic resolution, they were of great concern in our quantitative data acquisition. In order to obtain accurate quantitative data management, we had to identify the problems requiring image processor modification in collaboration with its manufacturer.

Because of such limitations in off-the-shelf frame grabbers, (which took a great portion of our time, mainly because of the demanding nature of our applications), it was decided to develop a new memory system with corresponding memory control package. This approach served two purposes: The digital data out of the A/D converter unit can store in our memory package as many images as the memory capacity permits, which is expensive to achieve otherwise. Next the above mentioned limitations by existing image processors can be circumvented. This is accomplished by digitizing and storing the imager

20 cm

Imaging (B)

10

Imaging (A)

Luminous
Zone

0

**Bunsen Burner
Fueled by
Natural Gas**
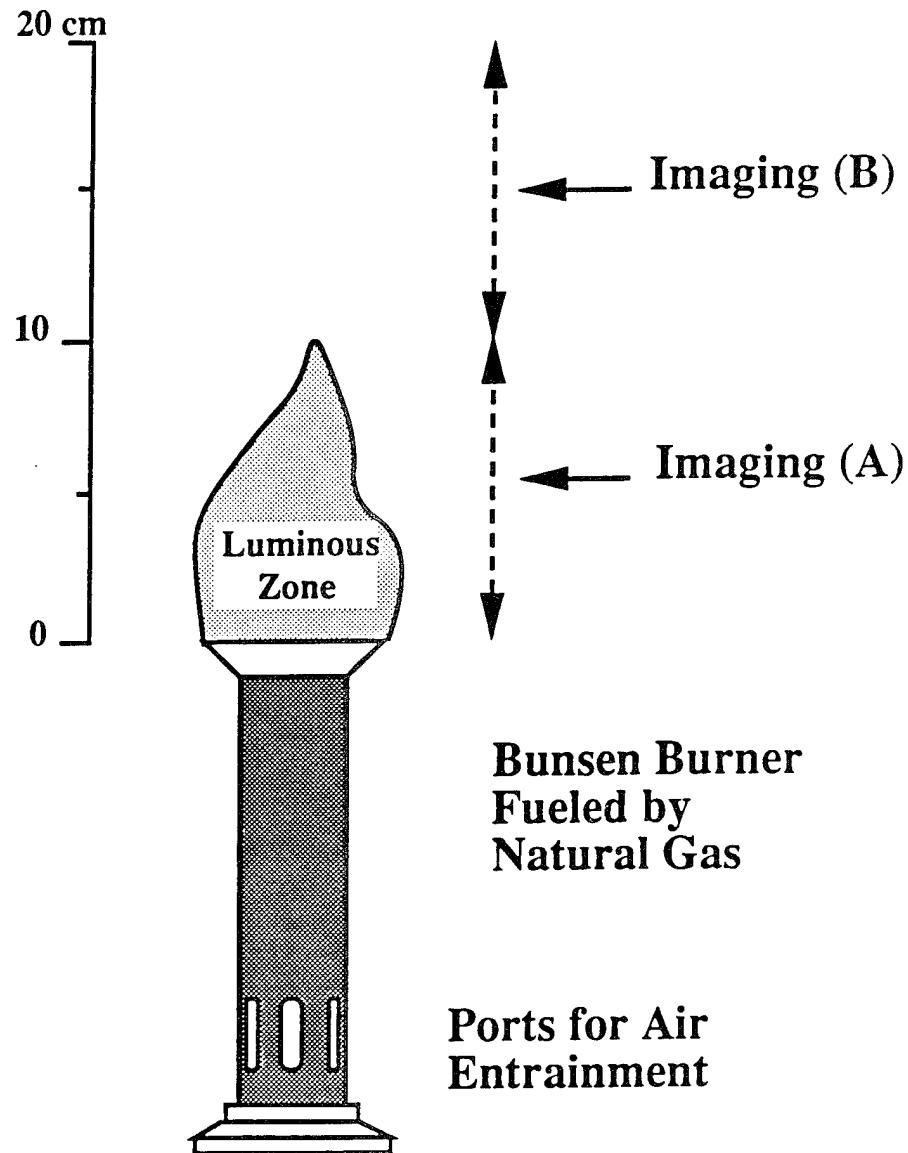
**Ports for Air
Entrainment**

FIGURE 2   Imaging Zones in a Bunsen Burner Fueled by Natural Gas.

output at the highest rate and retrieve them by using a low speed (and inexpensive) image processor because this processing time is less important.

It is noted that the timing signals for controlling the imager (and is also employed in the A/D converter unit as discussed above) are introduced into data compilation in the new memory package. particularly in the write-in stage. The readout of data from the memory is performed by using a separate clock for the sake of flexibility. As expected, the design/fabrication of the memory control package faced a lengthy debugging process due to severe tolerance limits in timing management to achieve high data acquisition rates
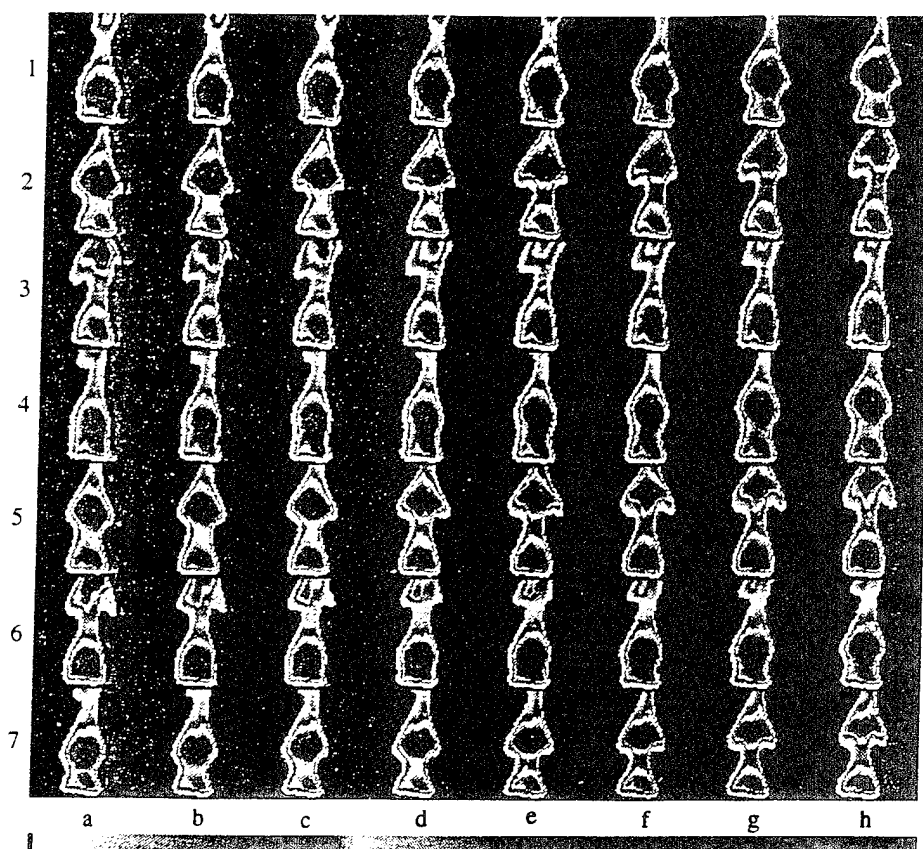
FIGURE 3   (A). Instantaneous Spectral (2.2-2.5 μm) Infrared Images of Natural Gas Fueled Bunsen Burner From Zone-A. 200 frames/sec with 90 μsec Exposure Period. See COLOR PLATE VII.

and other unique features to be met when performing (engine) combustion research. This potentially costly and time consuming work task was eased by using erasable and programmable logic gate arrays. In the memory unit we can store up to 256 image frames with 64 x 64 pixels in 12-bit. This capacity can readily be expanded.

Controlled Data Acquisition

The data acquisition by the present system can be achieved in ways similar to those employed in a modern digital oscilloscope, i.e., internal clock mode and external trigger imaging. The internal clock mode is straightforward: Once the imaging system is adjusted, e.g. setting the framing rate and exposure period, upon the initial triggering, images are continuously compiled until a designated amount of memory space runs out. Regarding the external trigger mode, the individual images can be obtained according to external signals. For this, the imaging system was equipped with a new data acquisition controller that enables image compilation according to combustion device operations, namely to obtain individual images triggered by coinciding engine crack angle (CA) markers in relation to TDC. This new unit is to control (e.g. in terms of CA markers): (1) delay
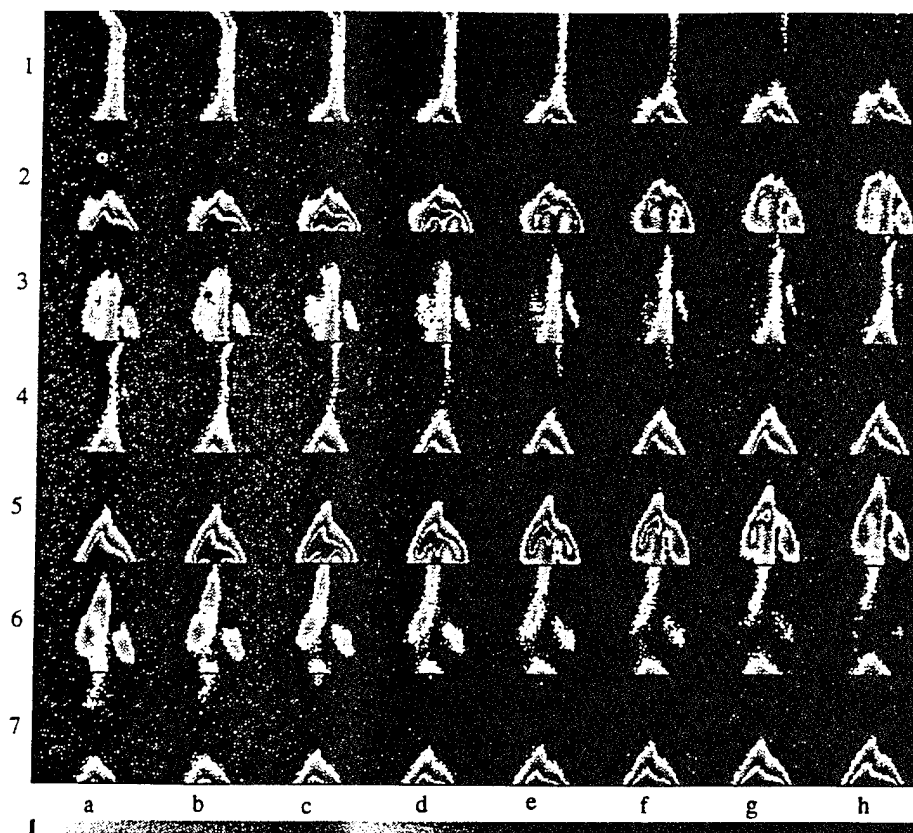
FIGURE 3   (B). Instantaneous Spectral (2.2-2.5 μm) Infrared Images of Natural Gas Fueled Bunsen Burner From View-B. 200 frames/sec with 300 μsec Exposure Period. See COLOR PLATE VIII.

period after the reference marker; (2) interval between successive images; and (3) total number of images per cycle. This device paves the way for consistent and efficient data acquisition. For example, selected sets of exactly timed images obtained from successive cycles at matching engine CA can be compared to each other for investigating the cycle-to-cycle variation of in-cylinder events, e.g. residual gas and its behavior.

Computer and Software

The only off-the-shelf unit packages (having no modification) included in this new diagnostic system are the computer and data displayer. We acquired several packages of image processing software but a great portion of the computer programs for the system control/operation and data reduction were newly developed to meet the needs of this prototype imaging and data processing system.

System Design Summary

The system design concept of the new device is verified by applying it to investigate reaction processes in combustion devices, as discussed next. The present system is
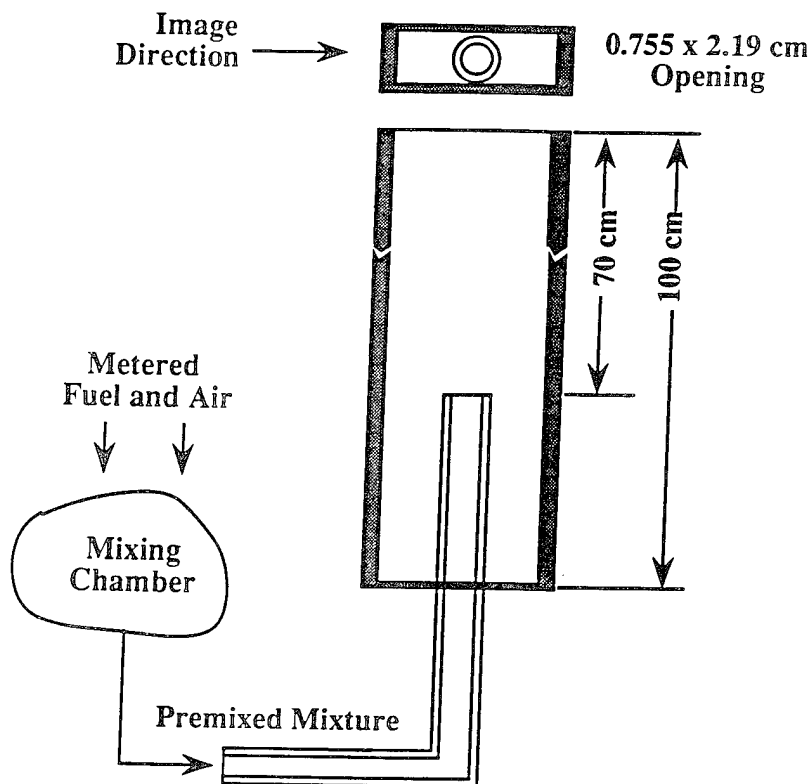
FIGURE 4   Poiseuille Burner employed by Lewis and von Elbe.

considered to stand alone as an independent data system that can be employed for various purposes of research and development, as demonstrated by some of the results from our ongoing experiments. Recalling the lengthy time required in obtaining even limited amounts of data by the high-speed cinematography applied for flame studies (Rhee, 1982), the promptness and versatility of obtaining new information offered by this spectral IR imaging device cannot be overemphasized. The system is applied for studying several combustion devices and some typical results are explained later. In addition, we are in the process of developing another imaging system to capture four simultaneous images (geometrically identical but in different spectral bands) at successive instants of time with the same high framing rates. This approach is taken in order to obtain the distribution of quantitative information from the combustion reaction volume, by employing conventional spectrometric data reduction techniques, including two-color and four-color methods.

SPECTRAL IMAGING OF BURNER FLAMES

The present imaging system was utilized to obtain images in the spectral band of 2.2-2.5 μm. which was to capture only emissive radiation from water vapor in the combustion products. Imaging in other bandwidths may be obtained by replacing the filter located between the lens assembly and the (liquid nitrogen cooled) Dewar where the imager is housed with one of choice. Since the half field of view angle (FOV) in our optical head
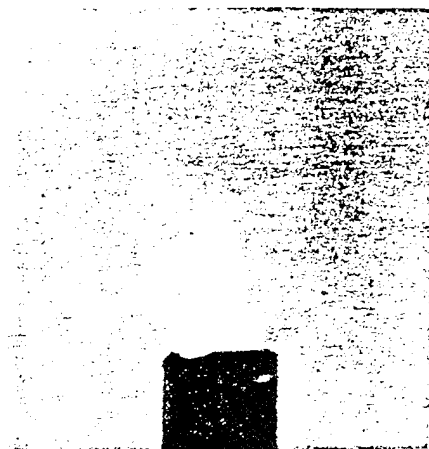
FIGURE 5   Flame Image of Poiseoulle-Flow Burner Obtained Using a 35mm Camera. See COLOR PLATE IX.
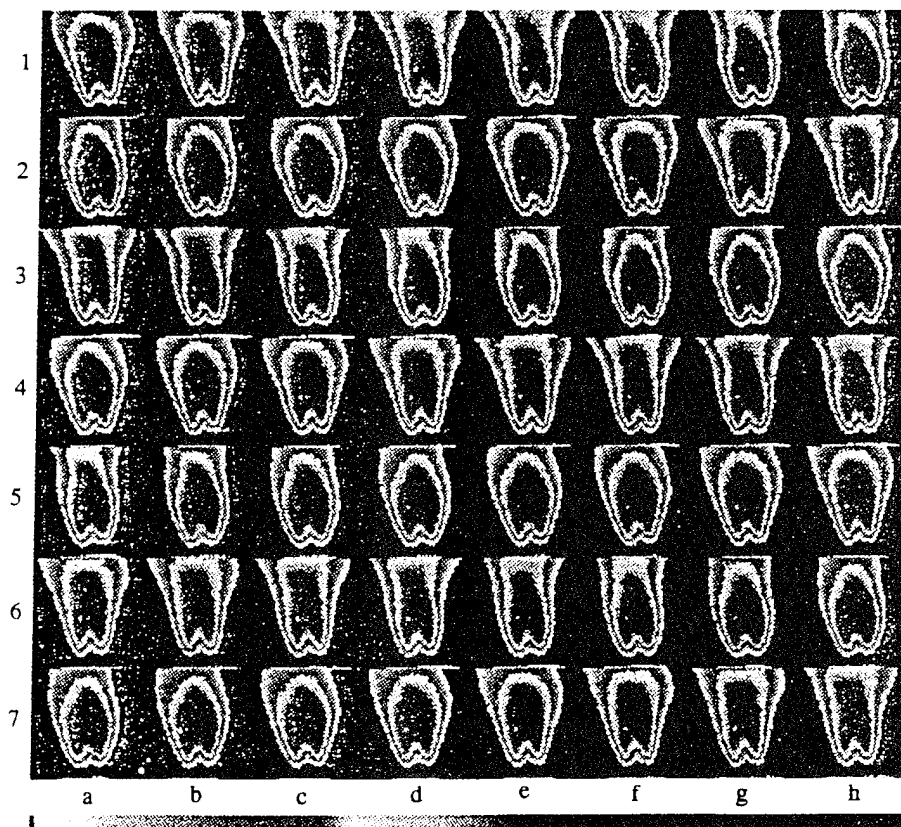
FIGURE 6   (A) High-Speed Spectral (2.2-2.5 μm) IR Images of Piseulle-Flow Burner with 200 cc/sec Flow of 9% Natural Gas in Air Obtained at 200 frames/sec Having 90 μsec Exposure Period. See COLOR PLATE X.

(C)

(B)
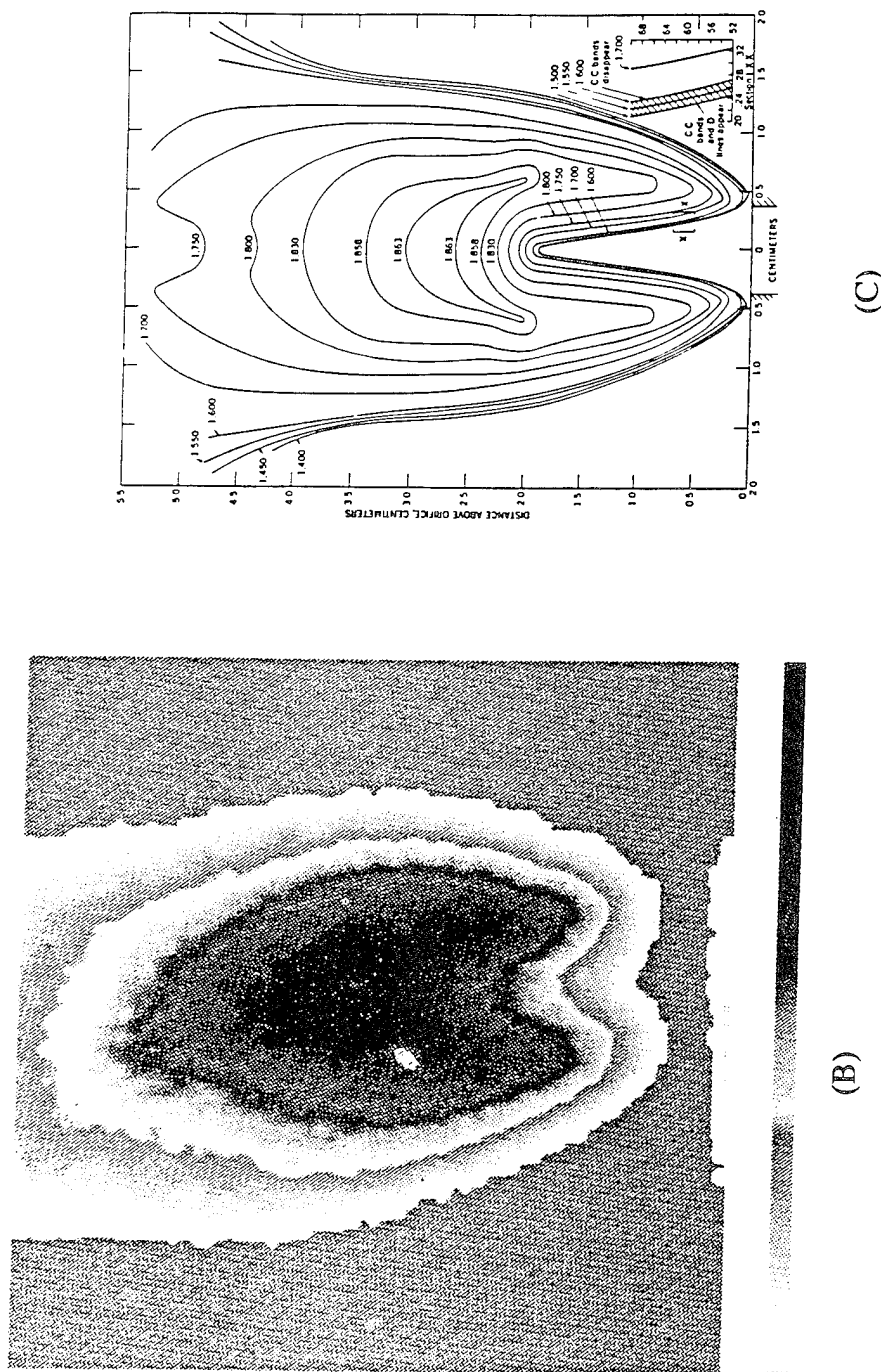
FIGURE 6   (B) & (C). Comparison of Spectral Image Averaged over Fifty-Six Successive Frames with Time-Averaged Temperature Contour Constructed Using Sodium-Line Reversal Method by Lewis and von Elbe (1961). See COLOR PLATE XI.

was narrow (4.6°) in order to help improve quantitative imaging, the typical objective distance ranged from 3 to 5 m depending upon the size of the object.

Imaging from a Bunsen Burner

A Bunsen burner with burner head diameter of 5.4 cm was fueled by natural gas with the air induction ports about half-way open. In a quiet laboratory environment, the fuel flow was adjusted to produce the flame height of about 10 cm. Two sets of images were obtained from respective sections as indicated in Fig. 2: (A) the luminous zone of the flame with about 10 cm length and (B) the invisible gaseous mixture above the flame. In order to find the temperatures of the imaging zone-(B), a thermocouple was used and it was found to range between 120-280°C. The flickering luminous flame represented the unstable nature of the reaction zone and also suggested time-varying motions and mixing of cold and warm gaseous mixtures in zone-(B).

A set of images obtained through zone-A at the rate of 200 frames/sec with exposure period of 90 μsec is shown in Fig. 3. This relatively low framing rate was chosen for the imaging in order to capture variations in flame behavior which are observable in the limited number of images displayable on our screen. The image sequence goes from left to right and succeeds from top to bottom. Relatively symmetric flame-cone images are displayed in line-1, which gradually form a neck. This trend becomes obvious with time, around image 1-e. This change in flame is exhibited more remarkably in the second line finally to produce a separate volume of high-temperature mixture, which detaches itself away from the main flame cone. Consequently, the separate volume of radiation source finally moves out of the imaging zone-A. This flame behavior repeated in a cyclic manner.

Under the same imaging condition, except for the exposure period, another set of images were obtained from zone-B, which is invisible to the eye (Fig. 2). The detached radiatively participating volume off the luminous zone, mentioned above, continues to move while dissipating. New cycles with nearly identical image sizes and shapes are repeated. This flow visualization may be the first observation of such a mode of sequential mixing process of combustion products with the entrained air.

The concentration of water vapor and temperature are the two main factors determining the pixel output in the present spectral imaging of 2.2-2.5 μm. Other species such as CO_2 and fuel molecules would not significantly emit in this range. The characteristics of the flame image, therefore, may be explained by using processes affecting their variations. Among those affecting the process are the entrainment of air into the high-temperature mixture and the buoyancy force. Both dictate the local mixing and convection of combustion species and the temperature redistribution. Note that the heat transfer, particularly radiation heat loss from this blue flame in the absence of carbon formation, is considered to play a minimal role in affecting the temperature. The effect of molecular diffusion in the large-scale transport of species in the flame zone is also negligible. In other words, a low water vapor concentration within the combustion products occurs due to dilution by air. The dilution of combustion products, containing water vapor, by the entrainment of cool ambient air is accompanied by quite the same redistribution of thermal energy, which is represented by changes in temperature. The variation of captured radiation energy in this imaging, therefore, indicates the temperature distribution at least in a qualitative scale. This consideration is supported by images obtained in the next burner, which was compared with some other reported measurements.

Looking at the periodic flame behavior and mixing of the combustion product separated from the initial reaction zone (Fig. 3), it is found that cyclic activity occurs about every 30 frames. With the imaging interval of 5 msec in this experiment, the cycle period

displaying repetition of the same flame pattern was approximately 150 msec: Several repeated measurements indicated the cyclic frequency ranged from 6-12 Hz. Initially this cyclic variation was thought to be associated with the flickering diffusion flame in the Bunsen burner. However, we also observed similar behavior in a quiescent laminar flow burner.

Flames and Combustion Products in a Laminar-Flow Rectangular Burner

Unlike the above Bunsen burner, a rectangular burner employed by Lewis and von Elbe (1961) is known to exhibit very stable flames. A new unit was fabricated in order to duplicate the same experimental condition employed in their flame studies. This laminar-flow premixed flame burner (cross section of 0.755 x 2.19 cm and length of 70 cm) was chosen for this investigation because, according to their report, it has advantages that in the flame no flow lines in the zone of illumination are refracted away from or toward the imager. The use of this burner offered additional advantages for us because much flame data from it was reported for studying combustion and mixing behaviors of gaseous mixtures. They may be compared with our findings obtained by our new device. The long travel distance (70 cm) for the mixture in the burner (Fig. 4) was sufficient to establish the normal Poiseuille laminar velocity distribution within the conduit before it reached the opening.

It was possible to reproduce quiet and steady flames as reported in literature when the burner (Fig. 4) was operated on a mixture of 9% natural gas in air (flow rate of 220 cc/sec). As illustrated in our photograph obtained by using a 35 mm camera (Fig. 5), the flame compares well with the published image of a sodium mist-laden fuel/air mixture (Lewis and von Elbe, 1961). Figure 6-(A) shows a set of high-speed spectral IR images from the burner under the same imaging conditions and laboratory environment as the previous Bunsen burner flame imaging. A new image was constructed by averaging over fifty-six successive frames as shown in Fig. 6-(B). First of all, it was unexpected to find the cyclic variation in the thermal images of this quiescent flame similar to that observed in the flickering Bunsen burner. Contrary to the initial interpretation of the cyclic flame behaviors that attributed to the flickering nature of the diffusion flame in the Bunsen burner, quite similar cyclic flames were found in this nominally stable premixed flame. What is common in both flames was the air entrainment, which is considered to cause the variation, but further investigation is needed. However, it is noted that there was no large-scale gaseous volume periodically detached from the main flame cone as was observed in the Bunsen burner.

An additional new finding was that the characterization of this burner flame as a laminar flame made based on a fluid dynamic observation that employed particle tracing may be questioned. It is particularly probable if the laboratory condition is not extensively controlled, as revealed in the instantaneous image. Some considerable amount of local variations in thermal radiation strength suggests the mixing of combustion products with the entrained air to be rather nonuniform. It is found, however, that a time-averaged thermal image over the above shown 56 frames (Fig. 6-(B)) compares relatively well with the temperature contour constructed based on time-averaged measurements by the sodium-line reversal method (Lewis and von Elbe) as included in Fig. 6-(C).

HIGH SPEED SPECTRAL IR IMAGING IN AN SI ENGINE

Gaining confidence by obtaining instantaneous spectral (water vapor) images from flames as applied in those burners, the new diagnostic tool was applied to a spark-ignition (SI) engine, as described in Fig. 7 in order to investigate the in-cylinder processes.
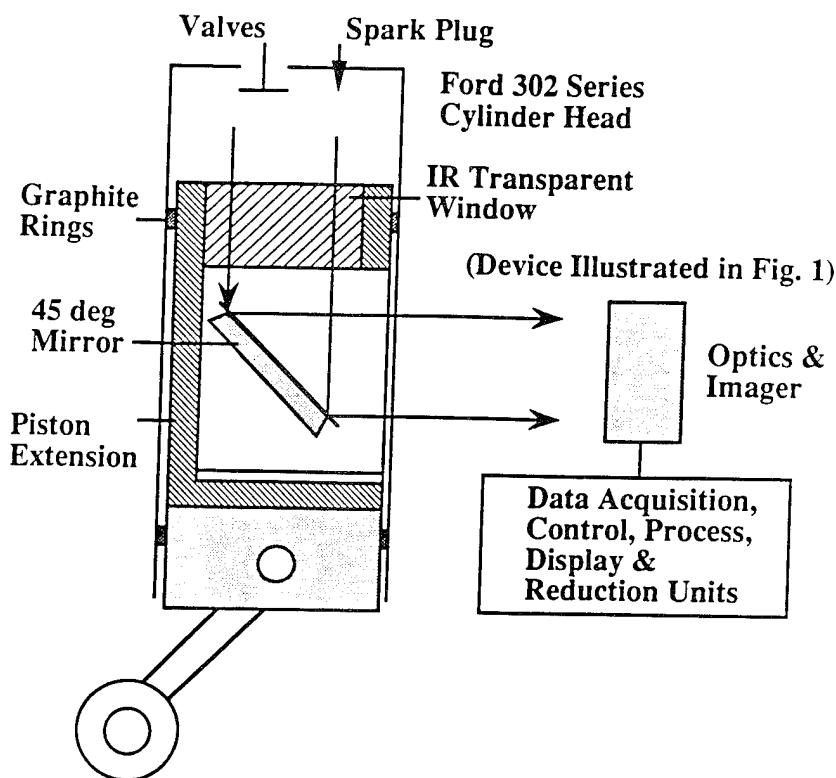
FIGURE 7.   Schematics of SI Engine Apparatus Lined up with New Imaging system.

In brief, a hollow piston extension with one side opened for optical access is connected to the piston head having an IR window. The window (82.55 ϕ x 19.05) was made of silicon, mainly because of its high mechanical strength, thermal conductivity and about 50% transmittance in 1.5-8 μm range even without any antireflection coating. Among other special considerations in mounting this optical window was to maintain it at low temperatures by enhancing heat conduction to the piston and cylinder. This was necessary in order to eliminate the interference in imaging by the radiation from the window and its reduced transmission at high temperatures (Zhao, et al., 1991). A special feature of this reciprocating engine apparatus is the graphite rings that replaced their metallic counterpart in order to eliminate the cylinder wall oil lubrication. This prevented window fouling by the lubrication oil.

The engine was equipped with a Ford 302 cylinder head and a matching intake manifold. This measure was taken in order to minimize potential uncertain effects during the gas exchange processes, which are likely to occur if an unrepresentative cylinder head was used. The engine set up was prepared to operate on either gaseous or liquid fuel for investigating fuel effects on the in-cylinder reactions. An encoder was connected to the engine crankshaft in order to generate crank angle pulses needed for compiling digital pressure-time data and for controlling individual images from the engine.

Figure 8 shows a set of spectral images from the natural gas-fueled engine operated at 500 rpm. The imaging was performed at the rate of one every three crank angle
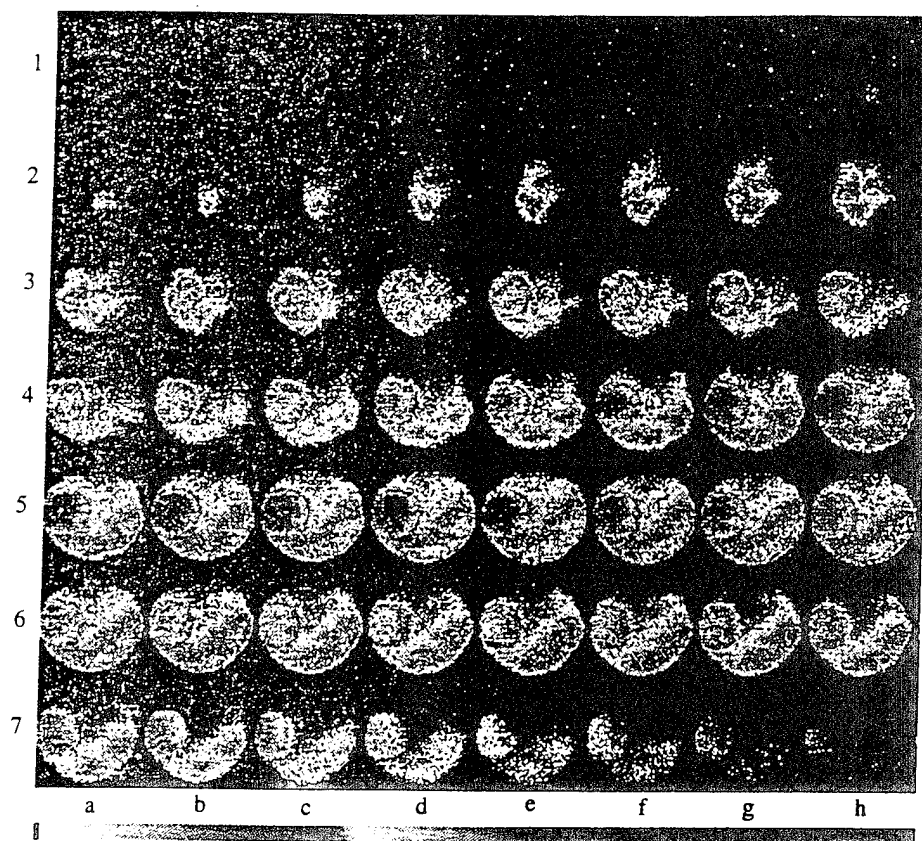
FIGURE 8   High-Speed Spectral (2.2-2.5 μm) Infrared Images of Combustion Reaction in a Spark Ignition Engine Operated by Natural Gas at 500 rpm. Three-CA Interval between Images with 80 μsec Exposure Period. Spark Ignition at Frame 1-c and EVO at Frame 7-b. See COLOR PLATE XII.

degrees with an exposure period of 80 μsec. Spark ignition took place at 3 degrees before top dead center (TDC), i.e., around frame 1-c and the exhaust valve opening (EVO) occurred at 135 after TDC (near frame 7-b). For reference, Fig. 9 is included which shows the view of the same imaging area obtained in a 35 mm photograph. In this view, the spark plug is located below the center of the chamber, between the intake valve on the right and the exhaust valve on the left.

The flame which is made visible by the emitted radiation of water vapor in the burned gas regions is seen in Fig. 8 to propagate to the left, presumably due to the gas motion in this direction. It then consumes the mixture in the lower portion of the chamber. The radiation from the mixture near the spark plug where the combustion started was strongest and that from the end gas portion stayed lowest throughout the imaging period. In view of the low radiation from the end gas, it is possible that mixture in the end gas did not burn during the observation. This will be further studied. The strongest radiation from the lower portion of the chamber may be explained by two possible reasons: This portion has a deeper volume (into the page, Fig. 9) than the upper half of the chamber allowing greater amounts of combustion product to emit more radiation. In addition, large portion of combustion products formed first may have stayed in near their initial position and were subjected to the increased cylinder pressure to attain higher
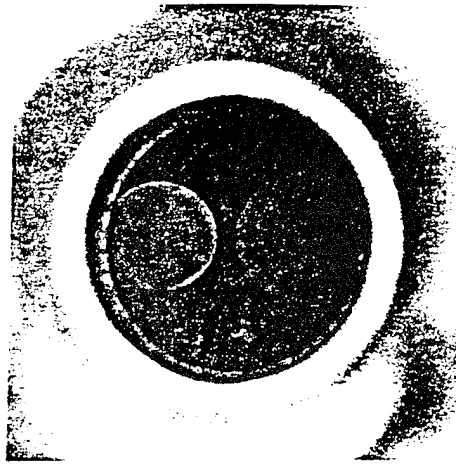
FIGURE 9   View of the Imaging Obtained by Using a 35 mm Camera. See COLOR PLATE XIII.

temperatures.

The strong observed thermal images from the exhaust valve prior to EVO are unexpected. The radiation from the combustion product was somewhat outshone by the emission from the exhaust valve starting as early as 30 after TDC (around frame 2-f). It is unexpected to find such early heating of the exhaust valve, even far before the blowdown process, because the strong convective heat transfer after EVO was considered to be responsible for the heating of the valve. After EVO (after frame 7-b), the radiative strength from the valve became weaker indicating rapid cooling of engine components taking place in the combustion chamber.

SUMMARY

A newly developed high-speed spectral imaging system is presented along with some results obtained from its application to flame studies. Its development was made possible by interdisciplinary participations on an extensive investigation of limitations and feasibility offered by recent advancements in imaging technology.

Among the unique observations is that the convective process of combustion products in and above the luminous flame zone of simple burners was observable by the implementation of high speed spectral IR imaging. The cyclic behavior of flames and mixing of combustion products captured by this device was unexpected. Temperature inferred from our thermal images obtained from a rectangular Poiseuille-flow burner compares with the temperature measurement reported by others.

In-cylinder spectral IR images of combustion in an SI engine obtained by using this new device offers not only the research convenience achieved using the conventional visible-range cinematography but also additional new opportunities for investigating the thermal state of gaseous products and solid surfaces that define the combustion chamber. It permits finding where combustion products at high temperature locate at successive instants of time within the chamber. Cylinder components heated up during the reaction period and their change with time were identifiable. Results obtained by using the present high frame-rate tool demonstrate that this new single-band spectral imaging system will facilitate various thermal and flame studies.

While our new four-spectra imaging system is being constructed for achieving quantitative imaging, the present single-band imaging system will be used for qualitative studies of thermal processes in combustion devices.

ACKNOWLEDGEMENT

REFERENCES

Cochran, B. L., "Signal Processing Circuit Development," RADC-TR-86-69, Final Technical Report, July 1986.

Jiang, H. and Rhee, K. T., "High-Speed Imaging of Bunsen Burner Combustion Products," Canadian and Western States Section, Combustion Institute Meeting, April 29-May 2, 1990, Alberta, Canada.

Kosonocky, W. F., "Review of Infrared Image Sensors with Schottky-Barrier Detectors, Schottky-Barrier Imager Technology." Optoelectronics-Device and Technologies, Vol. 6, No. 2, December 1991.

Lewis, B. and von Elbe, G., *Combustion, Flames and Explosions of Gases*, Academic Press, Inc., 1961, pp. 261-291.

Rhee, K. T., "Optimum Clearance for Rapid Flame Propagation," 19th Symposium (International) on Combustion. The Combustion Institute, 1982, pp. 607-613.

Rhee, K. T., "Spectral Infrared Imaging of Flames in Narrow Clearances," Combustion Science and Technology, 75, 4-6, p. 333, 1991.

Shephard, F. D., and Yang, A. C., "Silicon Schottky Retinas for Infrared Imaging," Int'l Electron Devices Meeting, Technical Digest, 310-313, 1973.

Zhao, H., Collings, N. and Ma, T., "The Cylinder Head Temperature Measurement by Thermal Imaging Technique," SAE Paper-912404, 1991.

High-Speed Spectral Infrared Imaging of Spark Ignition Engine Combustion

T. McComiskey, H. Jiang, Y. Qian, and K. T. Rhee
Rutgers, The State University of New Jersey

J. C. Kent
Ford Motor Co.

Abstract

In-cylinder flame propagation and its impact on thermal characteristics of the combustion chamber were studied by using a new high-speed spectral infrared imaging system. In this work, successive spectral IR images of combustion chamber events were captured while varying several parameters, including fuel/air, spark timing, speed, and warming-up period. Some investigation of cyclic variation, knock, and high-temperature components during the non-combustion period was also conducted.

It was found that the spectral images obtained in both short and long wavelength bands exhibited unique pieces of in-cylinder information, i.e., (qualitative) distributions of temperature and combustion products, respectively. During the combustion period, the temperature of early-formed combustion products continued to increase while the flame front temperature, e.g. near the end gas zone, remained relatively low. The exhaust valve emitted strong radiation starting from the early stage of the combustion period. The spark plug emitted the strongest radiation during the non-combustion period. Considerable cyclic variation in growth of the flame front and completion of the reaction was observable. The radiation from both spectral bands became stronger as the engine warm-up period increased.

While operating the engine with the addition of n-heptane in the intake to produce knock, we captured spectral IR images of the end gas right before it was abruptly consumed. The combustion products that were formed in the end-gas volume upon knock, showed no evidence of higher temperature than other zones in the combustion chamber.

Introduction

The formation of a reaction center initiated upon spark ignition is followed by the space and time dependent flame propagation within the combustion chamber. This process is affected by many variables including, engine design/operation parameters and fuel characteristics. Among their direct impacts is the temporal variation of the thermal conditions of the gaseous mixtures and reactor surface. We attempted to improve our understanding of these events in the present work by using a new diagnostic tool which we have been developing for some time at Rutgers.

In a study of in-cylinder processes, it is desirable to obtain clear pictures to show where, when and how the reaction fronts propagate, and also their effects on the thermal characteristics of the combustion chamber. This would be more desirable if it were achieved by quantitative measurement. There have been several difficulties limiting the achievement of this goal: (1) Some of the in-cylinder processes are invisible; (2) They take place fast; (3) The reaction events vary from cycle to cycle; (4) They are three-dimensional; (5) Modification of the combustion chamber for accommodating probe or optical access alters the target events; (6) The optical window may be fouled by deposit; (7) Some measurement methods are time-consuming in both data acquisition and processing; and more. Since they are rather self-explanatory and have been known within the field, no additional discussion will be added here. Nevertheless, a simple review of the list reminds us that there has been no previous diagnostic device which satisfactorily facilitates overcoming these difficulties.

Our early literature survey, however, suggested that rapidly advancing electro-optical technologies were so significant that development of a new diagnostic tool meeting those requirements, to a great extent, may be feasible. This motivated us to initiate design of a new high-speed infrared (IR) digital imaging system several years ago. The basic methodology and some description of the new IR imaging system were explained when its early applications were reported [1, 2, 3, 4][*]. Due to the need for extensive technology know-how and resources involved in the system development, the construction of a prototype unit was carried out with interdisciplinary participation and collaboration with industrial concerns.

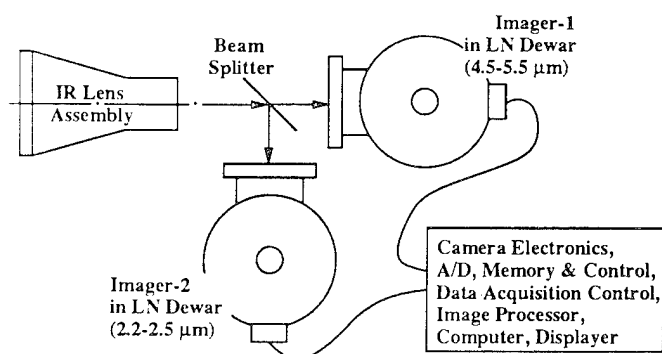[*]Numbers in the parenthesis designate references at the end of paper.

Fig. 1. High-Speed Two-Color Infrared Imaging System.

Why IR Imaging? Imaging in the IR range aids investigation of thermochemical processes in combustion devices in several unique ways. It complements visible range imaging by capturing more extensive "fingerprints" from the spectrum of reacting species in a wide range of temperatures. In particular, since IR imaging is capable of obtaining pictures of relatively low-temperature gaseous mixtures, which are generally *invisible*, some phenomena otherwise difficult to investigate can be examined with this method, as illustrated later. The IR spectral data may be used to perform quantitative analysis, such as determination of instantaneous spatial distributions of temperature and species concentration by employing the conventional two-color method or other spectrometric analysis techniques [5]. Among other advantages of this method over visible-range cinematography is that its imaging is performed without any lighting or chemical doping of the mixture, thanks to the highly sensitive (cryogenically cooled) imagers employed by the system.

Apparatus

IR Imaging System. Since this new diagnostic tool was described in the above mentioned literature, only a short explanation of the system is given here. Among the uniqueness of our approach over others' is that we developed a new operating method and electronic units to drive an existing IR area imager to achieve quantitative imaging at the highest possible framing rate. The imagers used are 64x128 PtSi Shottky barrier detectors operated through a CCD-scheme at a temperature of 77K which gives an effective spectral band of 1.5-5.5 μm and a 12-bit dynamic resolution. Our newly developed package includes a camera head, imager driving electronic boards, data processing and storage units, a data acquisition control unit, and a factory-modified image processor. They are all linked to a desk-top computer loaded with our image-process software (Fig. 1).

At present our imaging system can be operated at a rate of more than 1,800 frames/sec with exposure period as short as 20 μsec (when imaging is triggered by the internal clock, opposed to external signals). The independently variable imaging rate and exposure period of the camera unit

along with the aperture control in the optical train offer flexibility in acquisition of quality measurements according to the reaction rate and radiation intensity. The spectral bands of the present imaging were 2.2-2.5 and 4.5-5.5 μm, which captures radiation emitted by water vapor in high temperature mixtures. Note that there is infringement by strong radiation from CO_2 near 4.5 μm in hydrocarbon-air flames and its effect is taken into consideration.

Among the important adjustments made for quantitative imaging are (1) correction of pixel-to-pixel variation and sensitivity linearity; (2) background radiation/noise compensation; (3) simulated operation of the imaging system prior to each measurement. In brief, the output variation among the pixels (even upon the same incident radiation) is normalized by the two-point correction method for each set of raw image data, which is then followed by subtraction of the background image. They are standard practices performed by either software or hardware method. The simulated imager operation, however, is a new measure, which we discovered necessary for achieving consistent and quantitative imaging using the PtSi imager. According to our (calibration) study, the imaging system, however seemingly undiscernible to eye inspection, produced remarkable variations in digital output. This resulted from different engine running speeds, which affect the framing rates because the individual images were triggered by crank angle (CA) markers from the host engine. In order to overcome this problem, we fabricated a signal generator which produced a set of signal markers to be introduced into the camera. The preparatory camera operation under this arrangement simulated each engine measurement condition, which permits achieving a stabilized imaging performance. This eliminated unnecessary and often unwanted engine operation prior to each data acquisition.

Data Acquisition Control and System Arrangement. An additional new component developed for our engine investigation was a data acquisition control unit. This unit was designed to deliver the following features for the controlled imaging: (1) The start of imaging in each cycle is determined by a delay period (in terms of CA) from the reference marker, e.g. top-dead-center (TDC) signal; (2) The interval between images can be adjusted in terms of CA; and (3) The total number of images to be obtained per cycle are all predetermined. Since the captured images could be displayed for quick review while the engine was running, these features greatly improved consistency in acquisition of data and reduced/eliminated the editing time of images. A specific use of the third feature was that it facilitated investigation of the cyclic variation of in-cylinder events without requiring a large size storage-memory and data processing time. Integration of this engine-controlled imaging circuit-package with the 10 MHz CCD unit resulted in a lower top framing rate and a longer minimum exposure period (than those in an internal clock-trigger mode), i.e., somewhat over 1,200 frames/sec and 40 μsec, respectively.

This high-speed IR digital imaging system may be expanded in several ways for investigation of flames and combustion devices depending upon individual problem needs. They include: (1) single spectrum imaging; (2) dual-
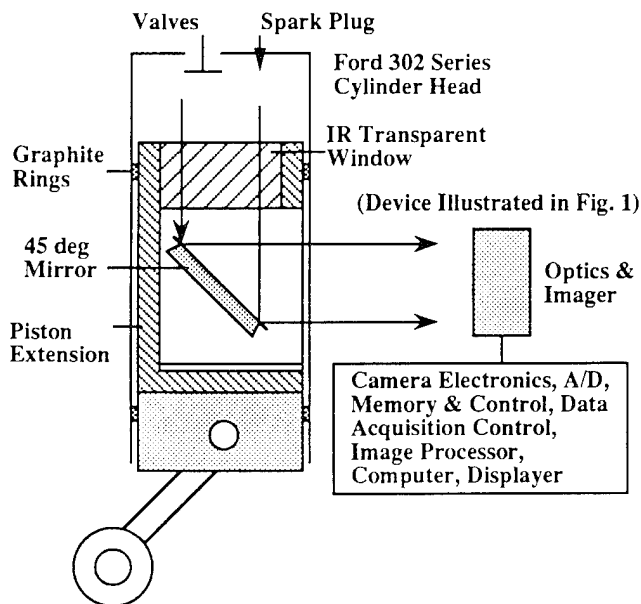
2

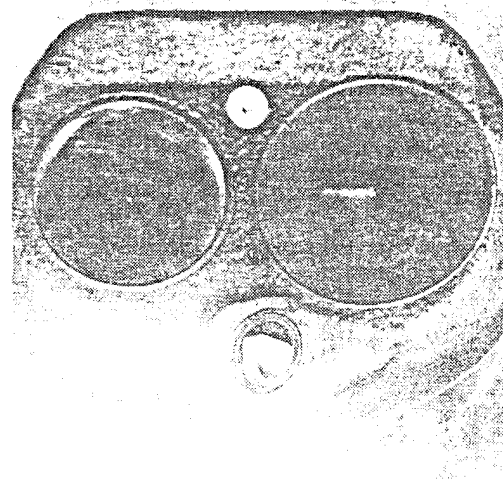Fig. 2. A Single-Cylinder Spark Ignition Engine with Optical Access.

band imaging; (3) quad-band imaging; and (4) magnified imaging. The present paper includes some results from layouts (1) and (2), and our continuing study is directed at investigation of combustion devices by employing layouts (3) and (4).

Mentioning the dual-band imaging arrangement, a beam splitter was placed between the lens and two camera units to give two spectral images. When these geometrically identical images are simultaneously obtained, alignment of the optical components is a necessary requirement. Precise alignment is particularly important because the digital output from matching pixels will be directly used for our spectral analysis. It turned out to be rather straightforward to achieve satisfactory alignment. Two image monitors were employed side-by-side, each displaying respective spectral images of a well defined blackbody object. The optical train was adjusted manually while visual inspection of the enlarged matching images was done on the screen. This led us to an alignment of the system to the pixel scale.

Single-Cylinder Engine with Optical Access. In order to accommodate the above mentioned new diagnostic tool, a single-cylinder CFR engine was modified as shown in Fig. 2. A hollow piston extension with one side opened for optical access was connected to the piston head having an IR window. The window (82.55 ϕ x 19.05) was made of silicon, mainly because of its high mechanical strength, thermal conductivity and about 50% transmittance in 1.5-8 μm range without any antireflection coating. The mounting of the window was implemented with a goal of maximizing the heat dissipation. This measure was taken because if its temperature exceeds about 250°C, its transmissivity

deteriorates and it may become a source of unwanted radiation emission [6]. (In view of temperatures under 200°C measured in a warmed engine by using a thin-film thermocouple implanted near the valves, to be mentioned later, the window temperature was not expected to exceed the critical value.) A special feature of this engine apparatus is the graphite rings that replaced their metallic counterpart in order to eliminate the cylinder wall oil lubrication. This prevented window fouling.

The engine apparatus was equipped with a Ford 302 cylinder head and a matching intake manifold. This approach was taken in order to minimize potential uncertain effects during the gas exchange processes, which is likely to occur if an unrepresentative cylinder head and peripheral components are used. In order to clarify the orientation of the IR images, a photograph taken through the imaging view without the silicon window (opaque to visible light) is shown in Fig. 3. Between the two valves, the exhaust valve on the left and the intake valve on the right, is the spark plug at the lower end and a fast-response thin-film iron-nickel thermocouple at the upper. The measurement obtained using the temperature probe was made to complement the spectral IR images in understanding the in-cylinder events and the thermal loading over the combustion chamber wall.

A careful design consideration was taken in the construction of cylinder block in order to maintain consistent cooling by directing coolant flow uniform over the outer surface of the cylinder liner. This cooling loop was separated from that in the cylinder head in order to exercise more flexible control of thermal balance in the engine. Ten thermocouples were implanted throughout the engine and the coolant loops in order to closely monitor temperatures at important places in the setup.
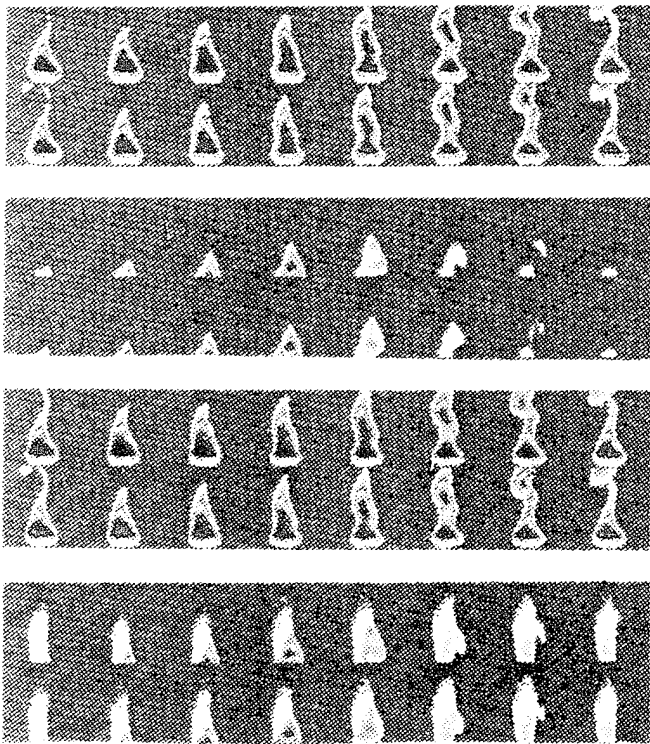
3

Fig. 4. Successive Spectral IR Images obtained at 67 frames/sec
and an Exposure Period of 90 μsec from Views:
  (A) Visible Flame in 2.2-2.5 μm Band;
  (B) Invisible Zone (above Flame) in 2.2-2.5 μm Band;
  (C) Visible Flame in 4.5-5.5 μm Band; and
  (D) Invisible Zone in 4.5-5.5 μm Band.

Among other instrumentation equipping the engine was an encoder connected to the crankshaft to generate crank angle pulses needed for compiling pressure-time (p-t), temperature-time (T-t) data from the surface thermocouple, and for triggering individual images. Except for design variables, several engine operation and fuel factors were readily changeable for the present exploratory investigation.

IR Images of a Simple Burner Flame. In spite of mutual similarities that may be found between an IR image and a visible ray photograph obtained of a solid wall, there are some distinctive differences between them, particularly when gaseous mixtures are imaged. In order to illustrate these differences, IR images of a Bunsen burner taken by this system are presented in an effort to help the reader interpret the high-speed spectral in-cylinder images that will be shown later. A Bunsen burner with head diameter of 5.4 cm was fueled by natural gas with the air induction port about half-way open. In a laboratory environment, the fuel flow was adjusted to produce a luminous flame height of about 10 cm.

At first, images were obtained of the luminous flame zone having an approximate height of 10 cm and are included in Fig. 4-(A). The imaging rate was 67 frames/sec with an exposure period of 300 μsec. This low framing rate was employed in order to display a full cyclic flame behavior within the set of images. In this set of sixteen images captured in the 2.2-2.5 μm band, one can find, in sequence

(going from right to left), relatively symmetric flame-cone images; those with a gradually developing neck; and those finally detached away from the burner base, occurring in a cyclic manner. Next, a similar set of images (Fig. 4-(B)) was separately obtained from the *invisible* zone right above the luminous zone with some overlap with the previous view. This had a similar height of view, 10 cm and the same imaging conditions. This direct flow visualization of an invisible object clearly illustrates the temporal and spatial dissipation process of combustion products.

Dual-Band Imaging. Expanding on our earlier application of a single band imaging (2.2-2.5 μm), the system was arranged to obtain dual-spectra images as previously mentioned: Sets of matching spectral images in 4.5-5.5 μm obtained at the corresponding imaging condition to the above are included in Figs. 4-(C) & 4-(D).

There are two main factors which cause differences between spectral IR images (of gaseous objects): temperature effect and spectral dependency. Images captured in the shorter wavelength band represent radiation from objects at *only* higher temperatures while those in the longer wavelength band exhibit combined effects by objects at a wider temperature range. For example, consider a blackbody at 600 K, which produces the peak spectral emissive power in the latter waveband, it emits a lower spectral power in the former band by almost an order of magnitude. In order words, combustion products at low temperatures will not be captured in spectral images of the shorter wavelength band, 2.2-2.5 μm, but they can be seen in the longer wavelength band (4.5-5.5 μm) images, as long as their population is sufficiently high.

As mentioned earlier, both spectral bands for the present imaging were chosen to capture the radiation from water vapor but the 4.5-5.5 band includes some significant CO_2 radiation. The spectral dependency of the absorption coefficient of those species, combined with the above mentioned temperature and population effects, will have to be taken into account while interpreting the spectral images. In the images obtained through the longer wavelength band, the radiation from a high-temperature object can, therefore, be overshadowed by that from a low-temperature object if its concentration and absorption coefficient are high.

The instrumentation is currently being arranged for quad-spectra imaging to implement quantitative spectral analysis (assuming molecular thermal equilibrium). Such an approach was not attempted using the present dual band imaging results (obtained from hydrocarbon flames) due to the abovementioned infringement of radiation by CO_2 in 4.5-5.5 μm band. However, some spectral analysis to determine spatial distributions of temperature and species was made on a hydrogen flame [5]. While such quantitative analysis is being pursued for the engine flames, the analysis of hydrogen flame seems to support the above suggestion, i.e., the images in the shorter wavelength band likely represent the (high) temperature variation and those in the longer wavelength band appear to more reveal the presence of combustion products (at even low temperature). This consideration is employed in explaining the results from in-cylinder imaging, as shown next.

Results and Discussion

It is pointed out that the present paper includes results from an *exploratory* investigation of in-cylinder events by using the new diagnostic tool. Some of the new findings made in this work, therefore, will have to be further studied in order to obtain more convincing explanations in the future. Several parameters were varied in this study. They are: spark timing; fuel/air ratio; warming period; fuel's knock tendency; and more.

Baseline Image. When the thermal imaging of in-cylinder reactions was performed by varying the above mentioned factors, other relevant engine information was also obtained, e.g. p-t data. The results from this parametric study were compared with a set of images obtained under the baseline engine operation condition (Fig. 5). The specifications of the baseline condition were: spark timing at nine degrees CA before top dead center (bTDC), which was the minimum spark advance for best torque (MBT), engine speed of 500 rpm, induction pressure of about one atmospheric pressure measured at the surge tank, over ten minutes of warming-up period, and fuel/air ratio of 19 to 1 of air/natural gas mixture.

The successive images were obtained starting from 10 bTDC with interval of 2.5 CA and an exposure period of 90 μsec. In order to help understand the high-speed IR image format, a look-up table (LUT) is offered as shown in Table-1. LUT-1 includes engine crank angles (negative sign representing bTDC) and other important events, e.g. exhaust valve open (EVO), which began at 135 aTDC, image 8-c. The figures shown are obtained in the two different wavebands: (A) 2.2-2.5 μm and (B) 4.5-5.5 μm. In general, the sharpness of the shorter wavelength images is better, which may be partially due to smaller diffraction by the shorter wavelength rays. The progressive change in both sets of images suggests the engine reaction is smooth without any measurable discontinuity, such as knock, which is confirmed by the p-t diagram (Fig. 8 or 10).

It is reminded that, except for the early stage of combustion when the piston is near TDC, the images of the in-cylinder events are accumulated effects through a line-of-sight (maximum about 10 cm at BDC) involving three-dimensional flow and flame propagations. Recall the discussion that low temperature objects can be captured in a longer wavelength band in the present imaging condition and review the images in line-1 of both picture sets. The earlier detection of flame formation and the greater size images in the 4.5-5.5 μm band seem to be reasonable in view that the growth of early flame front would be relatively slow and weak under low cylinder pressures. According to these thermal images, the flame growth progressively continued and the mixture was completely consumed leading to emission of remarkable radiation until around 30 aTDC. Except for the strong radiation from the exhaust valve, the variation of radiation out of the cylinder head wall seems undiscernible, mainly due to the presence of the combustion products in front. It is more obvious from the 4.5-5.5 μm band, which indicate the radiation emitted by objects in wide range of temperatures that it is difficult to infer the temperature variation over the wall. They, however, reveal the presence of the combustion products rather well.

On the other hand, those captured in the 2.2-2.5 μm band, represent radiation from products at higher temperatures and seem to exhibit obvious temperature variations. (Note that since uniform fuel/air mixtures were employed throughout the study, the concentration of water vapor in the combustion product is also uniform.) Looking at Fig. 4-(A), the strongest radiation from the early burned products near the spark plug and exhaust valve (particularly seen in lines 2 and 3) indicates correspondingly high temperature there. It seems to be quite reasonable that the continued increase in cylinder pressure results in higher temperatures in the early burned combustion products. The combustion chamber temperature, as inferred from images, decreased as the piston descended, yet maintained noticeable spatial variation, at least until 55 aTDC, frame image 4-c. This finding (particularly when the reaction is taking place) can not be seen in the long wavelength band images, seemingly due to the strong spectral radiation power contributed by low-temperature products which overtakes that from high-temperature objects.

This consideration brings on the question as to the nature of the products exhibiting low radiation at the upper portion of the pictures (in lines 2 and 3). This is before the volume expansion by the piston's descending motion, which results in lower temperatures throughout the imaging view, (those in lines 4 and 5). Again, since the water vapor concentration is expected to be uniform once the reaction is complete, low radiation indicates relatively low temperatures. Then it could be argued that the low-radiation zone may be a highly probable center for unburned hydrocarbon (UHC) formation, at least compared with the volume emitting strong thermal radiation.

Using the same argument, one may question about the significance of the combustion products emitting high intensity radiation throughout a great portion of the combustion period, which was found near the spark plug and exhaust valve. This may be a most probable localized volume of nitrogen oxide (NOx) formation.

Among other unexpected observations from the baseline images is the strong radiation by the exhaust valve, which started from the beginning stage of the combustion period, as early as 10 aTDC, image 2-a (Fig. 5-A). It was unexpected because the high temperature in the exhaust valve is considered to occur due to high convective heat transfer during the blow-down/exhaust period and poor cooling limiting dissipation of its energy. Two possible reasons for the unexpected observation are in order: As mentioned earlier, it is probable that the exhaust valve is indeed one of the highest-temperature components which retains a large amount of thermal energy during the entire engine cycle. The valve is expected to be cooled by dissipating this thermal energy out of its "skin layer" when a fresh intake charge is introduced hence its image is not captured before the presence of new flame front (images 1-a through -h in Fig. 5-A). As soon as the flame front sweeps over the valve, it may not need a long period of time before restoring the high skin temperature so that it again emits strong radiation (even at the early stage of combustion).

5
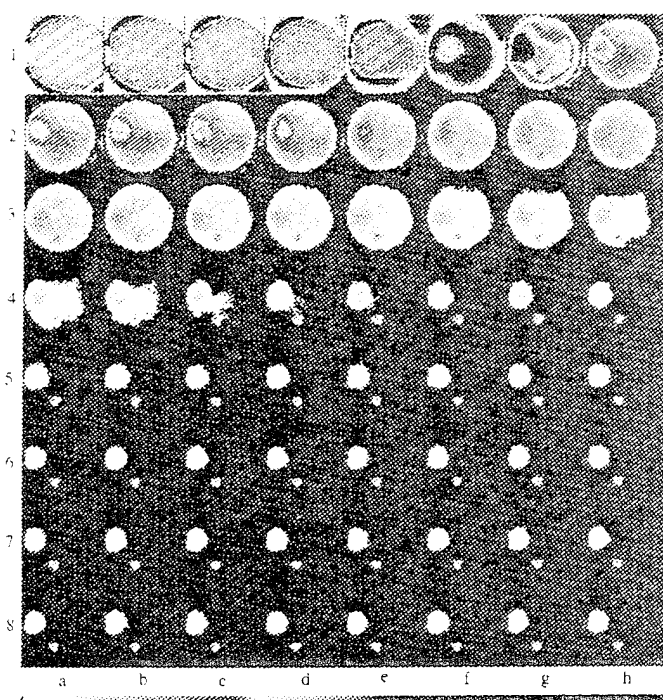
(A)
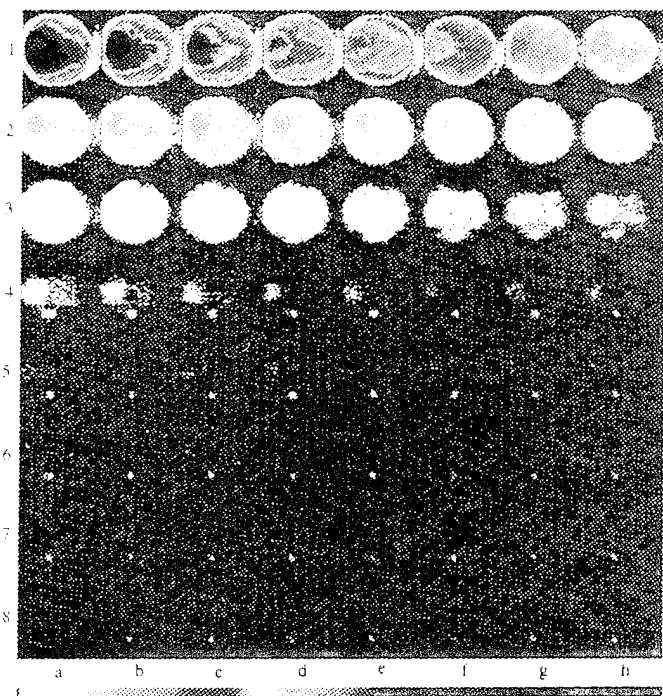
(B)

Fig. 6. High-Speed Spectral Images Obtained during Non-Combustion Periods under Baseline Condition:
(A) 2.2-2.5 μm band and (B) 4.5-5.5 μm band.
Refer to LUT-2 for Image Reading.

	a	b	c	d	e	f	g	h
1	-10	-7.5	-5.0	-2.5	TDC	2.5	5.0	7.5
2	10	12.5	15	17.5	20	22.5	25	27.5
3	30	32.5	35	37.5	40	42.5	45	47.5
4	50	52.5	55	57.5	60	62.5	65	67.5
5	70	72.5	75	77.5	80	82.5	85	87.5
6	90	92.5	95	97.5	100	102.5	105	107.5
7	110	112.5	115	117.5	120	122.5	125	127.5
8	130	132.5	EVO	137.5	140	142.5	145	147.5

Table-1. Look-up Table, LUT-1 for Image Reading.

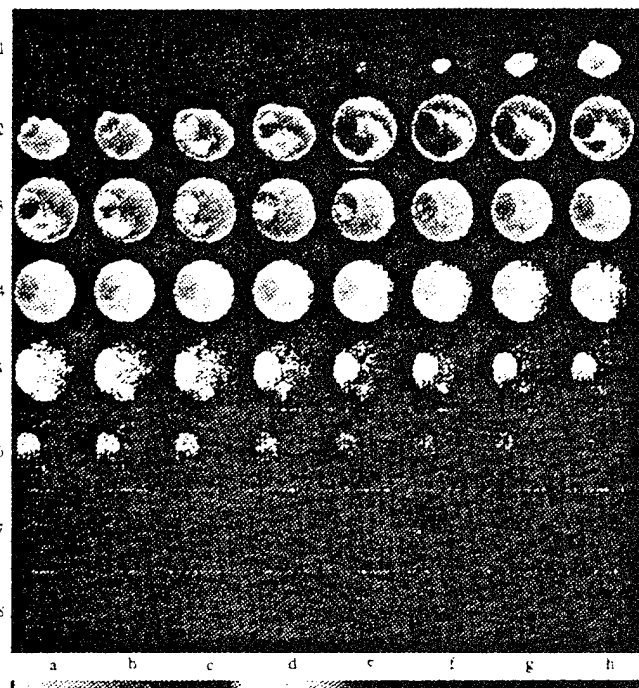|	a	b	c	d	e	f	g	h
1	120	128	EVO	144	TDC	160	168	176
2	184	192	200	208	216	224	232	240
3	248	256	264	272	280	288	296	304
4	312	320	328	336	344	IVO	360	EVC
5	376	384	392	400	408	416	424	432
6	440	448	456	464	472	480	488	496
7	504	512	520	528	536	544	552	560
8	568	576	IVC	592	600	608	616	624

Table-2. Look-up Table, LUT-2 for Image Reading.

Another probable reason is that the exhaust valve is more reflective of IR energy than other places in the combustion chamber. Although it seems probable, this consideration is rather unusual and an additional experiment is underway in order to explain the findings. Nevertheless, this hypothesis seems to be partially supported by the thermal images obtained at the very start of a cold engine, as explained later.

Images during Non-Combustion Periods. Similar sets of images were obtained under the above mentioned baseline conditions, except that imaging started at 120 aTDC with eight CA between frames and increased exposure period, i.e., 700 μsec (Fig. 6). A corresponding look-up table, LUT-2, is included. Note that the first several images obtained in 2.2-2.5 μm seem to be meaningless because they are flooded output due to an over-exposure of the incident radiation on the imager.

(A)

(A)

(B)

(B)

Fig. 5. High-Speed Spectral Images Obtained during
    Combustion Period under Baseline Condition:
    (A) 2.2-2.5 μm band and (B) 4.5-5.5 μm band.
    Refer to LUT-1 for Image Reading.

Fig. 13. High-Speed Spectral Images Obtained during
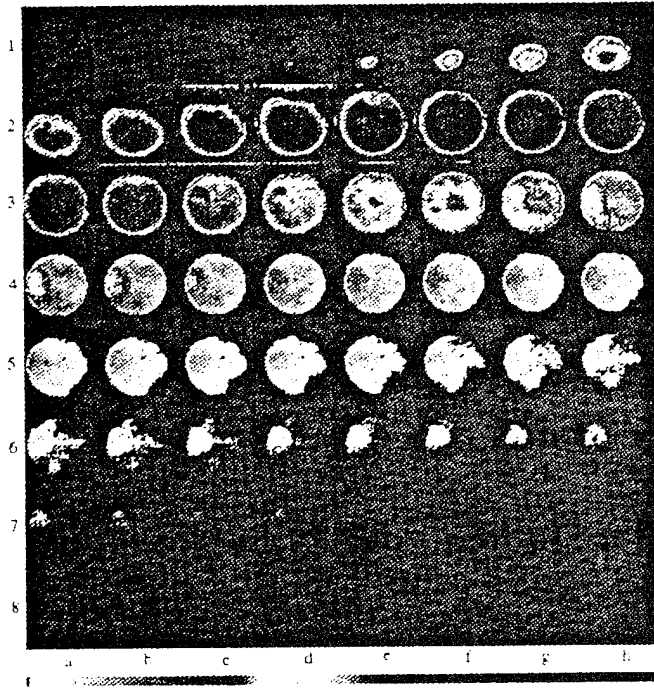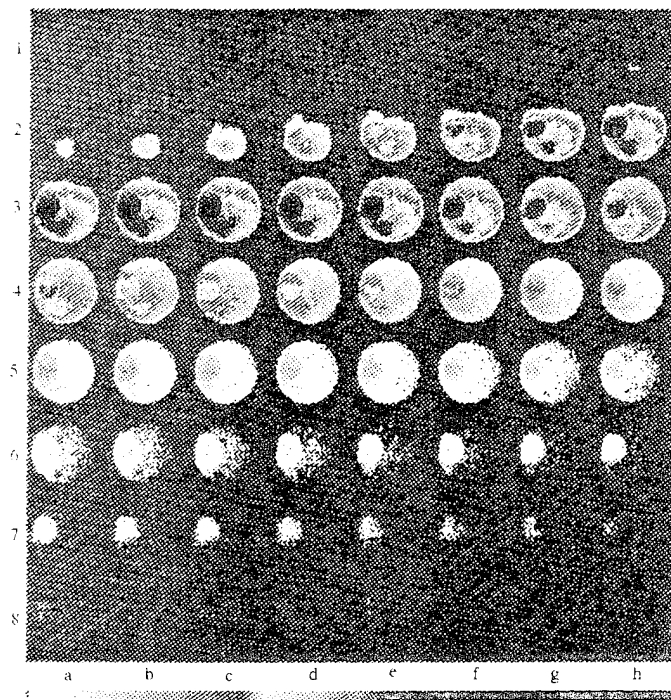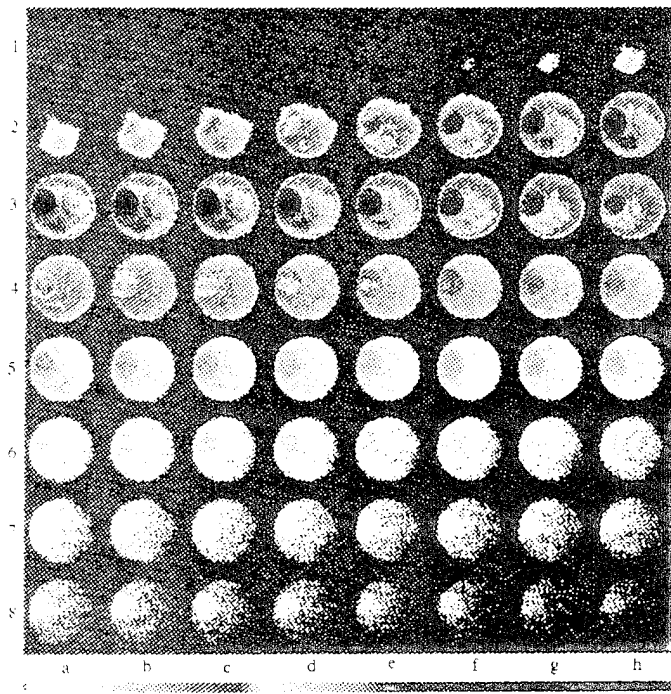   Combustion Period under Baseline Condition with
    Knock: (A) 2.2-2.5 μm band and (B) 4.5-5.5 μm band.
    Refer to LUT-2 for Image Reading.

7

(A)

	a	b	c	d	e	f	g	h
1	-30	-27.5	-25	-22.5	TDC	-17.5	-15	-12.5
2	-10	-7.5	-5.0	-2.5	TDC	2.5	5.0	7.5
3	10	12.5	15	17.5	20	22.5	25	27.5
4	30	32.5	35	37.5	40	42.5	45	47.5
5	50	52.5	55	57.5	60	62.5	65	67.5
6	70	72.5	75	77.5	80	82.5	85	87.5
7	90	92.5	95	97.5	100	102.5	105	107.5
8	110	112.5	EVO	117.5	120	122.5	125	127.5

Table-3. Look-up Table, LUT-3 for Image Reading.

The exhaust valve started to open at 135 aTDC, around image 1-c. The impact of the blow-down seems to be well indicated by the reduction of radiation from the products immediately thereafter. Similar findings are obtained from those in 4.5-5.5 μm. What is found unique in the latter set of images is that the spark plug emitted the strongest radiation in the combustion chamber, a probable indication that the plug was at higher temperatures than the exhaust valve throughout the non-combustion periods (assuming their emissivities are mutually comparable). By revisiting the images with LUT-2, the cooling effect of intake valve opening (IVO) can be seen from the subsequently reduced radiation after image 4-f.

During the intake period, the longer wavelength band images show some measurable variation of radiation (e.g. those in lines 5 and 6). Among the probable reasons for this variation may be the presence of residual gas, which is being further investigated.

Spark Ignition Time. Sets of images were obtained at three different spark ignition times: (1) late timing, 3 bTDC (Fig. 7-(A)); (2) baseline-MBT timing, 9 bTDC (Fig. 5-(A)) and (3) advanced timing, 20 bTDC (Fig. 7-(B)). LUT-1 may be referred for the late ignition timing and LUT-3 is included for Fig. 7-(B), images from advanced timing. As expected, imaging results show that the earlier the ignition, the sooner the reaction completion and the stronger the radiation. This in turn indicates higher peak product temperature. In addition, an advanced spark ignition time resulted in a shorter period of combustion, but had a longer duration of high temperature products. The higher heat transfer (to the combustion chamber wall) under such conditions, therefore, will occur due to both higher temperature difference and longer heat transfer duration, *not* longer overall combustion period.

Such effects on the reaction period and product temperatures were also indicated by p-t (Fig. 8-A) and T-t (Fig. 8-B) data. Advanced spark timing produced a shorter combustion period in the p-t history with a longer period of
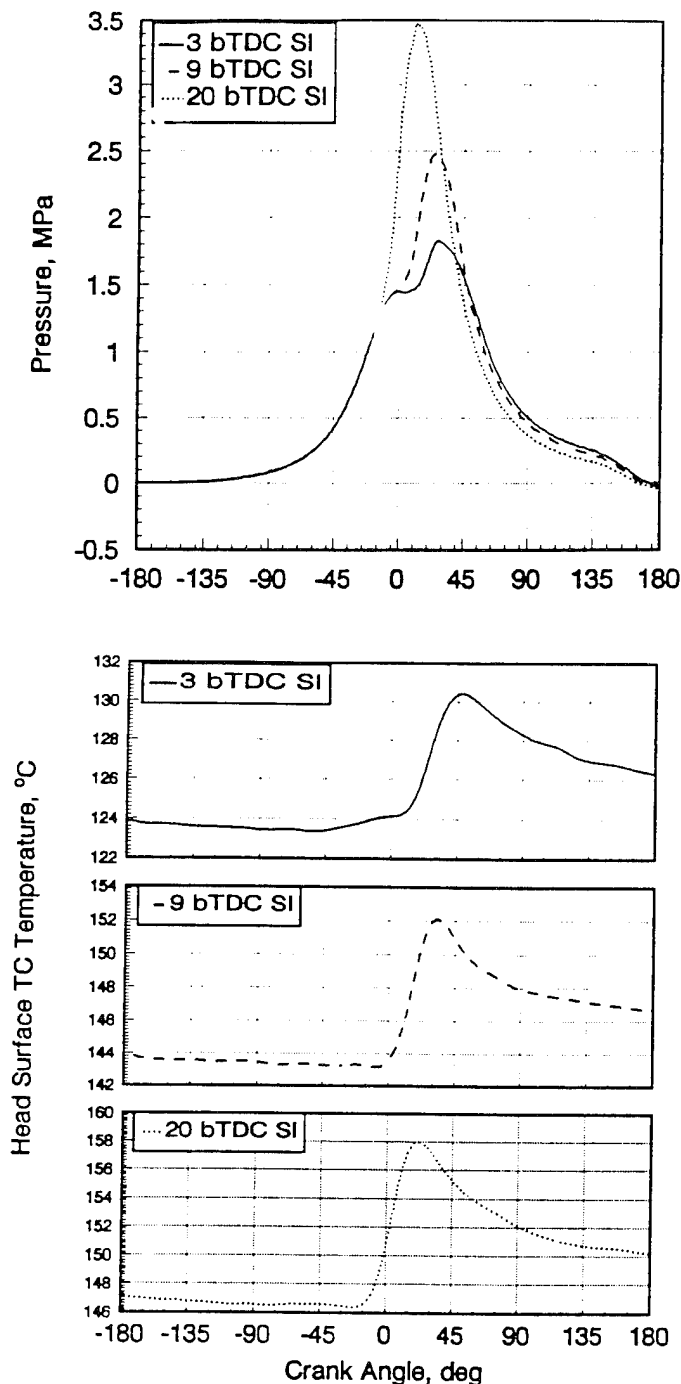

(B)

Fig. 7. High-Speed Spectral Images Obtained in 2.2-2.5 μm band at Varied Spark Ignition Time:
(A) 3 bTDC and (B) 20 bTDC.
 Refer to LUT-1 and -3 for (A) and (B), respectively.

Fig. 8. (A) P-t and (B) T-t Measurements Obtained for Varied Spark Ignition Timing.
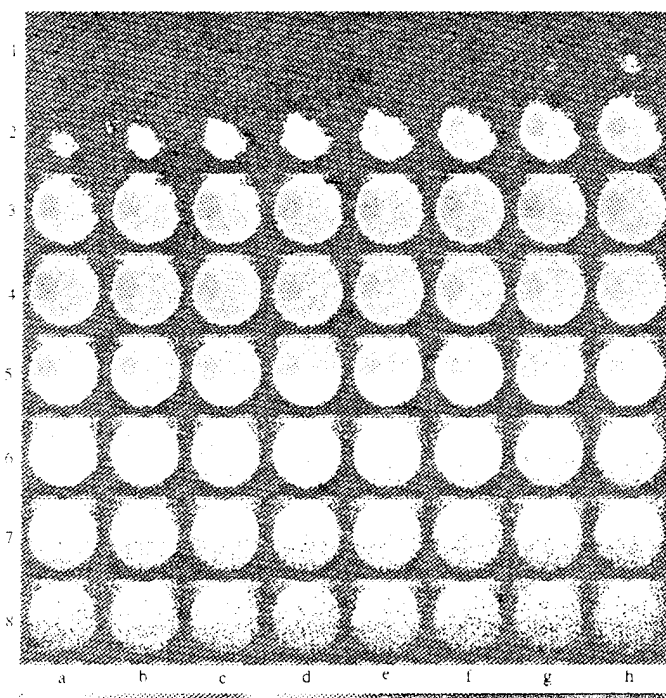
the engine is gradually warmed up, imaging was performed under the baseline conditions, but at progressively later times from the start of engine combustion: (1) imaging from one of the very first burning cycles (Fig. 9-(A)); (2) imaging after five minutes (Fig. 9-(B)); and (3) imaging after ten minutes (Fig. 5-(A)). They are all referred to LUT-1. The data obtained at startup reveal some unexpected results. The p-t history (Fig. 10-(A)) shows a mode of unusual double peaks (followed by high pressure at blowdown), for which reason is not known. The strength of thermal radiation captured in IR images is also very low compared with those obtained under conditions (2) and (3). Measurement of T-t (Fig. 10-(B)) made under the matching conditions shows temperature at the probe before the flame arrival increased with the warming period, but the temperature rise due to high-temperature combustion products remained about the same.

Recall the interpretation of the strong radiation from the exhaust valve when the baseline images were discussed earlier by mentioning one of probable causes being strong reflection by the valve surface. However unusual the interpretation might seem, it does appear to be supported by the IR images obtained at the very beginning (Fig. 9-(A)), which shows some measurable radiation from the (yet unheated) exhaust valve. In view that much more obvious radiation from the valve was observed when the engine was warmed up, the reflection may not fully explain the finding, however.
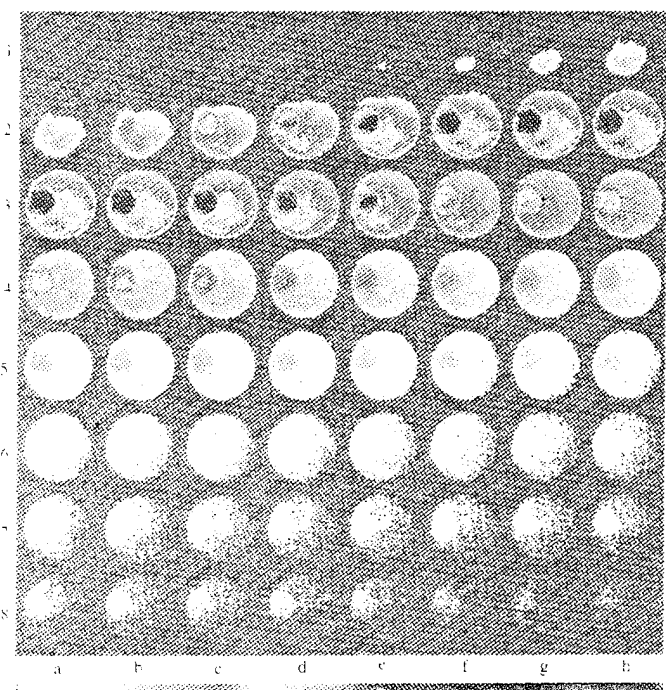
Cycle-to-Cycle Variation. The cyclic variation of the in-cylinder processes was studied by obtaining images under the baseline conditions starting from 10 bTDC at 10 CA intervals. Two set of images gathered in respective wavebands during four successive cycles are shown in Fig. 11. Since they were obtained at corresponding CAs, the imaging conditions are mutually comparable as shown in a new look-up table, LUT-4 (where only one cycle is indicated). The results are direct and indicative of significant cyclic variations occurring in this natural gas operated engine which exhibits differences in the flame front propagation even in the early stage of combustion, e.g. images in column-b and -c: When a cycle began with a strong flame front, the reaction was consistently completed sooner. What causes such cyclic variations remains be determined, which may be facilitated by obtaining images of the residual gas as briefly mentioned earlier.

The images captured in the longer wavelength band appear to complement their counterpart's finding of cyclic variation. For example, the weak radiation images, particularly when cylinder pressure was low, are captured more obvious in this spectral band.

Knock and Its Image. One of the most sought after investigations using our new diagnostic tool was the direct imaging of in-cylinder processes under a knock condition. In the present exploratory investigation of in-cylinder events, we chose to season the natural gas-air intake mixture with a small amount of n-heptane. This was to simulate occurrence of knock caused by fuel properties, opposed to the engine factors, e.g. deposit in the combustion chamber and temperature. Many sets of IR images were

high wall temperature. This is consistent with the above observation using IR imaging. The temperature measured at the surface thermocouple elevated during the combustion period, with the abovementioned spark advances, from 144 to 152, from 147 to 155, and from 178 to 191 °C, respectively.

Warming-Up Periods. In order to investigate the effect of the in-cylinder events on the thermal condition as

(A)

(B)

Fig. 9. High-Speed Spectral Images Obtained in 2.2-2.5 μm
Band for Varied Warming-up Periods:
(A) One of the Very First Cycle; and
(B) Five Minutes Warming. Refer to LUT-1.
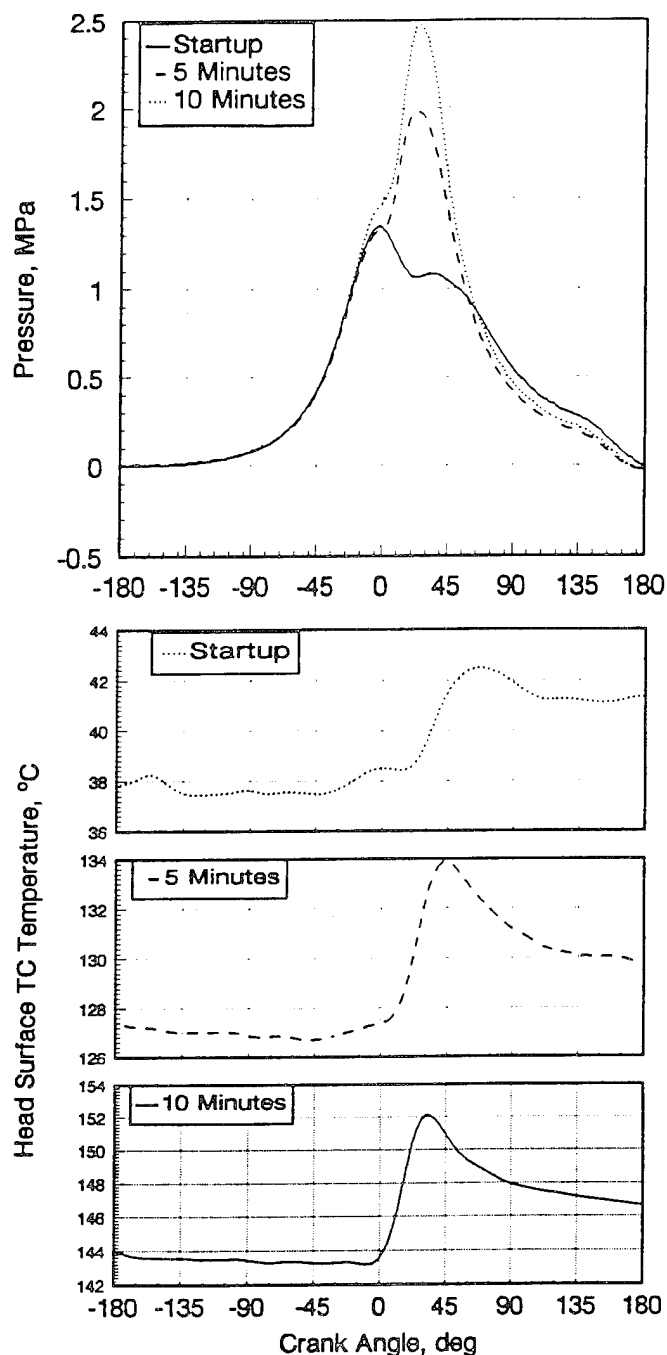
Fig. 10. (A) P-t and (B) T-t Measurements Obtained for Varied
Warming-up Periods.

obtained under exactly the same imaging condition
employed for the baseline images, except for the addition of
n-heptane to the intake charge. A small dose of n-heptane
injected into the surge tank produced continuous hard knock
for a period of about ten seconds, as indicated in p-t and T-t
measurements (Fig. 12). Figure 13 shows sets of results
obtained in both the short and long wavelength bands (2.2-
2.5 and 4.5-5.5 μm). Looking at those obtained in 4.5-5.5
μm first and referring to LUT-1, (which is expected to
indicate the species distribution more than those in short
wavelength images), the progress of the flame propagation

(A)

(B)

Fig. 11. High-Speed Spectral Images Obtained for Observing
Cyclic Variation in: (A) 2.2-2.5 μm Band; and
(B) 4.5-5.5 μm band. Refer to LUT-4.

1	-10	TDC	10	20	30	40	50	60
2	70	80	90	100	110	120	130	140
	a	b	c	d	e	f	g	h

Table-4. Look-up Table, LUT-4 for Image Reading.

Fig. 12. (A) P-t and (B) T-t Measurements Obtained under
Baseline Engine Condition with Knock.

11

(A)

(B)

Fig. 14. Radiation Intensity Distribution around the End Gas
Image 2-e of: (A) Fig. 13-(A); and (B) Fig. 13-(B).
(View angle of Corresponding Images in the
Counter-clockwise Direction by 180 degrees)

seems to be smooth until image 2-e (20 aTDC), when a low-temperature volume remains yet unburned or partially reacted (Fig. 14). (Determination of chemical species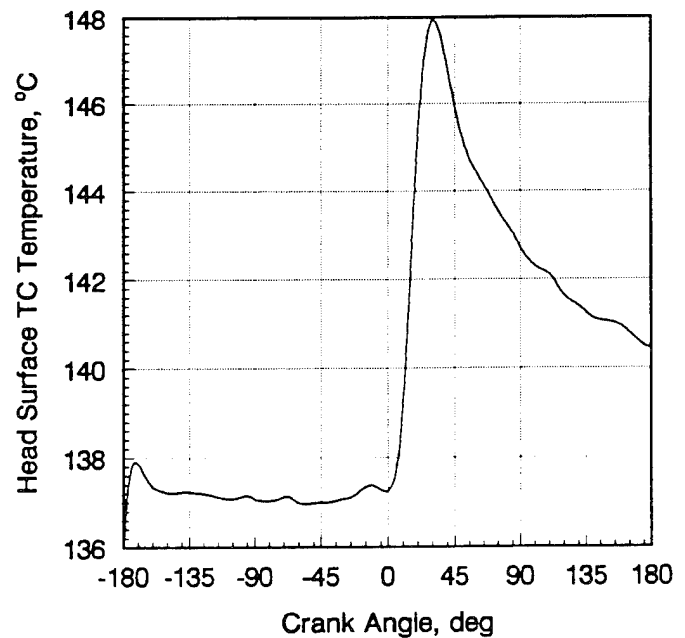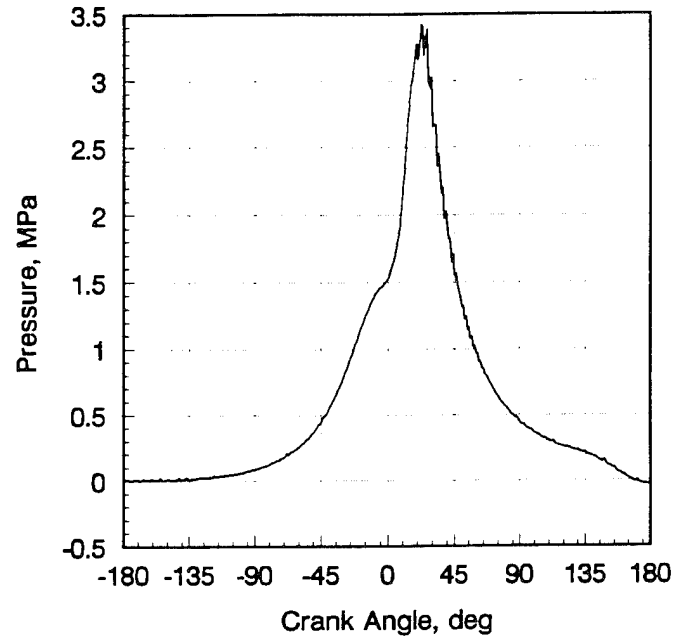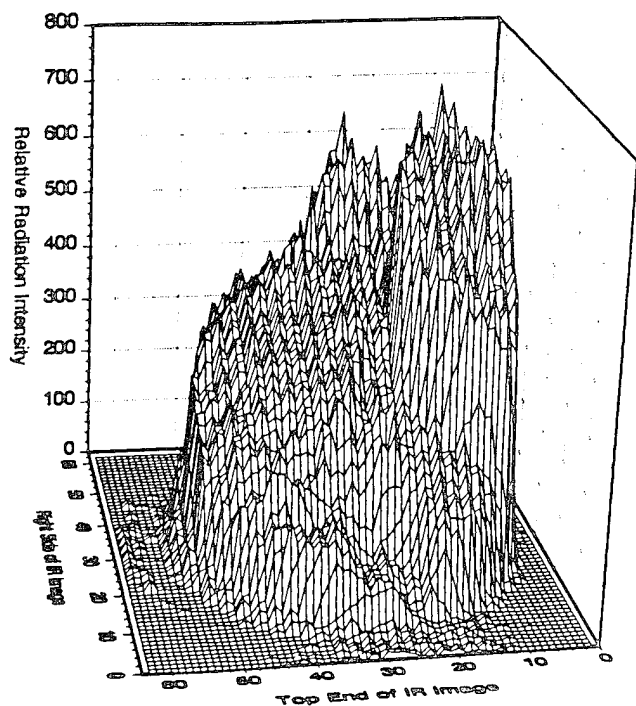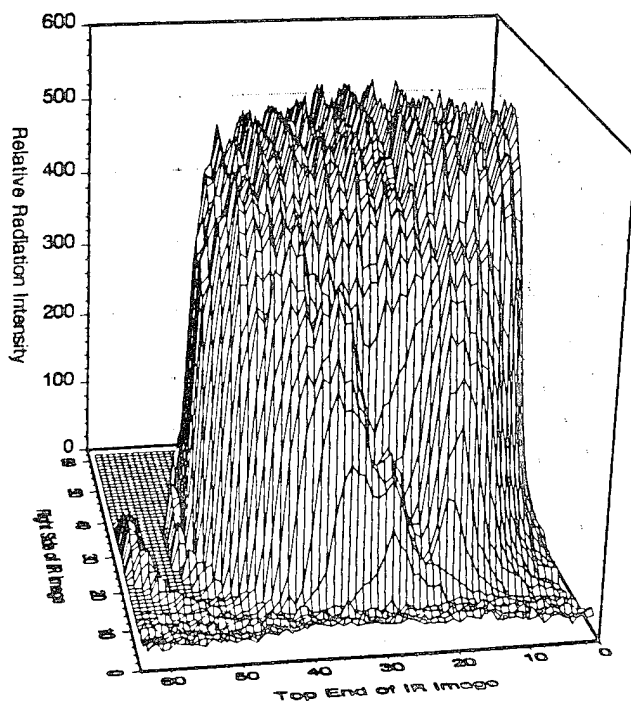 in this volume will be attempted by using our quad-spectra imaging unit.) Note that this three-dimensional presentation of digital output from the imaging results was made by rotating the view angle of corresponding images (2-e) in the counter-clockwise direction by 180 degrees.

The local volume, presumably at high density, is not seen in the following image, 2-f. Obviously, it was consumed during the period of 2.5 CA, the imaging interval. The disappearance of this volume is considered to be sudden by comparing the gradual progression of the flame front exhibited in the previous images, 2-a through 2-d and those in Fig. 5-(B). It is noted that the end gas volume may not be as dramatic as it appears to have a circular cross section in the image because what is observed by the imaging is that from a three-dimensional flow reactor. As expected, every cycle with knock occurrence had shorter reaction periods and weaker radiation from the combustion products by the time the exhaust valve opening was reached, compared with those in the baseline observation.

A mutually consistent observation may be made from those captured in 2.2-2.5 µm. Again, the flame propagation appears to be smooth up to image 2-e, where a low-temperature volume is spotted (Fig. 14-(A)). This volume is not found in the following image. The radiation from the local combustion products, upon rapid reaction in the end-gas volume, *does not* appear to be different from other regions as seen in images 2-f through 2-h. It is a quite contrast to the higher temperatures found in the early-formed combustion products, which is most likely due to after-compression.

Another finding worthy of emphasis is that the radiation from the (earlier-formed) combustion products abruptly increased when the end gas was consumed during knock. Such sudden increase of radiation most probably reflects correspondingly high temperatures, due to the higher cylinder pressure under knock conditions (as observed in p-t measurement). While the (global) cylinder pressure may explain the surge of radiation, one could also consider that the temperature was increased due to locally high pressures (spikes). Among other probable reasons for the finding is, instead of expecting increase of temperature, a sudden increase of absorption coefficient in the early-formed products, e.g. formation of soot or the like to result in strong radiation. This question may also be studied when the multispctra imaging system becomes operational.

The increased exhaust NOx emissions measured from knocking engines may help explain the cause of strong radiation from the early-formed products: our findings mentioned earlier as to temperature inferred in the end gas suggests that the formation of NOx in the end gas volume upon knock may be insignificant. It appears likely that a combustion product volume with greater NOx formation (to be consistent with its increased exhaust emission in a knock engine) is the early-formed products, instead of the end gas. However short of conclusive, this supports that the sudden and sustained strong radiation in the early-burned products (Fig. 13-(A), images 2-e through 2-h) occurs more due to similarly high temperature there.

12

As expected, the temperature of the combustion chamber surface was higher (compared with the baseline measurement (Fig. 10-(B)) when the knock was produced as indicated in T-t (Fig. 12-(B)) measured at the surface thermocouple. This may support the consideration of temperature rise but only to a limited extent because heat transfer coefficient also increases when knock occurs.

Repeated investigation revealed that under the present engine-fuel condition to produce knock, the last end gas image was captured at about the same location and piston position, i.e., around 20 aTDC.

Summary

The in-cylinder events in an SI engine were studied by obtaining high-speed spectral IR images and other engine information including p-t and T-t measurements (from a fast-response thermocouple in the cylinder head). The newly developed system employed for the imaging can be operated at a rate of over 1,800 frames/sec with exposure period as short as 20 μsec. The independently variable imaging rate and exposure period of our system complement the aperture control in the optical train in acquiring quality measurements. The spectral bands of the present imaging were 2.2-2.5 and 4.5-5.5 μm. The infrared images presented in the paper were plotted from the digital data obtained in a 12-bit dynamic resolution.

The imaging system was lined up with a single-cylinder SI engine having optical access. A special feature of this engine apparatus is the graphite rings that replaced their metallic counterpart in order to eliminate the cylinder wall oil lubrication. The encoder signals from the engine were used by the new data acquisition controller with predetermined imaging conditions, namely, the starting time, interval in terms of CA, and the number of images per cycle. (The incorporation of this controlled data acquisition mode resulted in a lower top imaging rate and an increased minimum exposure period than the case with internal clock-driven imaging.)

The sharpness of the shorter wavelength IR images appears to be better. The spectral images captured in both short- and long-wavelength bands showed, in a qualitative sense, distributions of temperature and combustion products, respectively. In the cylinder, the combustion products formed earlier attained higher temperatures due to after-compression, as expected. The spark plug seemed to be the highest temperature component during the non-combustion periods. Among unexpected findings was that the exhaust valve started to emit strong thermal radiation at the early stage of combustion. The cyclic variations in growth of flame front and length of reaction were readily observable by using the present tool. The radiation in both spectral bands became stronger as the engine warm-up period increased. The sudden reduction of radiation from the combustion products, upon the blow-down, was clearly observable.

Engine knock was investigated by running the engine with the addition of n-heptane to produce knock. We captured the spectral IR images of the end gas right before it was abruptly consumed. Under the present imaging condition, the last end gas image was seen at about the same location in the chamber and piston position. The combustion products formed in the end-gas volume, upon knock, exhibited no significantly higher temperature than other zones in the combustion chamber. As expected, the flame propagation completed earlier when knock occurred, and was accompanied by increased temperature on the combustion chamber wall. Upon onset of knock, the radiation from the early-formed combustion products suddenly increased and continued for a long duration. On the other hand, the combustion products formed from the end gas do not seem to attain higher temperature than other regions.

References

1. Jiang, H. and Rhee, K.T., "High-Speed Imaging of Bunsen Burner Combustion Products," Canadian and Western States Section, Combustion Institute Meeting, April 29-May 2, 1990, Alberta, Canada.

2. Rhee, K.T., "Spectral Infrared Imaging of Flames in Narrow Clearances," Combustion Science and Technology, 75, 4-6, p.333, 1991.

3. Jiang, H., McComiskey, T., Qian, Y., Jeong, Y.I., Rhee, K.T., and Kent, J.C., "A New High-Speed Spectral Infrared Imaging Device Applied for Flame Studies," in press, Combustion Science and Technology.

4. Kajitani, S., Sawa, N., McComiskey, and Rhee, K.T., "A Spark Ignition Engine Operated by Oxygen Enriched Air," SAE Paper-922174, 1992.

5. Jiang, H. and Rhee, K.T., "Dual-Spectra Method for Determination of Temperature and Species Concentration in Flames," Manuscript being Reviewed.

6. Zhao, H., Collings, N. and Ma, T., "The Cylinder Head Temperature Measurement by Thermal Imaging Technique," SAE Paper-912404, 1991.

High-speed dual-spectra infrared imaging

H. Jiang
Y. Qian
K. T. Rhee
Rutgers, The State University of New Jersey
Department of Mechanical and Aerospace Engineering
P.O. Box 909
Piscataway, New Jersey 08855-0909

Abstract. A new method of achieving controlled high-speed infrared imaging is presented, which has made it possible to overcome some of the limitations in current imaging technology, particularly in disposal of high-rate data flow synchronized with the event or object being investigated. This technique is employed to simultaneously capture two geometrically identical images in respective spectral bands for quantitative spectrometric data reduction. The system features 12-bit data processing capability from two pieces of 64×128 PtSi monolithic CCD FPA operated in a noninterlaced mode at pixel clock rates of up to 10 MHz by using new electronic units developed in our laboratory. The system consists of an electronic shutter unit, a programmable external trigger controller, a DRAM memory buffer per channel, a single-channel image processor, and a PC-AT loaded with our software package. Its independently adjustable framing rate and exposure period permit up to 1800 frames/s and as short as 20 μs, respectively.

Subject terms: infrared spectral; electronic maneuverability; memory subsystem; controlled imaging; dual-band spectrometry.

Optical Engineering 32(6), 1281-1289 (June 1993).

1 Introduction

Multispectra infrared (IR) imaging is desirable for achieving quantitative imaging whose application ranges from basic science research to product development as well as target identification for military purposes. Its application may become even wider when the imaging is obtained at high framing rates. Among other desirable characteristics of the system are short exposure period, digitizing the data in high dynamic resolution, acquisition of large amounts of images at once, and independent variation of such imaging parameters.[1] In spite of the promising potential and need for such a device, no commercial system has been made available to offer those features for a number of reasons, including peripheral technology limitations. Any attempt to construct such a system, therefore, has faced preceding development of custom subsystems (hereafter called units) at high costs.

Because of these difficulties, earlier applications of IR imaging were limited to either scanning using a single-cell detector[2] or adapting off-the-shelf camera heads.[3,4] Among the drawbacks of those applications are, for obvious reasons, low framing rate, long exposure period, and limited controllability of the hardware. Yet, recent IR imager development has been directed mostly to imaging in higher spatial resolution, greater charge-handling capacity, charge readout improvement, and yield increase.[5,6] Some remarkable prog-

ress has been realized in visible range imaging for capturing images at high rates,[7,8] but it has not been extended to IR range imaging, most probably because of a narrow market perceived for the new technology.

Realizing the absence of such a device that would meet our research needs for studying rapidly changing thermal processes, we decided to develop a new high-speed quantitative IR imaging system several years ago. Because the new imager development required substantial resources, the key consideration in our new system development was improving the electronic maneuverability of an existing imager, followed by high-speed data processing that eliminated the bottlenecks in the system. This approach of filling the technology gaps that we found in the current imaging method, by our new unit development, led us to construct a successful prototype system. In other words, we were led to develop an imaging system whose performance limit is solely dictated by that of the imager. This new single-band imaging system is being applied to investigate burner flames and in-cylinder processes of spark ignition and diesel engines.[1] Note that our new electronic-controlled shutter was proven successful even in our earlier application.[9,10]

2 System Description

Our new dual-spectra system for achieving quantitative imaging was developed in two steps, as schematically depicted in Figs. 1 and 2. Both configurations include the optical setup, camera electronic subsystem, image processor, PC-AT computer, and RGB monitor. At first, the camera subsystem was
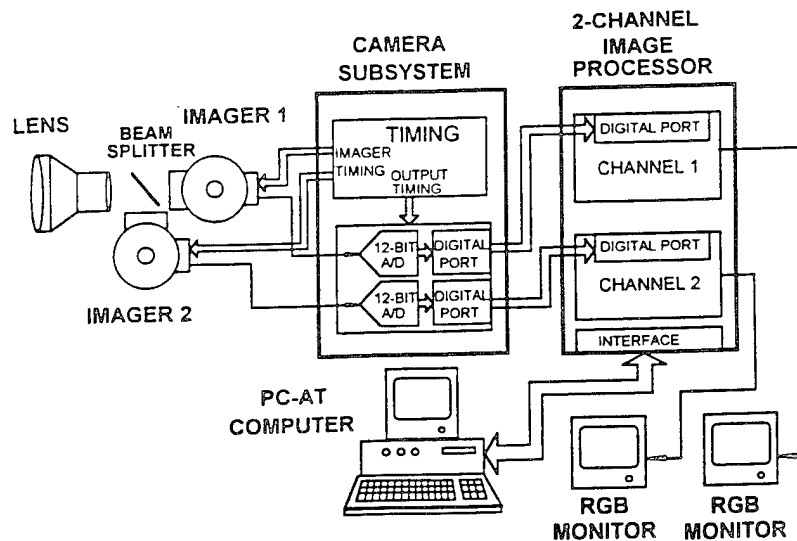
Fig. 1 Block diagram of dual-band high-speed IR imaging system without memory subsystem.
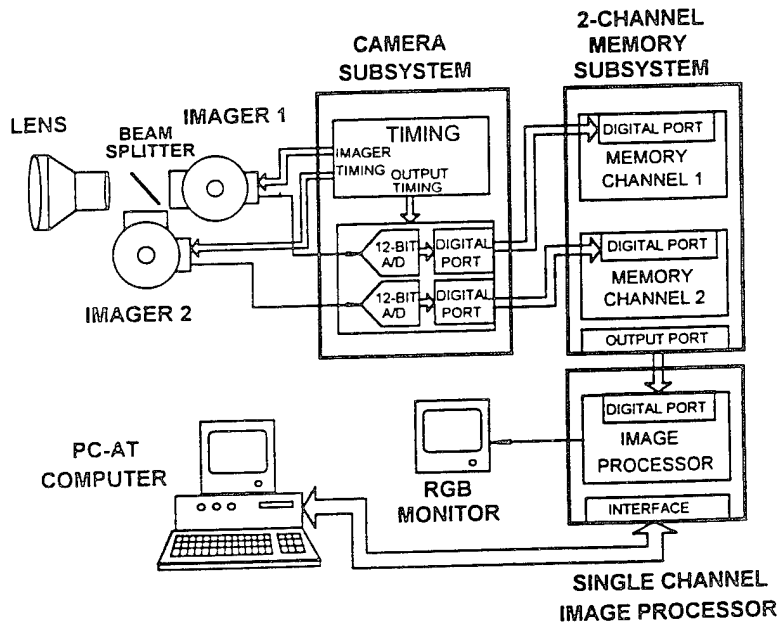
Fig. 2 Dual-band high-speed IR imaging system with memory subsystems.

the only portion of the system that was newly developed; it was connected to a factory-modified dual-channel image processor (Fig. 1). Some initial application was attempted using this device.

The first system configuration, after lengthy testing during the course of system development and calibration, was found to be inconvenient and expensive for obtaining large numbers of images at once. Furthermore, when the system was operated at 10 MHz, the image processor exhibited some missing images and other erratic performances, the reason for which is discussed later. Consequently, it was decided to develop a new memory subsystem, which was placed between the camera subsystem and the existing image processor, as shown in Fig. 2. The basic idea of the second system configuration was to capture sequential images at the highest

rate that the imager permits, to digitize them in 12 bits using our new analog-to-digital (A/D) unit, and to store the data in our memory buffer. This enabled eliminating problems associated with the speed of data flow to the image processor, the number of images, and the number of channels, which reduced the cost of the system package. This was possible because once the image acquisition is performed for each measurement, the buffered image data can be read out at lower rates using even a low-cost single-channel image processor. Considerations associated with our dual-band system development are discussed next.

2.1 Optics

The dual-band optical setup consists of an IR lens, a beam-splitter, and two band filters placed in front of respective

Fig. 3 Schematic presentation of camera timing logic.

liquid-nitrogen Dewars that house imagers. The lens assembly has four lenses made of germanium with transmission range from 2.1 to 5.5 μm. It has a diameter of 50 mm with $f/2$ and a field of view (FOV) of 4.6 deg.

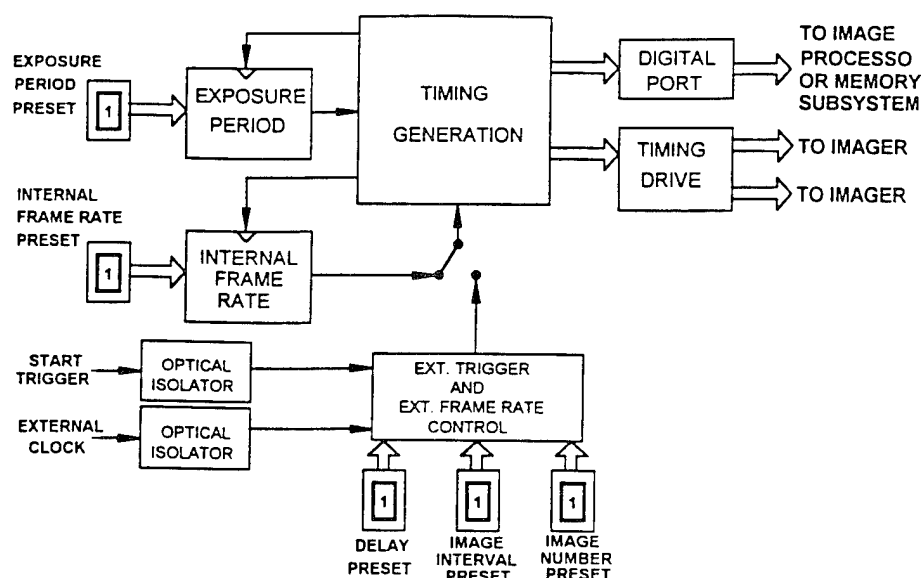### 2.2 Imager and Data Readout

The selection of the imager, which preceded the optics setup design, was made as a practical compromise to achieve the highest framing rates and at the same time obtain a reasonable spatial resolution of the image. Our system employs PtSi 64×128 monolithic CCD FPA imagers manufactured by David Sarnoff Research Center in 1985. These are interlaced devices, that is, they have a 64×64 charge register array (called the B register) with each register cell gated to two respective sensing cells from the even and odd fields. In the interlaced operation, the charge in the sensing cells is transferred twice to the B register, i.e., from even and odd fields to make an entire 64×128 image. Between the transfers, the charges from a field sent earlier to the register are read out line by line through a C register having 64 cells (and the same is repeated on the following transfer). This mode of operation, however, is not suitable for imaging rapidly changing thermal events because the separate sequential charge transfer causes the exposure periods of two field transfers to differ. On the other hand, this same imager can be operated in the noninterlaced mode, i.e., the charges from the even and odd field cells are simultaneously transferred to the corresponding cells in the B register, which is followed by the same readout process through the C register. This method was employed in our system, as is more fully discussed later.

2.3 Image Processor and Limitations

To meet the requirements of our quantitative imaging, an Imaging Technology 151 system was custom modified to have two channels. Each channel has three different units: a variable scan interfacer (VSI), a frame buffer (FB) board, and an arithmetic and logic unit (ALU) board, which performs real-time image processing. This package is connected to a PC-AT via another interface board placed in the computer.

The VSI board receives timing signals from the camera unit for orderly data acquisition via either the analog or digital port, and the image data in the board can be displayed on the RGB monitor. The image buffer banks in the VSI board are capable of storing real-time image data, but only one image at a time regardless of the input format.

When continuous image acquisition is to be achieved at high framing rates, a two-step process is taken in image data transfer, which poses a serious limitation. The first step, the VSI acquisition, transfers the image data from the input port to the VSI buffer bank; and the second step, FB acquisition, sends the image data from the VSI buffer bank to the FB buffer at the programmed location. Although VSI acquisition is controlled by the camera timing, the FB acquisition is driven by the internal timing generated within the image processor. Because both timings are asynchronous, the imaging rate cannot be achieved according to the top pixel clock rate, and it often results in erratic system performance.

2.4 Camera Head Electronics

Two functional circuits are included in our camera electronics package: timing generation and A/D conversion (Fig. 3). The timing circuitry generates timings to drive two imagers, and is also used for controlling operations in the A/D converter, image processor, and memory subsystem, which are further discussed in the next section. The A/D converter unit was newly designed to produce 10 MHz in 12 bits employing a Comlinear CLC925, which has a data rate on par with our data readout frequency from the imager.

2.5 Memory Subsystem

To overcome the various briefly mentioned limitations, it was decided to develop a memory subsystem, as indicated in Fig. 2. Because of the importance and extensive consideration given to achieving its development, a separate discussion on the subject is included later.

2.6 Alignment of Optical Components

When two geometrically identical images are obtained in

respective spectral bands, i.e., dual-spectra imaging, alignment of the optical components is a precondition to meeting the goal. Precise alignment is particularly important because the digital output from matching pixels is used directly for our spectral analysis. It turned out to be rather straightforward to achieve satisfactory alignment when we employed two image monitors, side-by-side, simultaneously displaying respective spectral images out of a well-defined blackbody object. Visual inspection of the enlarged matching images on respective screens, which were reflected on manual adjustment of the optical train, led us to achieve an alignment of the system even at the pixel scale.

3 Camera Electronics and Control

3.1 Basic Timing

A brief explanation of the CCD readout scheme of our imager is as follows: two sets of clocks are required to obtain output from the present 64×128 PtSi Schottky barrier CCD imager—the line clock, or B clock, and the pixel clock (PCLK), or C clock. During each horizontal line time, the B clock sends charges in individual lines to corresponding cells in the adjacent lines in the direction toward the C register, which has the same number of cells as in each line of the B register. This action places charges in the last line in the B register into the C register. The C clock timing pulses, which are more frequent than the B clock pulses by at least the factor of the number of pixels in each line, sequentially push the charges in the C register into the charge amplifier, which produces video output in series. This imager can be driven by either four-phase or two-phase timing. The latter has an advantage of driving faster charge transfer but with a potential disadvantage of low charge transfer efficiency. There are blanking periods between the line readout of data and the frame readout completion.

Extensive testing was performed to maximize the performance of the imager, which was originally designed to operate the C clock around 2 to 3 MHz, its extreme performance limit, however, had not been evaluated in the past. Repeated modifications were made to improve our circuits after receiving initial help from outside experts. Even driving the imager by the two-phase timing method, it became possible to achieve output that was quantitative at C clock rates of up to 6 MHz and qualitative with 10 MHz.

3.2 Frame Rate Control

Two methods of varying the framing rate of the camera were considered: changing either the PCLK rate or the vertical blanking period. From the circuit design point of view, the former is easier, but has some drawbacks. First, the variation of framing rate is determined by the increment for which the master clock rate is divided, which does not allow continuous variation of the framing rate. Second, the charge accumulation in the pixel and its transfer efficiency vary with changes of the PCLK rate. This causes inconsistent video output, even under the same length of exposure period, because the framing rates differ, which makes it difficult to perform quantitative imaging.

On the other hand, while the C clock and B clock rates are maintained the same, the vertical blanking period is simply varied to achieve change of the framing rate. This method offers consistent control of the exposure period and permits selection of any framing rate (within the upper limit), opposed to discrete and finite number of choices in framing rate that results in the former method.

3.3 Exposure Period Control

Systematic variation of the framing rate is a desirable feature of an imaging system, and versatile control of exposure period is as important a requirement. This is to attain quality imaging, e.g., to freeze a rapidly changing event and to allow a desired amount of radiation received by the imager per exposure.

Unlike optical control of the exposure period (e.g., a shutter or intensifier employed in the visible band domain), the determination of our exposure period of imaging was made by varying the charge accumulation period in the sensing area, which involves manipulation of the charge transfer pulses. The uniqueness of our system lies in the continual transfer of the charge from the sensing area to the B register, which is read out by the aforementioned CCD readout scheme. By this process of eliminating unwanted charges, the "dumping period" is stopped at the start of the exposure period, which defines a designated charge integration until this fresh charge is transferred into B register. When this new "electronic shutter," which was proven to be successful in our first system,[9] was combined with the independent framing rate control explained earlier, it was possible to achieve an exposure period of under 20 μs at a framing rate of over 1800 frames/s.

3.4 External Trigger and Controlled Imaging

When a rapidly changing event or object is investigated, in addition to controlling the start and framing rate of the imaging using the internal clock rate, it is desirable to capture images in synchronization with the event. For example, in capturing images of the in-cylinder flame propagation in an engine, because the engine angular speed varies in response to the periodic pulsed power stroke, it is often necessary to trigger the individual images not only by engine crank angle markers but also by the internal clock timing. Because the present system development was directed to immediate applications for engine study in our laboratory, further details of system operation are elaborated next to illustrate the system's flexibility for other applications.

3.4.1 Control features

Two different input signals, a start trigger and an external clock, are utilized to perform the following special measures in our imaging system: (1) control of the start of imaging, (2) imaging of individual frames triggered by predetermined intervals of the external clock, and (3) compilation of a preset number of images in each cycle. These features can be individually programmed for each experiment. Recall a similar control methodology of data acquisition employed in modern digital oscilloscopes.

3.4.2 Engine study

Consider imaging of in-cylinder processes of a reciprocating four-stroke internal combustion engine to which an encoder is connected to produce the top dead center (TDC) reference marker, when the piston locates at the top, and engine crank

angle (CA) markers, two different signals to be fed into our control circuit via respective optical isolators (Fig. 3). In the control circuits, the external trigger feature determines the delay period from the TDC reference marker to the start of imaging in each cycle. To determine the imaging interval, the acquisition of individual images is performed by skipping a preset number of CA or external clock markers. The total number of images to be obtained each cycle (at corresponding CA markers) can be determined by the preset image number feature.

3.4.3 Examples

In addition to the system's capability of continuous imaging at a preset framing rate, the new features greatly improve experiment efficiency and reduce the data processing/editing time. Examples include the following: (1) When the combustion stroke is the only period to be studied from successive cycles, the control unit can be set to capture images starting from 10 deg before TDC (bTDC) with an imaging interval of 2.5 CA to obtain 64 successive images in each cycle. (2) If cycle variation of flame propagation within the combustion chamber is to be investigated, the imaging system can be set to obtain successive in-cylinder images, starting from 5 bTDC to compile only eight images per cycle with a preset interval, e.g., 10 CAs. This allows us to compare flame growth at corresponding piston locations from 32 successive cycles.

4 Memory Subsystem

One of the main problems faced in modern high-speed, high-definition imaging is how to store the captured images as rapidly as they are read out from the imager, in an economical manner. Probably the most widely used method at present is to store the image data in the memory buffer in the imager processor. Several limitations of the image processors presently available on the market are explained next.

4.1 Limitations of Image Processor

4.1.1 Memory size and cost

The FB board may include 512×512 or 1024×1024 16-bit memory capacity, which is, in general, only sufficient for single-channel and single-frame imaging. When imaging in multiple channels is performed to obtain large numbers of images per channel, it is necessary to equip additional FB boards assigned to each channel of the imager processor, which drives the system cost very high.

4.1.2 Data transfer speed

As briefly mentioned earlier, the image data transfer from camera to VSI is driven by the camera timing, whereas the data transfer from the VSI buffer to the FB is controlled by timing generated within the image processor. In general, these two timings are asynchronous, which results in low framing rates. This problem may be compounded when a two-channel mode is employed.

4.1.3 Video channels

When multiple channel imaging is performed, each imager is most likely assigned to a corresponding image processor channel, if the imager speed is to be fully achieved. This is a costly measure, as we faced when we designed the present

two-band imaging system as well as the four-band system that is under construction.

4.1.4 Control of image acquisition

The special control features that facilitate image compilation in synchronization with the changes in event or object, as described earlier, are neither available in the existing image processor nor applicable at reasonable system modification and cost.

4.2 Development of Memory Subsystem

To overcome the limitations involved in achieving high-speed imaging, including those previously explained, it was decided to explore the possibility of developing a new high-frame-rate buffer that can readily be controlled for meeting the needs of various applications. The approach was to assign a separate memory board to each channel to store digitized images as they are captured out of the imager (Fig. 2), which were to be retrieved using a simple image processor for retrieving image data to a permanent storage, e.g., a hard disc.

Setting up an initial objective of having memory capacity of $1 M \times 12$ bit per channel, which can store 256 frames of a 64×64 image, and with an option of increasing the capacity as needed, the following steps were taken. In the beginning, we studied whether an off-the-shelf item, an inexpensive PC memory board, could be modified to meet our needs, mainly to take advantage of its low cost. After some extensive investigation, it was concluded that this approach was not feasible because of the inadequate bus architecture and low data clock rate. This led us to begin development of an entirely new memory subsystem.

4.2.1 Selection of memory chip

The very first consideration associated with the design of a chip that delivers performance of 10 MHz in 12 bits, was to determine the type of memory chip to be used in the memory buffer: DRAM, SRAM, or VRAM.

The VRAM chip, which has dual-port architecture, allows simultaneous processing of the image input and output, permitting increased data processing. Because the cost of this chip is very high, when large numbers of images are compiled at high framing rate, such real-time data processing does not offer any obvious advantage simply because the human senses cannot keep up with the speed. The SRAM is the fastest memory chip available on the market with the typical access time of 20 to 30 ns, which is much shorter than the target system required write/read cycle time of 100 ns. It can be used for direct address mapping without the need to refresh circuitry, making the circuit design relatively simple and easy. The main drawback with the chip is its cost, which is higher by 5 to 10 times than that of the DRAM chip. Another drawback, less severe than the former, is that it has a large outlet having twice as many address pins as the DRAM chip has, so that the memory subsystem becomes relatively bulky.

The DRAM chip is much slower, and its control circuit design is more difficult than the SRAM's. The typical DRAM access time is 70 to 80 ns and the read/write cycle is about 150 ns, which is longer than the requirement of 100 ns in our subsystem. The bright side of this kind of chip is that the speed limitation can be overcome by employing the memory interleaving technique. Because of fierce market competition
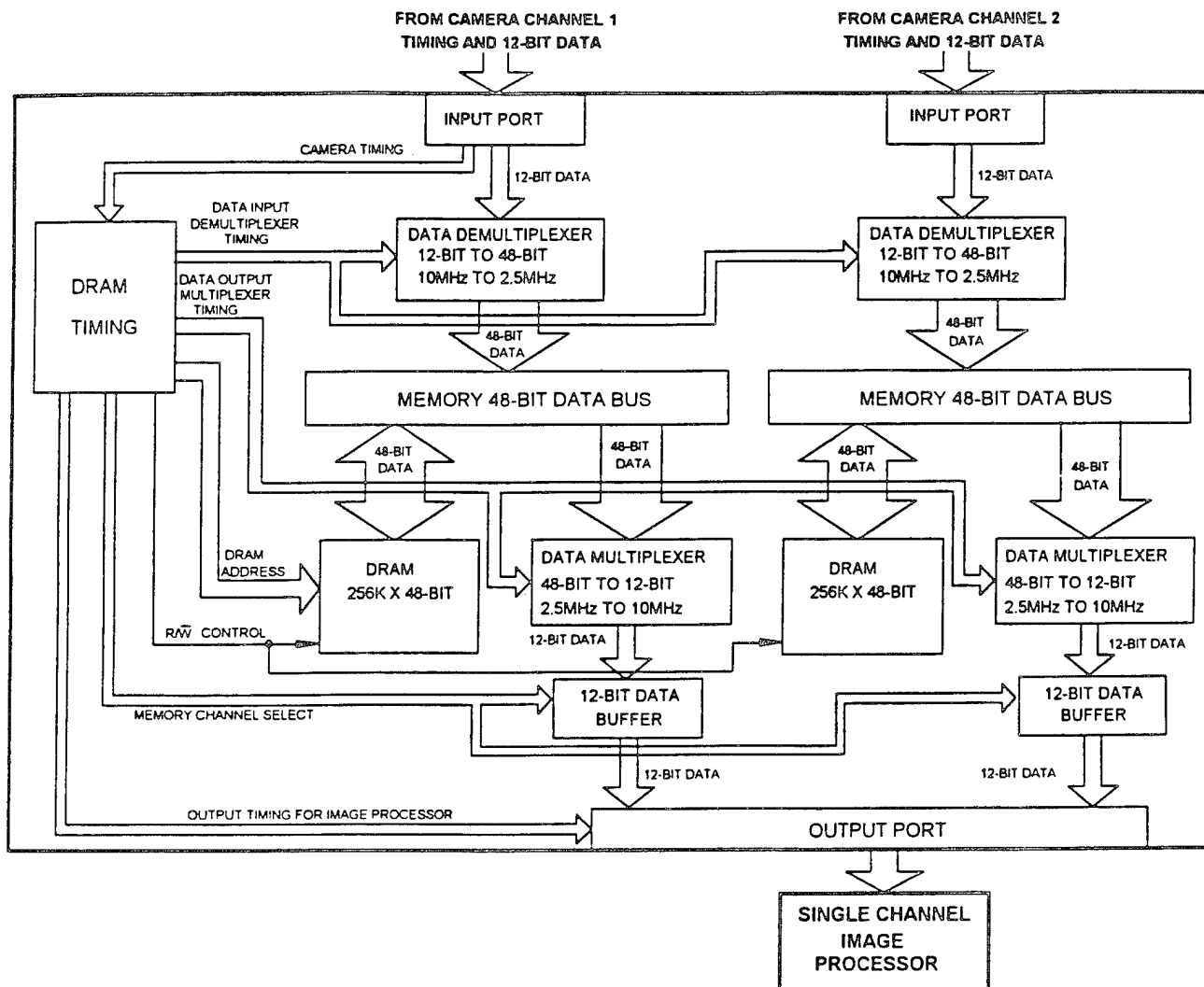
FROM CAMERA CHANNEL 1
TIMING AND 12-BIT DATA

FROM CAMERA CHANNEL 2
TIMING AND 12-BIT DATA

Fig. 4 Block diagram of memory subsystem.

and wide application, its cost is much lower than SRAM's. Also, the memory subsystem made of DRAM chips is more compact than the counterpart using SRAMs. Fortunately, there are versatile DRAM controller VLSI chips available on the market, which paved the way to easy refresh control counting, address multiplexing, and others.

4.2.2 New memory subsystem

Realizing the considerable cost advantage of using DRAM and aforementioned technical feasibility of developing a new memory subsystem, a new prototype memory subsystem was developed for completing our high-speed imaging system. Figure 4 schematically shows our new memory subsystem. By employing the memory interleaving method, image data in 12 bit issued out of our A/D circuit are delivered to four memory banks via a set of 1-to-4 demultiplexers to write them on 48-bit DRAM. In the data retrieval out of the memory, the 48-bit data are read out from DRAM by converting to 12 bit through a set of 4-to-1 multiplexers, leading them into a single channel image processor. This four-bank interleaving memory method requires a read/write cycle period

of 400 ns (4 × 100 ns), which is a long enough time to meet the system requirement.

In our memory subsystem, the image input and output operations are performed by our timing logic using a Texas Instrument DRAM controller. The timing signals required for controlling the image input, which are derived from the camera timing, include the input demultiplexing, refreshing, and address mapping. Those required for retrieval of image data from DRAM, which are generated from the timing logic, are image processor timing and DRAM readout timing. To simplify the requirements by the image processor, those timings were designed in a fixed 512 × 512 format, instead of the 64 × 64 camera format. Similar to the data input process but in reverse sequence, the DRAM readout timing signals include address mapping, refreshing, and the data output multiplexing.

5 Dual-Band Spectrometry

One of the main purposes of obtaining a greater number of spectral images is to improve accuracy in the spectral analysis of object characteristics. For example, in temperature mea-

surement, the two-color ratio method produces a lower error than the single-band pyrometry. When more than two spectral images are obtained, the accuracy is further improved by eliminating additional uncertainties in solving the Planck's equation.[11]

An improved dual spectrometry is employed in our spectrometric analysis.[12] Briefly, the pixel output V_η for a given wavenumber η, in our spectral IR imaging of gaseous mixture can be expressed by

$$V_\eta = \int_{\Delta\eta} K\varepsilon_\eta \frac{2C_1\eta^3}{\exp(C_2\eta/T) - 1} \, d\eta \ ,$$

where K represents the system response as a result of sensitivity of imager, optical characteristics of the lens, transmissivity of beamsplitter and band filter, aperture, gain/offset of amplifier, A/D converter, etc.; ε_η is the spectral emissivity of the gaseous mixture volume determined by the length of optical path, partial pressure of species, total pressure, and temperature T; and the remaining portion of the expression is Planck's equation expressed in terms of wave number and radiation constants. Note that K is determined experimentally using a blackbody source.

Calculation of ε_η (unlike in applications of solid wall temperature measurement where the graybody assumption can be employed), even if the optical length and species concentration are known, is not readily feasible because of highly nonlinear irregular behaviors of gaseous molecules. Therefore, one has to resort to experimental data to calculate ε_η even for a simple geometry gaseous mixture under a well-defined measurement condition. What is different in our improved dual-band spectrometric approach is the development of a new algorithm for implementing the single-line group model[13] by including tabulated absorption coefficients of all relevant gaseous species in our computer program. This solves two simultaneous equations, in the above equation for two wave numbers, to determine two unknown values, i.e., temperature and partial pressure of the target species, which is feasible only if the aforementioned table values are incorporated.

As long as the value of K is determined and measurement is clearly defined, including the optical length and total pressure, the solution can be found by an iterative method. The typical time required in processing equations using a pair of sets of spectral pixel output by our program loaded in a 33-MHz 486 PC was about 20 s, which amounts to over 2 h for processing a set of data from 64×64 imagers. To facilitate the process, however, we developed a new numerical mapping technique,[12] which reduced the processing time of a full image to less than 30 s.

6 Results and Discussion

Although the main objective of this paper is to report the core methodology of our new high-speed dual-band spectral IR imaging system, some imaging results are included here to illustrate its operational characteristics.

6.1 High-Speed Synchronized Imaging

The new IR imaging system was lined up with a single-cylinder spark-ignition engine, which was modified for obtaining full optical access.[14] In brief, an IR transparent win-
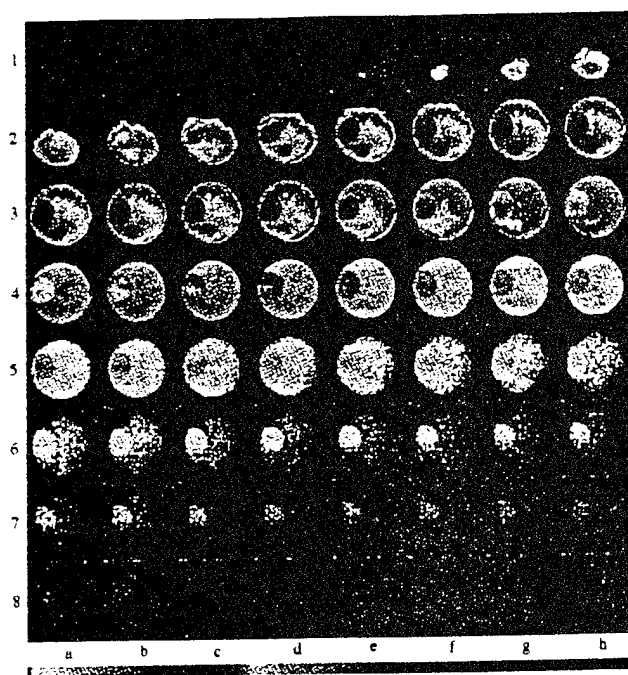

Fig. 5 High-speed spectral IR images of flame propagation in a spark-ignition engine.

dow was installed on the piston crown and the in-cylinder image was captured through the optical path made by a 45-deg mirror, a hollow piston-extension, and the IR window. This permitted viewing the flames by "looking up" the cylinder head. Figure 5 shows a set of spectral images of the engine flame by using the imaging control device with features as discussed in detail earlier. They were taken starting from 10 CA before TDC with an exposure period of 90 μs and a 2.5 CA interval between successive images from an engine speed of 500 rpm with a spark ignition time at 9 CA before TDC. The engine was fueled by natural gas to have induction of a mixture slightly leaner than the chemically correct ratio. Note that unlike in the visible range imaging where some chemical additives are introduced into the fuel to enhance the flame luminosity, thanks to the high sensitivity of our imager, the present spectral (2.2 to 2.5 μm) images were taken without such an extra measure.

6.2 Hydrogen Flame

Our aforementioned dual-band spectrometry method was applied to a hydrogen flame, which produces only water vapor as main combustion product. A simple Poiseuille burner (cross section of 0.755×2.19 cm and length of 70 cm) employed by Lewis and von Elbe[15] was fueled by hydrogen to produce a stable diffusion flame in a quiet laboratory environment. This produced a relatively stable triangular-shaped flame (as viewed from the side) attached on the burner head. Figure 6 shows two spectral images obtained from water vapor emission bands and the distributions of temperature and water vapor calculated using the spectral digital data (using the dual-band spectrometric method explained earlier) and plotted on the same geometric plane. It will be useful to compare these calculated distributions with measurements obtained by using other methods, which were not available to us.
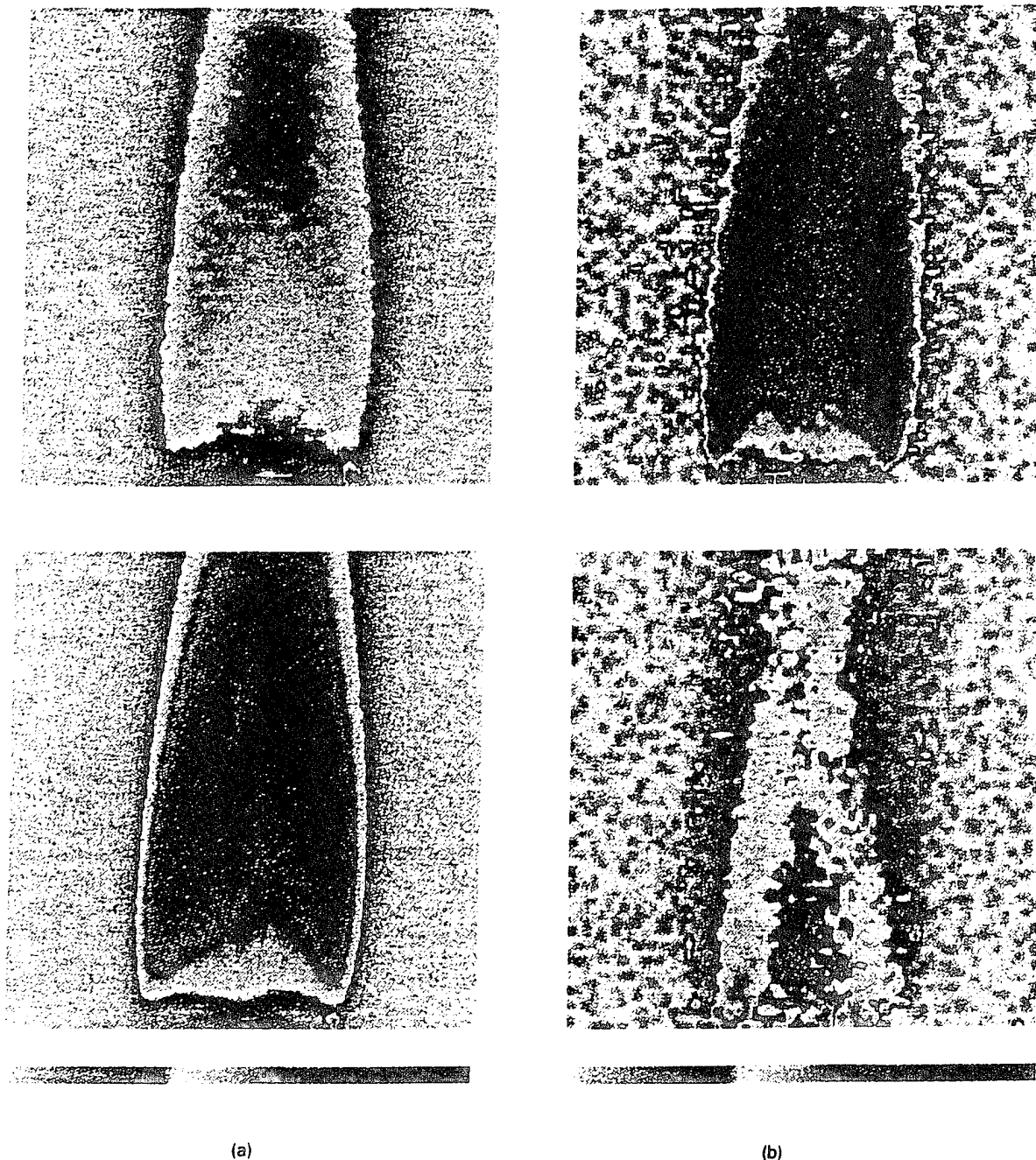
(a)

(b)

Fig. 6 (a) Spectral images of hydrogen flame produced using a Poiseuille burner in spectral bands of 2.2 to 2.5 and 4.5 to 5.5 μm, and (b) temperature and water vapor concentration calculated using results from (a) and plotted over the same plane.

7 Concluding Remarks

This paper reports the method used to develop a new dual-spectra high-speed IR imaging system. The design considerations include the limitations in the current image processor, which were overcome by developing new electronic units including a new high-frame-rate memory subsystem. This new system development has enabled the achievement of extensive control over image acquisition, namely flexible determination of the start of imaging by external triggering, individual image by external signal markers, and control of imaging interval and the number of images to be obtained each cycle.

Some typical results obtained using this high-speed, dual-band system are included to illustrate validity of our methodology in developing the new system.

References

1. G. Jiang, T. McComiskey, Y. Qian, Y. I. Jeong, K. T. Rhee, and J. C. Kent, "A new high-speed infrared imaging device applied for flame study," *Combus. Sci. Technol.*, in press.
2. H. Uchiyama, M. Nakajima, and S. Yuta, "Measurement of flame temperature distribution by IR emission computer tomography," *Appl. Opt.* 24(23) (1985).
3. X. Maldague and M. Dufour, "Dual imager and its applications to active vision robot welding, surface inspection, and two-color pyrometry," *Opt. Eng.* 28(8), 872–880 (1989).
4. S. M. Shepard, D. T. Sass, and A. Meng, "Time-resolved video thermography at above-frame-rate frequencies," in *Thermosense XIII,* G. S. Baird, Ed., *Proc. SPIE* 1467, 234–238 (1991).
5. F. D. Sheperd, "Silicide infrared image starring sensors," in *Infrared Detector and Array, Proc. SPIE* 930, 2–25 (1988).
6. W. F. Kosonocky, "Review of infrared image with Schottky-barrier detectors, Schottky-barrier imager technology," *Opt. Device Technol.* 6(2) (1991).
7. K. S. Balch, "Technique for capturing over 10,000 images/second with intensified imagers," *Proc. SPIE* 1358, 358–373 (1990).
8. G. C. Damstra and A. H. Enink, "A 10 MHz multichannel image detection and processing system," *Proc. SPIE* 1358, 644–651 (1990).
9. H. Jiang and K. T. Rhee, "High-speed imaging of bunsen burner combustion products," *Canadian and Western States Section, Combustion Institute Meeting,* April 29–May 2, Alberta, Canada (1990).
10. K. T. Rhee, "Spectral infrared imaging of flames in narrow clearances," *Combust. Sci. Technol.* 75(4–6), 333 (1991).
11. G. Barani and A. Tofani, "Comparison of some algorithms commonly used in infrared pyrometry: a computer simulation," in *Thermosensor XIII, Proc. SPIE* 1467, 458–468 (1991).
12. H. Jiang and K. T. Rhee, "Dual spectra infrared spectrometry for quantitative measurement of gaseous combustion products," manuscript being prepared.
13. C. B. Ludwig, W. Malkmus, J. E. Reardon, and J. A. L. Thomson, *Handbook of Infrared Radiation from Combustion Gases,* NASA SP-3080 (1973).
14. T. McComiskey, H. Jiang, Y. Qian, K. T. Rhee, and J. C. Kent, "High-speed spectral infrared imaging of spark ignition engine combustion," submitted to *SAE J.*
15. B. Lewis and G. von Elbe, *Combustion, Flames and Explosions of Gases,* pp. 261–291, Academic Press, Inc., New York (1961).

H. Jiang has been a graduate student in the Mechanical and Aerospace Engineering Department of Rutgers University since 1987. He obtained BS and MS degrees from the Beijing Institute of Technology. He is about to complete his PhD thesis at Rutgers under supervision of Professor Rhee. Among the main activities for his thesis is the development of a new high-speed IR imaging system in collaboration with Dr. Y. Qian.

Y. Qian joined Professor Rhee's laboratory in 1991 as a research engineer after obtaining his PhD in mechanical engineering from the Beijing Institute of Technology. His contribution in IR imaging studies at Rutgers include the development of a high-speed memory system. He is presently enrolled in the graduate program in electrical engineering at Rutgers.

K. T. Rhee has been a professor in the Mechanical and Aerospace Engineering Department of Rutgers University since 1979. Prior to coming to Rutgers, he served with the faculty at the University of Miami, Florida, for two years. He obtained a PhD degree from the University of Wisconsin-Madison with a major in engine combustion. He has been involved in the research areas of flame propagation, radiation heat transfer, species measurements, thermal loading of engine components, high-speed infrared imaging, and others.

Partial-load and Start-up Operations of Spark-ignition Engine with Oxygen Enriched Air

Shuichi Kajitani
Ibaraki University, Hitachi, Japan

E. Clasen, S. Campbell, and K.T. Rhee
Rutgers, the State University of New Jersey

Abstract

Effects of the intake air oxygen enrichment (IOE) on the combustion processes and performance of a spark ignition (SI) engine were investigated when the engine was operated under part load conditions both after and during the warm-up period.

The study was performed by comparing the direct measurements of engine performance and emission characteristics with instantaneous digital imaging of in-cylinder reaction processes obtained using our high-speed dual-spectra infrared imaging system developed at Rutgers.

The IOE under the partial load operations of an SI engine produced some comparable improvements in the thermal efficiency and mean effective pressure to those from the full load operations. Although no dramatic reduction of unburned hydrocarbon emissions with the IOE was realized in the present measurement, the insignificant increase of NOx under the same condition is noteworthy.

On the other hand, the reduction of emission and increase in performance by the IOE during the warm up period were as comparably significant as those observed in the full throttle open operations.

The high-speed in-cylinder IR imaging obtained under corresponding conditions exhibits some consistency with the above findings. The instantaneous successive digital IR images did not show an obvious difference between those obtained with and without the IOE in the partial load experiment. There was observable difference, however, in the results during the warm-up period: with the IOE, the combustion started earlier and burned stronger, which was followed by a shorter combustion period.

Introduction

A small increase of oxygen content in the intake-air alters in-cylinder reactions affecting performance and emission characteristics of the spark ignition (SI) engine, which was studied as reported last year [1]*. This initial study was an evaluation of the engine responses to intake-air oxygen enrichment (IOE). The IOE may be achieved in the real world by means of a newly developed membrane technology that can be incorporated in the intake-air system through the cleaner or other means [2]. The present study is a continuation of this earlier investigation.

In the authors' previous study, the impacts of IOE on SI engine performance and emission characteristics, were found to be significant and mostly desirable. The oxygen concentration was increased from the nominal 21% found in ambient to 22% and 23% as it was introduced into the engine. Both brake thermal efficiency (η_b) and mean effective pressure (P_{me}) increased; exhaust unburned hydrocarbon (UHC) and carbon monoxide (CO) emissions considerably decreased; exhaust gas temperature increased; the combustion duration was shortened; stability of in-cylinder flame was higher; and the flame reaction was stronger by exhibiting increased radiation intensity. In particular, since the extra oxygen by the IOE permits introduction of corresponding amounts of fuel per cycle into the engine, it was also possible to obtain some remarkable P_{me} increase under naturally aspirated operation modes. On the other hand, the exhaust nitric oxides (NOx) emission was very high with IOE, which was undesirable although expected.

The findings from this study suggest that the IOE approach may help solve some of persisting problems in modern internal combustion engines (ICE) technology. Among such problems to be eliminated are the low thermal efficiency and the large amount of UHC emission of the SI engine under partial load operations, particularly during the warm-up period. One of the recent approaches being taken for reducing such emissions is to use new absorption and desorption type post-combustion treatment devices until the exhaust catalytic converter reaches sufficiently high

---

*Numbers in the parenthesis designate references at the end of paper.

temperature [3]. In view of favorable engine responses in emissions and performances with the IOE method, as mentioned earlier, the same method was expected to help reduce the excessive UHC emission and increase the thermal efficiency during the engine warm-up period and the partial load operations. This motivated the present study. The same chain of thought may also be extended to the IOE in compression ignition (CI) engines expecting reduction of the particulate emissions.

As mentioned above, the main drawback to the approach of the IOE is the considerable increase of NOx emissions, even though other emissions decrease in some cases by an order of magnitude. This unusual pattern of low emission of other pollutants except for NOx emission from a fully warmed engine may pave the way to some economical control of emissions. Possibly a lean-burn one-way NOx catalytic converter can be used in both SI and CI engines. This consideration may be somewhat differently applied in the SI engine during the warm-up period, as explained below.

Low UHC Emissions during the Warm-up Period? Among the key considerations for performing the present study was the fact that when the throttle valve opening is small for part-load operations, including during the warm-up period, the portion of residual gas and EGR accounts as much as 40% of the entire cylinder mixture at the spark ignition. Such engine conditions result in highly oxygen-starved and inert-rich mixtures in the cylinder. These measures are taken in order to reduce NOx emission. This does not seem to necessarily be an effective emission control strategy during the warm-up period when UHC and CO emissions are unacceptably high, which the catalytic converter is unable to eliminate.

Some promising observations from the above mentioned SI engine study conducted in our laboratories suggest that the IOE method, during the warm-up period, will lead to the reduction of UHC and CO emissions as well as NOx emissions. The present study is based on the expectation that the extra oxygen enhances the oxidation of UHC and CO, otherwise in a cold cylinder, which will also increase thermal efficiency. At the same time, the inert EGR is expected to play a diluting role to slow down NOx formation and improve in-cylinder combustion by the IOE, which also accelerates heating of the catalytic converter.

This new strategy of reducing emissions and increasing thermal efficiency, η_b during the engine warm-up period was studied through the collaboration of two separate laboratories: the engine emission and performance characteristics were measured at Ibaraki University and the in-cylinder reactions were studied at Rutgers using a high-speed spectral infrared imaging system which has been developed during the last several years. Again, since the present work was performed based on the findings from the previous investigation and since it is in direct comparison to the earlier results, only minimum changes were made to the apparatus and basically the same measurement methodology was employed.

Experimental Apparatus

The engine performance and emission characteristics were measured using a single cylinder air-cooled side valve engine (Fuji Heavy Industry Co., EY44-2D). The high-speed in-cylinder IR imaging was performed at Rutgers University by using a CFR engine reciprocating system mated with a Ford 302 series cylinder head.

The main specifications of the former engine includes: bore x stroke, 90 x 68mm; stroke volume, 433cc; and compression ratio, 6.35. The corresponding dimensions in the latter engine are 101.6 x 101.6mm; 823cc; and 9.0, respectively. Both engines were sufficiently instrumented for performing characterization of IOE engine operations [1]. The only significant change made to the apparatus was that the latter engine is now outfitted with a latest-version of 302 cylinder head with in-cylinder deposit. Note that the deposit formation on different cylinder heads was made by operating a V-8 engine. They then were transferred to the single cylinder setup for IR imaging.
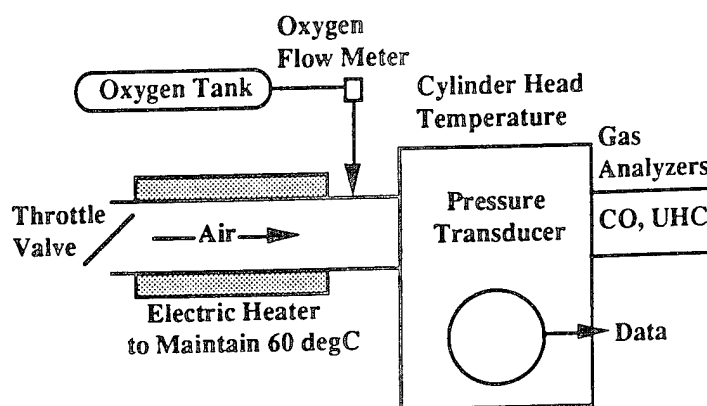

Fig. 1. Ibaraki Engine Apparatus and Data Acquisition Unit Arrangements.

The new high-speed dual-spectra infrared (IR) imaging system was developed at Rutgers and has proven itself satisfactorily operational. This was demonstrated by results reported on in-cylinder thermal events of an SI engine and other combustion devices [4, 5]. In brief, this dual-color high-speed system employs a pair of 65x128 PtSi imagers housed in respective cryogenically-cooled Dewars each having a corresponding filter. The filter band employed in the present study was 4.5-5.5 μm, which permits capturing images of water vapor and carbon dioxide. Among the features of the imaging system are variable high framing rate, as high as 1,800 frame/sec; variable electronically-controlled exposure period, as short as 30μsec; 12-bit dynamic resolution of data obtained from individual pixels; and individual images triggered by corresponding crank angle markers generated by an encoder connected to the host engine. The Ibaraki's engine apparatus and Rutgers' system are shown in self-explanatory schematic figures (Figs. 1 and 2), respectively. Further details of these experimental setups may be found elsewhere [1,4,5].
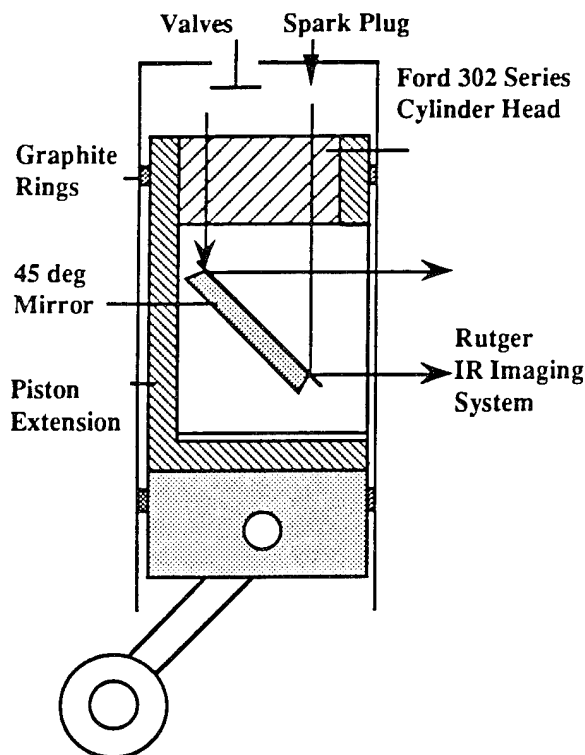
Fig. 2. Rutgers Engine Single-Cylinder Engine with Optical Access for High-Speed IR Imaging.

In the experiment of IOE, simply an extra amount of oxygen was added into the intake air and this extra oxygen was balanced by the corresponding amount of extra fuel when the engine performance and emissions were measured. It was also desirable to find the engine's response to an IOE measure without the addition of extra fuel, so in-cylinder thermal imaging was performed under these conditions. The engine operation of both engines was made under a 1/3 throttle valve opening, which resulted in an intake manifold vacuum of about 24 KPa.

Results and Discussion

The results are presented in five groups. They are measurements obtained after the engine was fully warmed up and include information characterizing the IOE induction, some of performance measurements and emission data. In addition, some results obtained during the warm-up period are presented, which are followed by inclusion of high-speed in-cylinder spectral IR images captured during and after the warm-up period. It is noted that the Ibaraki engine was operated at 1,500 rpm through the experiment.

Engine Operation Data-Warm Engine. Figure 3 shows measurements indicating the engine induction characteristics with the IOE, including (A) the air flow rate; (B) the oxygen flow rate for the IOE; (C) the fuel induction; (D) the excess oxygen factor; and (E) volumetric efficiency. The results seem to be reasonable and mutually consistent.
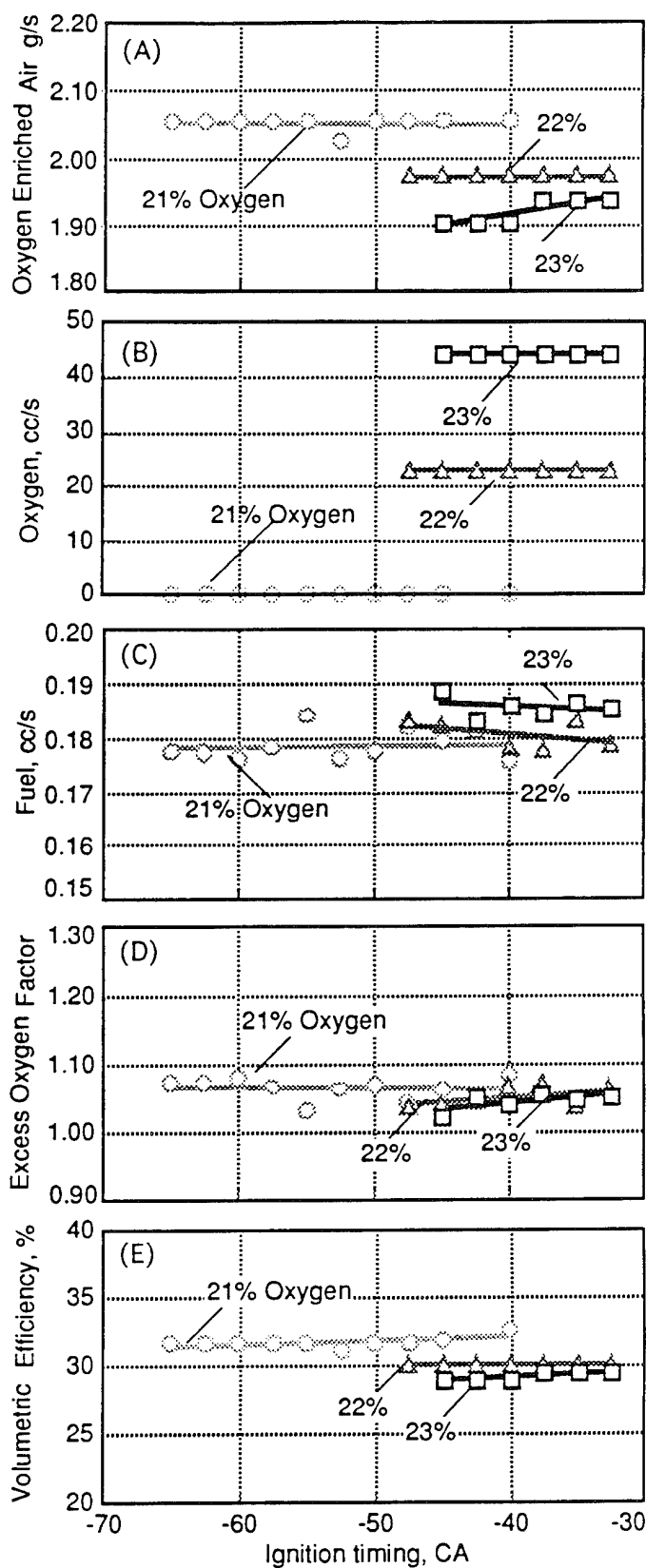

Fig. 3. Measurements Characterizing Engine Operation Conditions with the IOE.
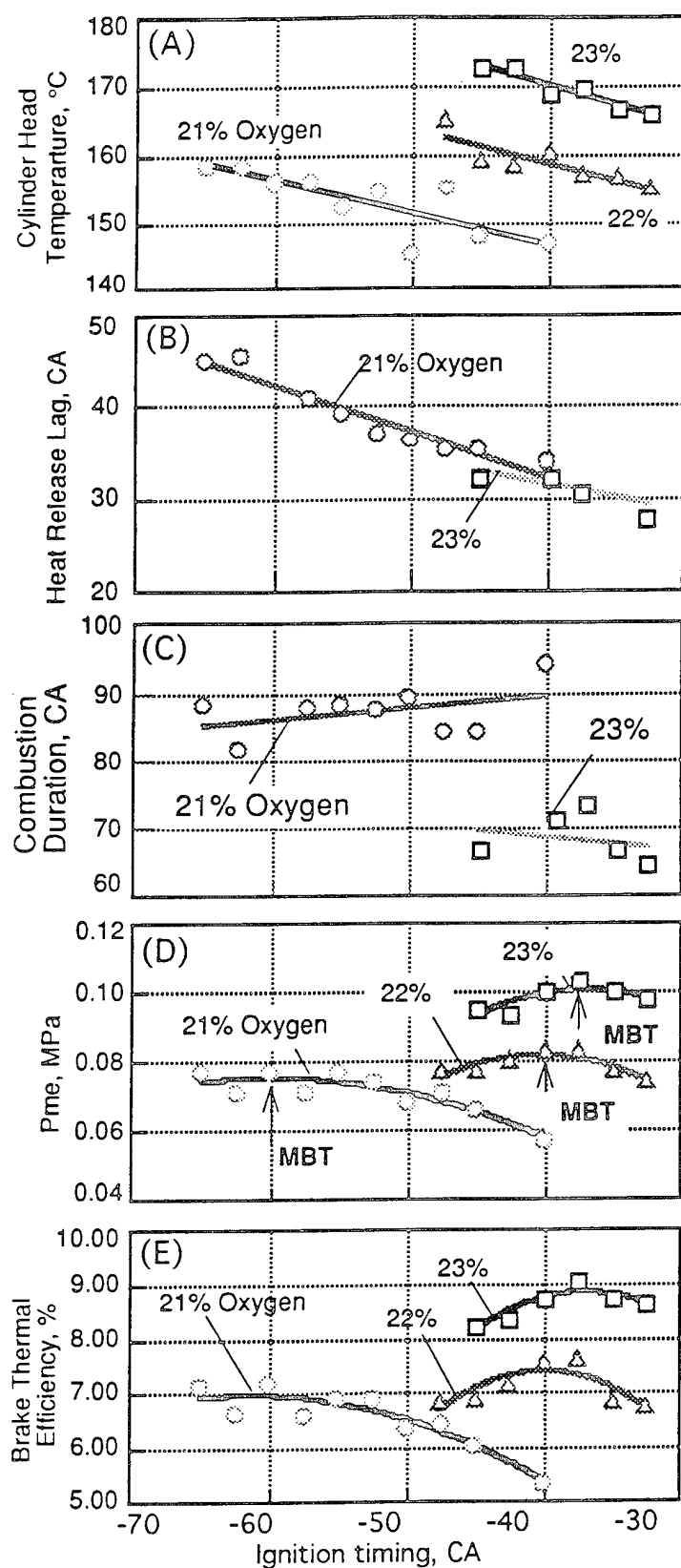
The addition of extra amounts of oxygen causes decreases in the air induction, which is considered to occur due to both replaced volume flow by the oxygen and the reduced volumetric efficiency. The deteriorated volumetric efficiency may be explained by the extra fuel added to utilize the excess oxygen in the IOE. This also caused the increased cylinder head temperature. In order to maintain controlled air induction under such complex engine conditions, a new term was defined and used in monitoring the IOE. It is the excess oxygen factor (φ) which is the ratio of the mass of oxygen in the intake mixture to the mass of oxygen in the stoichiometric mixture. Since extra amounts of fuel were introduced with the IOE, the excess amount of oxygen in the mixtures which were employed in the present performance and emission characterization had about five percent more than theoretical oxygen for that fuel.

Performance Measurements-Warm Engine. Some of the performance data obtained in the above warmed engine experiment are shown in Fig. 4: (A) cylinder head temperature; (B) the heat release lag; (C) the combustion duration; (D) the mean effective pressure (P_{me}); and (E) the brake thermal efficiency (η_b). As mentioned before, the cylinder head temperature increased with IOE, which is due to corresponding additional amounts of fuel introduced into the mixtures. In the actual engine design with the IOE, however, this temperature increase may be eliminated by increasing the coolant flow to the head, which will minimize the deterioration of the volumetric efficiency. In spite of such unfavorable thermal conditions, the IOE significantly increased the mean effective pressure (P_{me}) and the brake thermal efficiency (η_b) as shown in Figs. 4-D and -E. The increase of P_{me} may be explained by the extra amounts of energy release made possible via the additional amounts of fuel inducted (Fig. 3-C) and the increased η_b. The P_{me} could have been made even higher if the cylinder head temperature increase was eliminated to avoid the deteriorated volumetric efficiency (Fig. 3-E). Among the engine data which help explain the increased brake thermal efficiency are decreases in the heat release lag and the combustion duration which were inferred from the pressure-time measurements (Fig. 4-B and -C). That is, in the IOE engine operations the time period from the spark ignition to the rapid pressure rise, the heat release lag, was shorter, although it was relatively less obvious compared with the full-throttle IOE experiment [1]. The combustion duration defining as the period with most significant heat release became shorter by the present IOE. The short combustion duration results in greater portions of heat release while the piston is near the top-dead-center (TDC) permitting the engine combustion to take place at more of a constant-volume process.

Emissions-Warm Engine. The emission data obtained at the same time as the performance measurements include: (A) CO emission; (B) UHC emission; and (C) NOx emission (Fig. 5). Note again that the present data were under fully warmed partial throttle engine operating conditions.
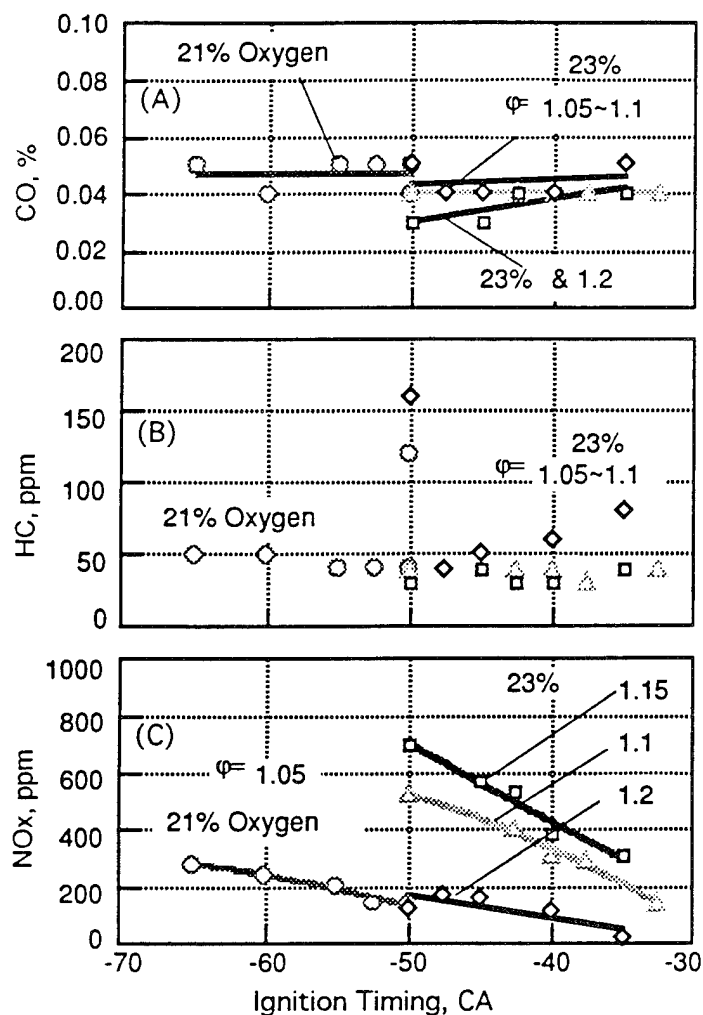

Fig. 4. Engine Performance and Condition Changes with the IOE.

Fig. 5. Exhaust Emission from a Warm SI Engine with the IOE.

Fig. 6. Pressure-time Histories during the Warm-up Period

In general, unlike the substantial reduction of UHC and CO emissions observed in the full throttle operations with the IOE [1], the reductions were relatively small in the present results. Particularly, the UHC measurements were erratic, which may partially be attributed to difficulties encountered with the measurement processes and instrumentation. However, the reduction did become somewhat significant when the excess oxygen factor (φ) was higher. The NOx emissions was high in general with IOE, but in the present experiment, it became very low as φ was increased, i.e., when more oxygen was included than the chemically correct amount. The relatively low NOx emission during partial load is noteworthy in comparison with its excessively high emission observed under wide-throttle-open combustion. This may be attributed to the strong diluting role of high content EGR during the partial load operations, even under the operation with the IOE, as discussed earlier.

Engine Measurements during the Warm-up Period. Recalling the need for some period of running time before an engine reaches the operating condition when it delivers acceptable performance, it is not difficult to expect
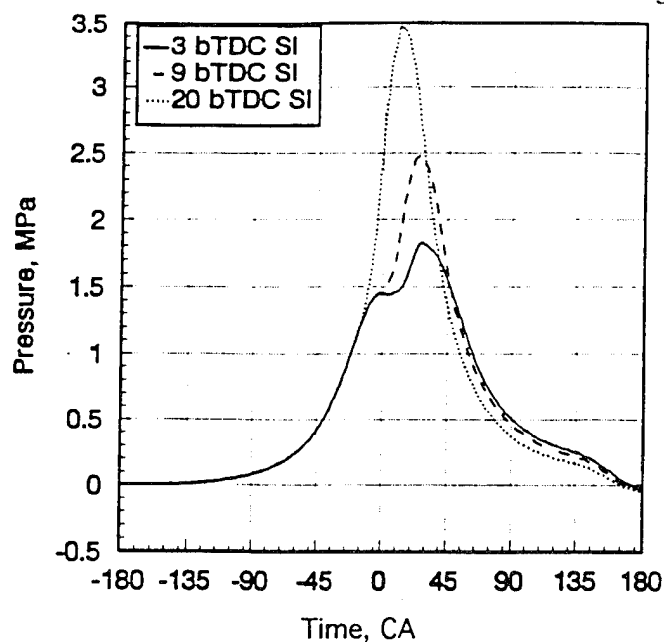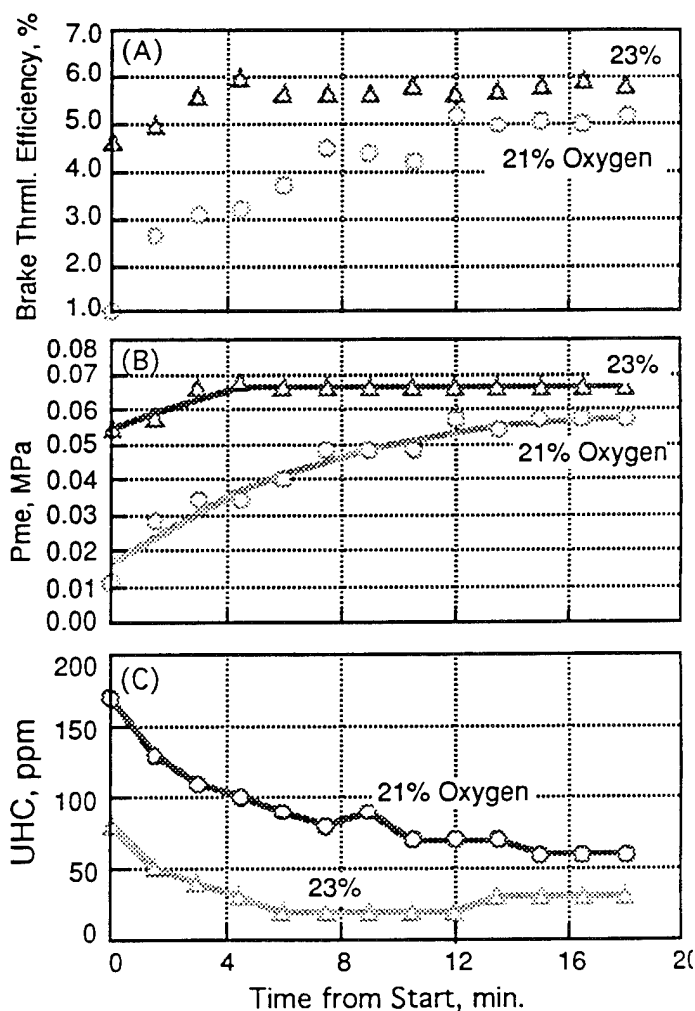

Fig. 7. Measurements during the Warm-up Period.

the in-cylinder reactions to vary with time during the warm-up period. This may be seen from the pressure-time (p-t) history obtained at different times after the start-up from the SI engine apparatus (Fig. 2) with Ford 302 cylinder head [6] (Fig. 6): (A) immediately; (B) five minutes; and (C) ten minutes. It is pointed out that the engine was fed with gaseous mixtures of fuel and air, which could have exhibited more extreme transitional p-t histories than if the fuel was in liquid phase. These p-t results obtained from an engine without the IOE obviously indicate progressive changes in various parameters associated with the fuel-air induction and engine conditions. The convergence of their change finally delivers a p-t history expected under the spark timing of the minimum spark advance for best torque (MBT). In other words, the MBT timing during this warm-up period also varies. One has no doubt that there is a need for better understanding of in-cylinder reactions during the warm-up period in order to improve the engine's performance and emission characteristics. This will be demonstrated in the additional results shown below.

In order to help understand the transient process and its response to the IOE during the warm-up period, several sets of engine measurements are shown here (Fig. 7): (A) brake thermal efficiency; (B) mean effective pressure (P_{me}); and (C) exhaust hydrocarbon emission. Despite some variations in φ encountered during this transient engine operation condition, the following results may be noted. An increase of a minute amount of oxygen concentration in the intake air of an engine during the warm-up period produces increased η_b and P_{me}, and higher cylinder head and exhaust gas temperatures. This IOE also causes the engine to rapidly reach the fully warmed condition, as much as three times sooner. These engine responses to the IOE seem to be consistent with the exhaust UHC emissions (Fig. 7-C). The results show that the emission was very high in the beginning, which decreased with time thereafter to achieve a steady state. Incidentally, UHC's steady state was reached at approximately the same time when the P_{me}'s was.

High-Speed Spectral IR Images. As indicated earlier, the in-cylinder imaging was taken from a separate engine apparatus, but the IOE and the key engine operation conditions were maintained as close as possible to those employed for obtaining the emission and performance characterization. In taking the images, the engine apparatus was installed with a cylinder head having some amount of surface deposit from a continuously used engine. As briefly mentioned earlier, the deposit formation was obtained by placing this multicylinder head on a Ford V-8 engine and running it for a period of over one hundred hours. Only one representative cylinder out of the four cylinders was examined in the experiment.

Four sets of high-speed spectral IR images obtained under respective conditions are included in Fig. 8: (A) fully warmed engine without the IOE, i.e., 21% oxygen in the air; (B) fully warmed engine with 23% oxygen in the intake air; (C) start-up engine without the IOE; and (D) start-up engine with 23% oxygen. The imaging was made using a 4.5-5.5μm band filter which permits imaging of both water vapor and carbon dioxide in the combustion products. The

key parameters employed in the imaging and the engine operation are: the start of imaging at 10° bTDC; an exposure period of 50μsec; an imaging interval of 2.5 crank angles (CA); propane/air mole ratio of 0.0433; the spark ignition at 6° bTDC; the engine speed of around 500 rpm; and the exhaust gas temperature of 325° C. It is noted that the in-cylinder imaging at the start-up was made within several cycles from the first ignition of the engine motored at around 400 rpm. Note that upon ignition the engine speed increased to attain near 500 rpm by the time of imaging.

The sequence of images in the figure goes from top to bottom and from left to right. Ignition occurred between frame 1-b and 1-c, i.e., 6° bTDC. Note that the exhaust valve opened around frame 8-c. An obvious image of combustion product was captured earlier from the warm engine than the cold engine, which was 2.5^o bTDC and TDC, respectively. Since the pseudo color presentation of these spectral IR images taken from the same engine was made in the same relative scale, the respective thermal conditions are comparably indicated by the results. It is quite clear the the combustion product radiated much stronger in the warm engine than in the start-up engine although the fuel/air ratios were maintained as close to each other as possible. This result compares well with the p-t history (Fig. 6) indicating the in-cylinder thermal events are highly transient with time. In order to further investigate the transition processes during the warm-up period, a new study is in progress.

When the engine was fully warmed up, no obvious difference was observed in IR images obtained with and without the IOE unlike engine emission and performance measurements shown earlier. A probable reason for this observation may be the fact that in the IR imaging no extra fuel was added to the mixture when the IOE was employed. The IR images captured during the warming period, however, exhibited a clear difference between them: With the IOE, the flame propagation became stronger in the early stage of combustion period and the period ended sooner, compared with those without the IOE, which is consistent with most measurements made in the other engine apparatus.

In spite of some considerable differences between the two engine apparatuses and measurement implemented at two separate laboratories, the results are in general comparable as summarized next.

Summary

In order to investigate the engine responses to the intake air oxygen enrichment under the partial throttle opening operations during and after the warm up period, engine emission and performance measurements were made. In addition, in-cylinder high-speed IR imaging was conducted under the similar engine and measurement conditions and compared with those results.

When the oxygen content of the intake air is raised from the nominal ambient 21 to 22 and 23%, SI engine in-cylinder reactions started earlier and stronger, which were followed by a shorter combustion period. This observation
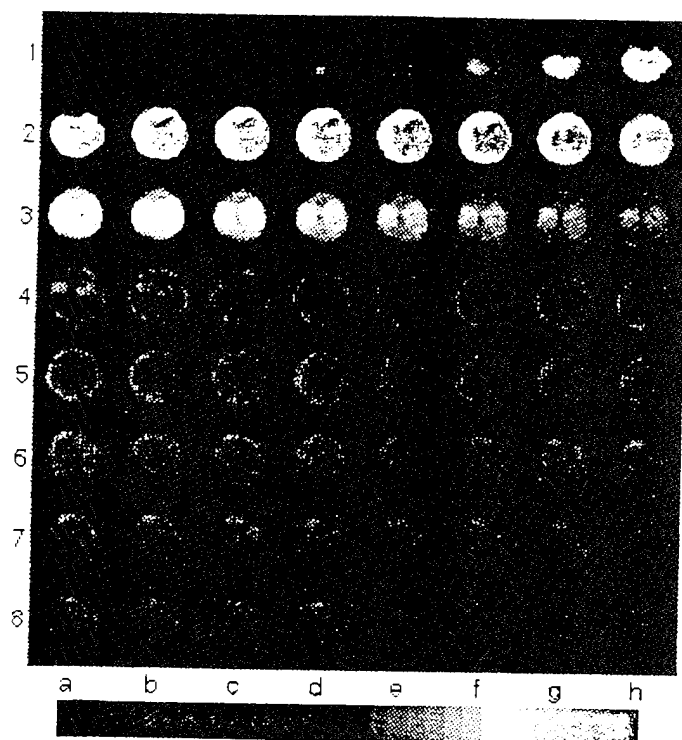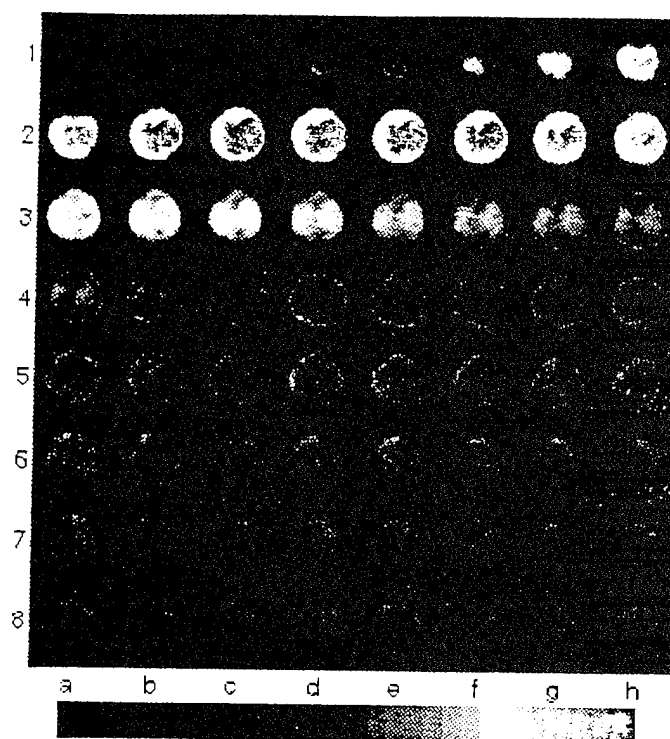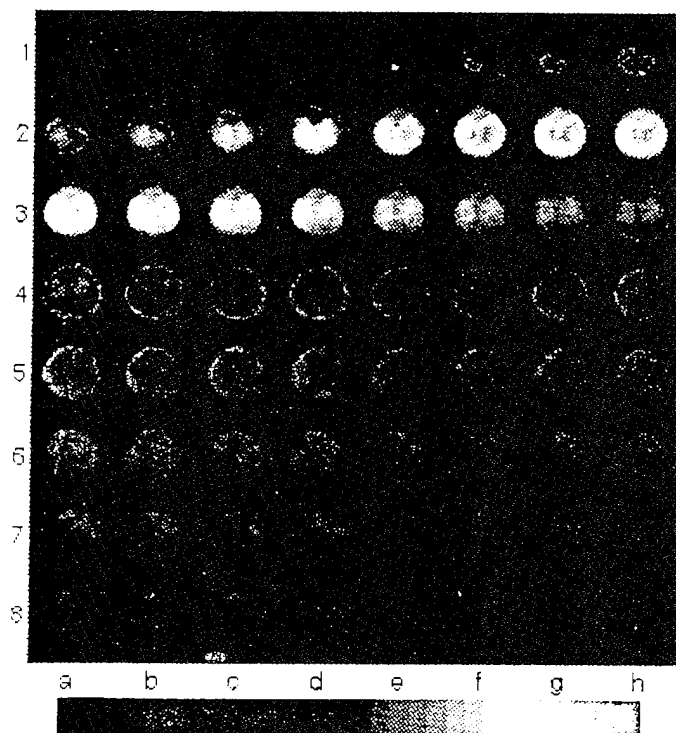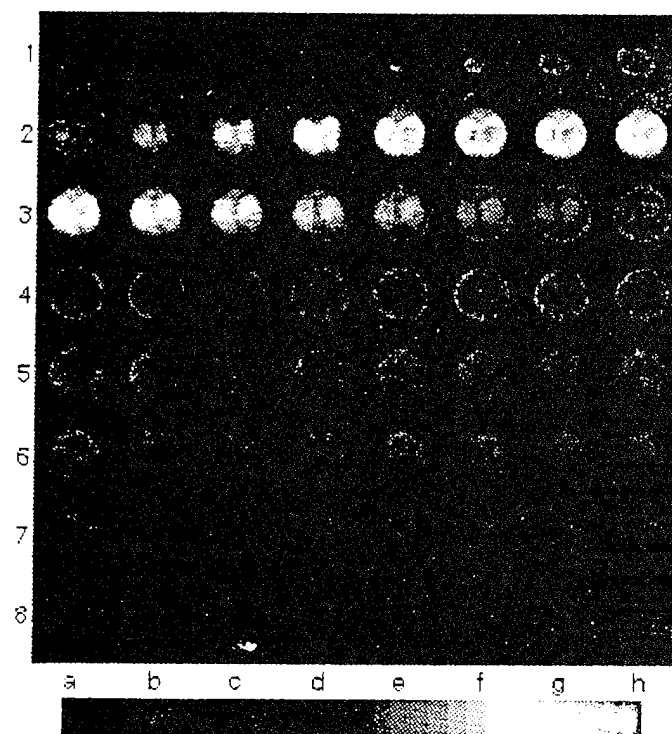
Fig. 8. High-Speed IR Images Obtained in 4.5-5.5μm Waveband from: (A) Fully Warmed
Engine without the IOE; (B) Fully Warmed Engine with the IOE of 22% Oxygen;
(C) Start-up Engine without the IOE; and (D) Start-up Engine with the IOE of 22% Oxygen.

made by both pressure-time history and the in-cylinder high-speed IR imaging is consistent with the emission and performance measurements. When the engine was operated at *partial* load conditions with the IOE:

    (1) the UHC and CO emissions decreased (this was significant during the warming period, although no such dramatic results were found in the partially loaded fully warmed engine;

    (2) the NOx emissions were not very high as in the full throttle operation, which became lower with the excess oxygen factor;

    (3) the brake thermal efficiency and mean effective pressure were considerably improved;

    (4) the engine warmed up much sooner; and

    (5) both the UHC emission concentration and P_{me} reached a steady state at about the same time.

In view of the shorter warm up period producing smaller amounts of emissions with the IOE, it is warranted to study the engine responses to a similar measure in a low temperature environment.

Acknowledgement

References

1. Kajitani, S., Sawa, N., McComiskey, T. and Rhee, K.T., "A Spark Ignition Engine Operated by Oxygen Enriched Air," SAE Paper-922174, 1992.

2. Willument, H.P. and Bauer, M.,"Emission and Performance of an SI Engine Inducting Oxygen-Enriched Combustion," MTZ Mptrtechischrift, 1989, 49, pp 149-152.

3. Hochmuth, J.K., Burk, P., Tolentino, C., and Mignano, J., "Hydrocarbon Traps for Controlling Cold-Start Emissions," SAE Paper-930739, 1993.

4. McComiskey, T., Jiang, H., Qian, Y., Rhee, K.T., and Kent, J.C., "High-Speed Spectral IR Imaging of Spark Ignition Engine Combustion," SAE Paper-930865, 1993.

5. Jiang, H., McComiskey, T., Qian, Y., Jeong, Y.I., Rhee, K.T., and J.C. Kent, "A New High-Speed Spectral Infrared Imaging Device Applied for Imaging Gaseous Mixtures from Combustion Devices," Combustion Science and Technology. 90, 5-6, p. 341, 1993.

6. McComiskey, T., "An Experimental Investigation of a Spark Ignition Engine Using High Speed Spectral Infrared Digital Imaging," M.S. Thesis, Rutgers University, January 1993.

Investigation of a Direct Injection Diesel Engine by High-Speed Spectral IR Imaging and KIVA-II

Y. I. Jeong
Korea Institute of Machinery & Metals
Daejeon, Korea

Y. Qian, S. Campbell and K.T. Rhee
Department of Mechanical and Aerospace Engineering
Rutgers, The State University of New Jersey

Abstract

In-cylinder process of a direct injection (DI) compression ignition (CI) engine was studied by using the Rutgers high-speed spectral infrared (IR) imaging system and the KIVA-II computer code. Comparison of the engine measurements with the computational prediction was attempted.

In order to perform the instantaneous IR imaging, a Cummins 903 engine cylinder head was modified by installing an optical access in place of one of the intake valves, which required designing a new rocker-arm mechanism. The measurements obtained using the high-speed dual spectra IR imaging system were processed by the conventional two-color method which employed soot as the radiating target. The KIVA-II program was coded in order to match engine and operation conditions to those employed in the present measurements for achieving mutual consistency of the analysis.

In the study, the thermochemical progress over a spray plume was measured by simultaneously obtaining IR digital images in two spectral bands at successive instants of time during the reaction period, which generated some new findings. In general the thermal image appeared strong after the premixed combustion stage. The results processed by the two-color method indicated that there were low temperature zones near the spray axis. This phenomena was explained to take place due to either the spray formation process involving the hollow spray injected into a narrow-height combustion volume or the unstable high-speed flows compounded by the latent heat of evaporation. The soot concentration distributions inferred from KL values were compared with the temperature distributions obtained from the spectral digital images. High soot concentration zones indicated by KL were found between the low temperature and high temperature zones. This is interpreted that zones at low temperatures were not expected to produce large amounts of soot because the reactions there were expected to be slow while those at high temperatures consumed the soot at high rates. Under the engine and operating conditions investigated in this study, the computational results failed to predict the measurement results.

Introduction

Among the improvements being implemented in modern Diesel engines are increasing the thermal efficiency and at the same time reducing the emissions of both NOx and particulates. Because of the mutual exclusivity involved in achieving these goals for the existing Diesel systems, e.g. a design change for reducing the NOx emission generally results in an increase of particulate emission and vice versa, one may suggest that some radical changes will have to be made in the engine or fuel for achieving advancement of the Diesel engine technology. New measures presently studied for achieving the objectives are reflected in some recent literatures: injection rate shaping [1]*; ultra high fuel injection pressure [2]; sensor-electronic controlled engine [3]; low-heat rejection engine [4]; unconventional fuels and additives [5]; and even intake-air oxygen enrichment [6]. The use of exhaust gas treatment devices [7] is also a part of those changes being investigated for solving the problems.

A similarly important strategy being taken for improving modern Diesel engines is to achieve a better understanding of the events taking place in the combustion chamber, particularly when such new unconventional changes are made on the engines. While the computational modeling approach is possibly an economical way of helping design a desirable Diesel engine, the modeling method itself implies imperfection and indicates the need for experimental verification in order to get more out of it. Realizing the limitations in producing useful in-cylinder measurements by means of the existing diagnostic tools, one may also suggest that some radically new methods will have to be employed for obtaining better pieces of in-cylinder information. There have been such methods recently introduced for engine studies, and one of them is discussed in this paper.

The research approach taken for this paper was to employ a newly developed diagnostic tool and to compare the results obtained using this device with the predictions made by the KIVA II computer code.

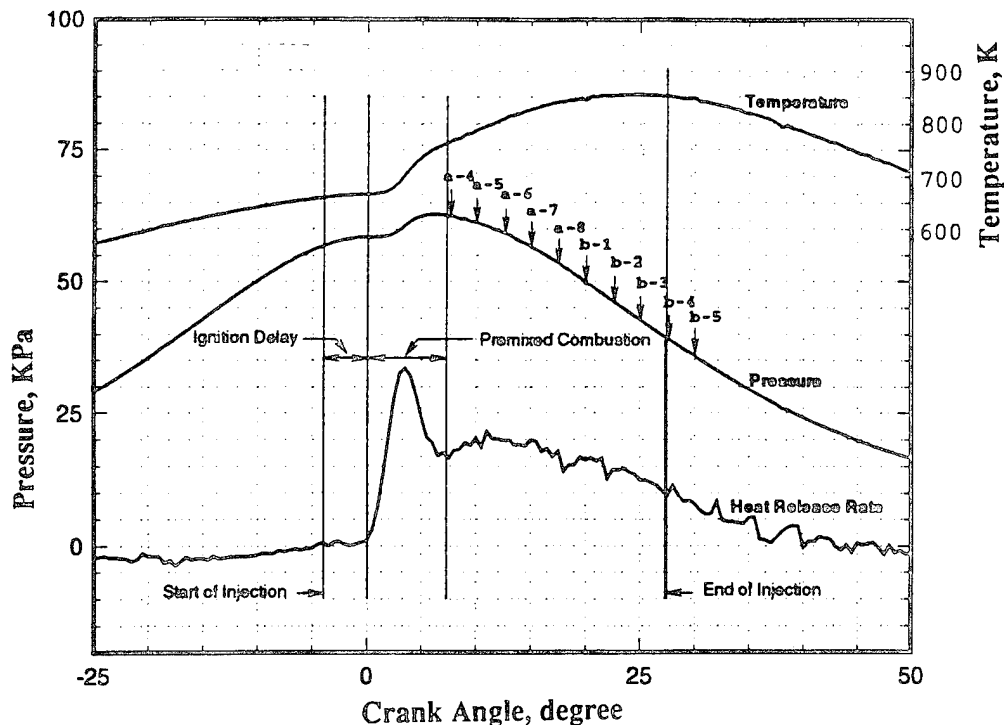*Numbers in parentheses designate references at end of paper.

Fig. 1. Pressure-Time (p-t) Measured of Single-Cylinder Engine and Markers to Show Corresponding Imaging Times.

Experimental

In this section, two main topics are explained: the high-speed two-color infrared (IR) digital imaging system and the engine constructed to accommodate a new diagnostic tool. A single cylinder direct injection (DI) compression ignition (CI) engine was newly designed and fabricated for facilitating investigation of in-cylinder events and some of its new design considerations are explained. Since the IR imaging system and its use on a spark ignition (SI) engine has been reported elsewhere [8-12], a brief discussion is made on the system application in a DI CI engine here.

Engine Apparatus and Operating Conditions. After searching for a CI engine apparatus which permits easy access to the combustion chamber and also maintains engine characteristics representing a large population of DI CI engines, it was decided to newly design and fabricate a system in our laboratory, under a sponsorship of the U.S. Department of Defense University Research Initiative. Among the key considerations taken for this goal was to employ the existing engine components as much as possible (that also reduced the cost of fabrication and maintenance) and to modify the engine cylinder head to facilitate the use of either intrusive or nonintrusive engine diagnostic tools.

Upon investigating what was available for the work and evaluating the basic layout of the engine, it was decided to use components of the Cummins 903 engine and the complete engine design was carried out in collaboration with Power Energy International and BKM, Inc. In taking such measures into consideration so as to preserve the representative engine characteristics, a section of the

multicylinder 903 engine head was modified. The modifications include: conversion of one of the intake valves to the optical access; a new rocker-arm mechanism; a measure to use either a Cummins unit injector or a BKM's electronic controlled injector; and separate control of both coolant and oil flows in the cylinder head and the block, respectively; reserving a provisional large amount of space in the crankcase for facilitating installation of a linkage system that retains thermocouple wires from the piston-crown to the data system outside the engine crankcase. The intake air was supercharged, which partially compensates the eliminated intake valve.

In this engine, the start of fuel injection varied with load but the end of fuel injection stayed about the same, which was typically around 27 crank angle (CA) after the top-dead-center (aTDC). These were reflected on the subsequent combustion processes. For example, this can be seen from the two engine operating conditions employed for in-cylinder measurements as summarized in Table-I and Fig. 1. Some more details of the engine are: borexstroke, 139x117mm; connecting rod length, 201mm; compression ratio, 13.5:1; injector hole diameter, 0.19mm; and number of holes, 7.

The engine was sufficiently instrumented in order to monitor engine operation parameters including those listed in the above mentioned table. The pressure-time (Fig. 1) history obtained in Load-1 was used to calculate the heat release rate (HRR) and accumulated heat release (AHR). In the same figure, a typical strain gage output is shown, indicating the start of injection by the sharp deflection point near 4 CA bTDC. Note that the strain gages were mounted on the rocker-arm and push-rod for this observation.
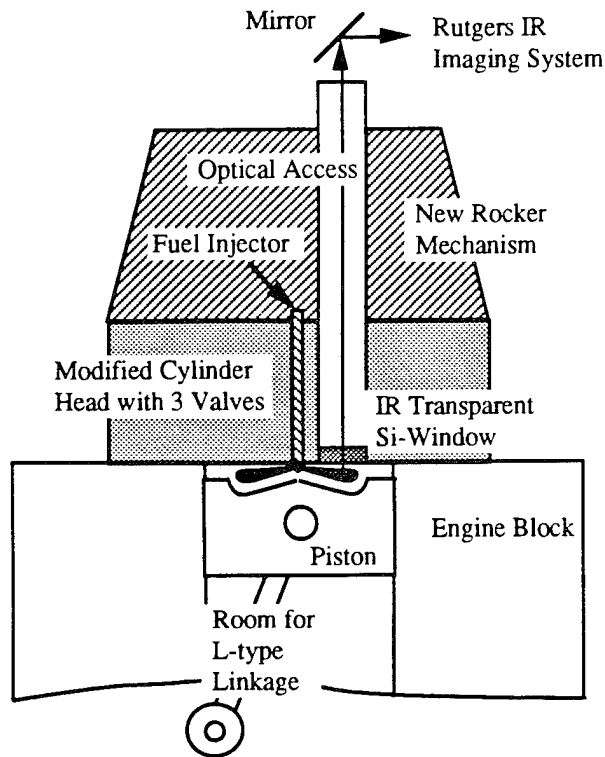
2

Fig. 2. Schematic Presentation of the Single Cylinder
Engine with Optical Access Lined up with the
Rutgers High-Speed Imaging System.

Fig. 3. Optical Window Installation using an O-ring.

A schematic presentation of the cylinder head with optical access is shown in Fig. 2. The optical access was made barely big enough to cover the projected view of a spray plume produced by the fuel injector seven-hole (0.19mm diameter) tip having flow rate of 70.3 Kg/min. This assumes all spray plumes to be identical. Note again that one section of a 903 multicylinder head was cut out and fitted to the new single-cylinder block/reciprocating unit, which was followed by installation of the optical access and other modifications such as a new rocker-arm unit. The engine construction was done in such a manner that it can be mated with an electronic controlled fuel injector in place of the mechanical PT-type injector which was mainly used for the present work. The unit, therefore, was a single-cylinder 903 engine. The engine was operable at speeds as high as over 2,000 rpm.

Table-I. Engine Fuel Injection and Combustion.

Engine Variables	Load-1	Load-2
Injection Start (bTDC)	4	11
Injection End (aTDC)	27	27
Injection Period (CA)	31	38
Combustion Start (bTDC)	0	7
Premix Comb. End (aTDC)	7	3
Ignition Delay (CA)	4	4

One of the new design features of the present optical access was to use an o-ring as shown in Fig. 3. This method was proven to be highly satisfactory in eliminating some serious problems encountered by others. Because of the need for frequent cleaning of the soot deposit on the window, its quick removal-cleaning-installation was a key consideration. This was achievable in the present design providing excellent sealing by this ring even under a preload of slightly more than hand-tightening on the retaining sleeve. At the same time, it facilitates completing the entire cleaning process for fresh in-cylinder imaging typically within three minutes. Note that the engine warming-up was done by installing a dummy steel plug in place of the silicon window. The new o-ring also permitted the direct contact between the silicon IR window and the cylinder head near the combustion wall without introducing any soft material for maintaining seal. The direct contact was an essential measure to increase cooling of the window in order to minimize its absorption and emission of radiation [11]. Any extra material introduced between the contacting surfaces, which is in general required for maintaining seal (if an o-ring were not used), would have considerably reduce the cooling effect of the window.

Mentioning another successful measure introduced in this experiment, an annealed aluminum ring was introduced in the beginning at the upper end of the window in order to eliminate any excessive stress spot on the Si window. The aluminum ring was found to cause serious damages on the silicon window, however. This was due to its reduced thickness by the repeated compression of the ring by the window exposed to cyclic combustion pressure, which produced a new clearance for the window to (vertically) vibrate between the metallic holders. In order to rectify this problem, after the metallic components housing the window were precision finished, particularly at both the upper and lower end surfaces touching the window, the original aluminum ring was replaced by a thin paper-gasket ring, followed by a preload equivalent to a bit more than hand-tightening: No more damage on the window occurred.

It may be worthy to mention that the soot deposit layer over the IR window is a less severe problem compared with that in visible-ray imaging because the layer is relatively transparent in the IR regime.

3

High-Speed Two-Color IR Imaging System.

When one investigates thermochemical molecular characteristics, such as distributions of temperature, reaction fronts and species population, the signatures exhibited by species in (spectral) infrared radiation images are more indicative than those obtained by the (photographic) visible-ray method. Furthermore, when such signatures are captured in high dynamic-resolution digital numbers over time and space, some useful pieces of new information can be found about the thermal reactions in the cylinder otherwise difficult to achieve. Realizing the great potential of infrared imaging as a (engine) research diagnostic tool, it was decided to undertake development of such a system by taking advantage of the continuing advancements in the areas of electro-optical and imaging/computer technology.

This IR system development at Rutgers has been a progressive course of work. The first generation of the research tool was to capture successive flame images at high rates using a single camera head [8,9]. The next system was to employ two camera heads in order to capture two geometrically (pixel-to-pixel) identical IR images in respective spectral bands, a two-color system [10,11], which permitted determination of temperature distributions in flames [12]. Its prototype electronic systems were all fabricated via hand-wiring directly using many transistor-transistor-logic (TTL) components. Among the main functions of the camera circuits was to generate the timing signals required to readout the charge-coupled-device (CCD) output. While the next generation four-color system was concurrently developed in our laboratory [13], this two-color system was redesigned (using Protel and Orcad design systems) and constructed in printed boards, which included several programmable logic gate arrays (using Max-Plus, Altera Corp.) that replaced most TTL components to produce quantitative IR images having minimum noise. The results reported in this paper were obtained using this improved IR imaging system.

The IR system is equipped with two units of 64x128 PtSi Schottky-barrier detector imager housed in respective (liquid-nitrogen-cooled) cryogenic Dewars. The imaging rate is changeable to obtain over 1,800 frames/sec and the exposure period is adjusted at the same time to have as short as 30μsec. The imaging system was integrated in a new package of electronic circuits to independently vary the start of imaging, the interval of imaging individually triggered by the corresponding engine CA markers, and the number of images to be captured per cycle of the engine.

Although the imaging can be made through various IR bands, the present imaging was performed using filter bands of 2.2-2.5μm and 4.5-5.0μm. They were chosen in the beginning to capture emission from the water vapor of the combustion products, but the latter band has a strong infringement by emission of carbon dioxide. During some portion of the combustion period of the in-cylinder combustion, the strong radiation from soot seems to dominate over the radiation from the gaseous species. In spite of a small amount of radiation passing through such narrow band filters, unlike in most high-speed visible ray imaging, because of the sufficiently high sensitivity of the present cryogenically cooled PtSi imagers, no separate (IR) light source was needed.

Computational

KIVA II Code. Expecting a meaningful comparison of predictions made by the KIVA II computer program of Diesel engine combustion with present measurements, this three-dimensional finite difference method program was adjusted by including corresponding engine data as close as possible to those in the experiment. Some progressive steps were taken for this work in order to eliminate or minimize probable misuse of the code by consulting with KIVA-II user group members and by conducting a parametric analysis of the combustion processes. The values introduced for the key code parameters are listed in Table-II. Two different grids were employed in the study: case-(1) nx=26, ny=20 and nz=18; and case-(2) nx=14, ny=8 and nz=18. The typical CPU time in the Pittsburgh Super Computing Facility required per computation for the former and latter grids were 35.5 and 2.4 hours, respectively. Because of the limited amount of CPU time available for the present work, i.e., total about 250hrs at the Computing Facility, only a few computations were performed using the former grid and the main portion of parametric study was performed by using the latter.

Table-II. Computational Parameters

DTI, initial time step	2.0×10^{-5}
RPM, engine speed	500
STROKE	11.66
CONROD	20.66
THSECT, azimuthal dim. of mesh	51.4286
SWIPRO, initial swirl	3.11
TSPMASS, mass injected	0.0390
CALINJ, injection time	-11.0
CADINJ, injection duration	38.0
TILTXY, rotation of injector	25.714
TILTXZ, injector incline	84.0
DCONE, injector thickness	5.0
ANOZ, injector hole area	2.859×10^{-4}
TKESW, turbulence on	1.0
SGSL, k-ε model	0.0

Two-Color Method

When the spectral measurements obtained in the experiment were processed by using the conventional two-color method, some unexpected results were obtained. In order to identify these problems encountered in applying the technique for the present engine studies, a brief discussion is made on the method. The relatively continuous and strong IR radiation emission (over the wavelength) by soot in the combustion products often amounts to several times or more the band emission by gaseous species. When this happens, the former radiation shields the latter making it difficult to measure the spectral characteristics of gaseous products. Because of such a difficulty, the spectrometric analysis of spray combustion such as in a Diesel engine was attempted by measuring the radiation from soot. On the other hand, when the measurements of radiation supposedly mainly from
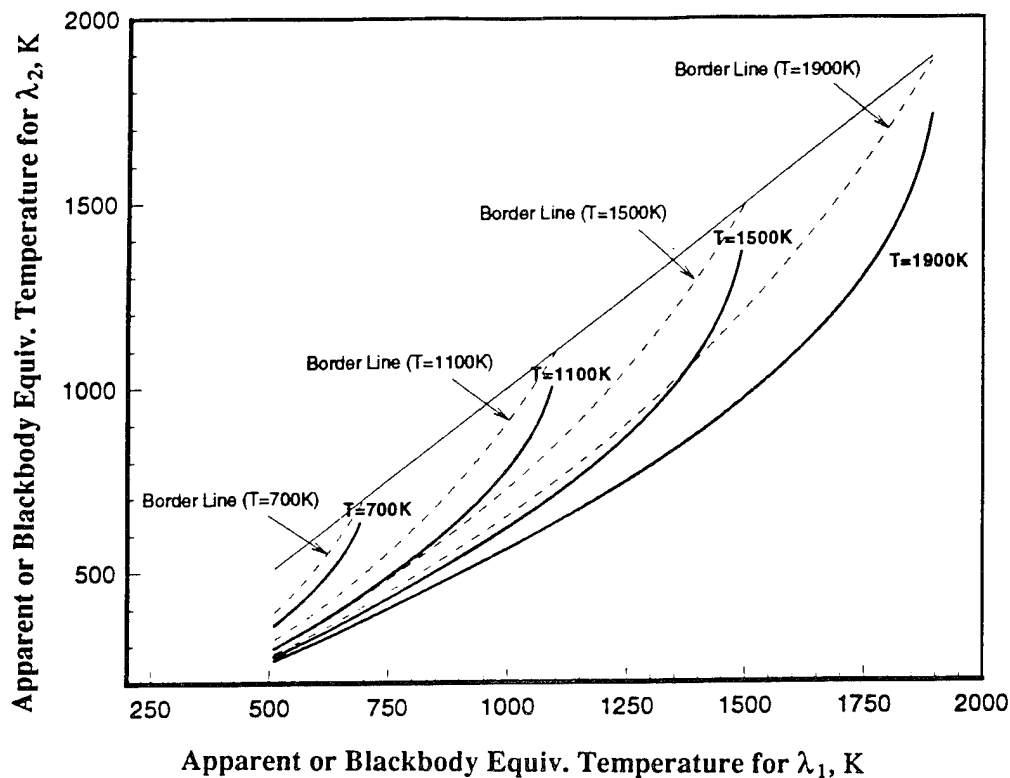
4

Fig. 4. Solution Domain of Two-Color Method.

soot are employed for such a spectrometric analysis, the effect of radiation from gaseous mixtures does not seem necessarily to be negligible as mentioned later.

In brief, the method was to obtain two measurements of radiation intensity [14].

$$I_{\lambda i} = 2 \, \varepsilon_{\lambda i} \, C_1 \, \lambda^{-5} \exp(-C_2/\lambda_i T_a). \quad (i = 1,2) \quad (1)$$

From the measurements, the temperature, T and a representation of soot concentration, K are determined along the line of sight. In this method, instead of using the conventional Lambert Beer's law, the spectral emissivity, ε_λ was expressed by an empirical relationship,

$$\varepsilon_\lambda = 1 - \exp(-KL/\lambda^\alpha) \quad (2)$$

where, the value of α was given 1.38 for the visible region and 0.95 for the infrared range and L was the length of the optical path. In implementing the solution, eq. (1) was rewritten by defining a new term, T_a, which may be termed the blackbody equivalent or apparent temperature, namely,

$$I_\lambda = 2 \, C_1 \lambda^{-5} \exp(-C_2/\lambda T_a). \quad (3)$$

Combining eqs. (2) and (3), the KL factor, an index of soot, is expressed by,

$$KL = -\lambda^\alpha \ln[1 - \exp\{-C_2/\lambda \, (1/T_a - 1/T)\}]. \quad (4)$$

The above equation is then extended for two wavelengths as,

$$[1 - \exp\{-C_2/\lambda_1 \, (1/T_{a1} - 1/T)\}]^{\lambda_1^\alpha} =$$

$$[1 - \exp\{-C_2/\lambda_2 \, (1/T_{a2} - 1/T)\}]^{\lambda_2^\alpha}. \quad (5)$$

One of the ways of determining temperature is, after T_{a1} and T_{a2} are found from the spectral intensity measurements and using eq. (3), T is calculated from eq. (5).

Validity of Measurements. When the measurements obtained using the new spectral IR imaging system were processed for finding T and KL by this method, however, some of the results were found unreasonable. In order to identify reasons leading to this observation, the above equations were used for constructing a graphical presentation of the solution domain of the method as shown in Fig. 4. This was a plot for the (central) wavelengths of filter bands employed in the experiment, $\lambda_1 = 2.35$ and $\lambda_2 = 5.0\mu m$. Note that the solid-lines indicating temperature solution were obtained with $\alpha_1/\alpha_2 = 1$, and the dotted-line solutions were calculated for $\alpha_1/\alpha_2 = 1.88$, an extreme case, which is considered almost unreal. The figure indicates that temperature, T can only be determined when the corresponding values of T_{a1} and T_{a2} fall within each region bordered by the pair of lines. It is pointed out that the

5

realistic solution, however, will exist along or near the solid line. The unreal results mentioned above mean that some of the measurements led to values falling out of the regions, even the upper side of the diagonal line. Among the probable reasons for such invalid solutions is the radiation from gaseous mixtures compounded over the soot radiation.

Experimental Results

As mentioned above, one of the seven sprays was investigated through the optical access in the cylinder head. Figure 5 shows the top view of the sprays whose axes are represented by corresponding lines, two exhaust valves, an intake valve and the optical access (shaded portion with a plume axis).
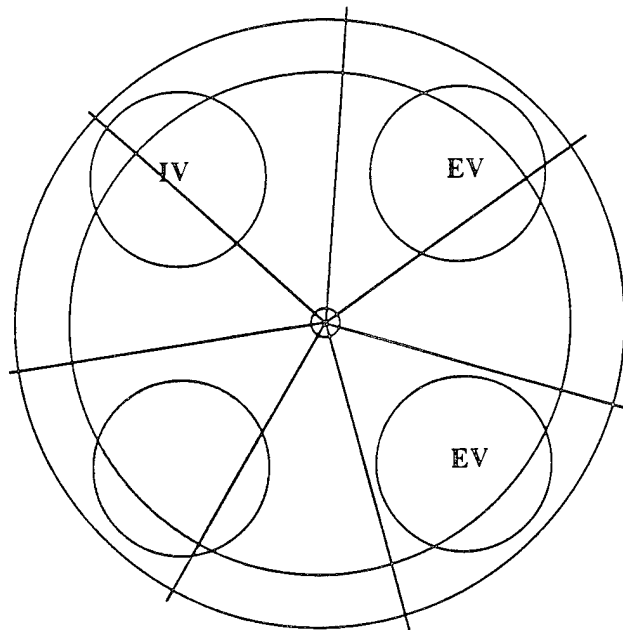
Spectral IR Images and Combustion Period. A typical set of high-speed spectral IR images are shown in Fig. 6, which can be compared with the spray axis shown in Fig. 5. Among the engine operating and imaging conditions for the result are, engine speed of 500rpm; fuel injection at 11bTDC; exposure period of 90µsec; imaging interval of 2.5CA; and spectral bands of 2.2-2.5µm and 4.5-5.5µm. In the same figure, the flame temperature and KL factor calculated by using the above mentioned two-color method are also shown. In order to compare the imaging results with the pressure-time (p-t) history, the imaging times are indicated on the p-t curve (Fig. 1), which may also be compared with the HRR and the average mixture temperature plotted on the same plane.

Explaining the imaging results shown in Fig. 6, the sequence of images goes from left to right and from the top to the bottom. The first thermal image captured of the combustion process was at 2.5aTDC as shown in Figs. 6-(A) and-(B). If the combustion products are directly indicated in the regions exhibiting strong radiation, the growth and relocation of those regions also show the combined effect of flame propagation and gas motions such as gas swirl. The present results show that the swirl is the counter clockwise direction as seen via the optical view.

It is noted that when some earlier images are obtained by extending the exposure period and using a large size aperture, those captured thereafter become overexposed, meaningless results. The engine CAs at which individual images were taken are indicated on the p-t diagram. According to the measurement, the first image (image a-4) was obtained near the end of the premixed combustion stage. The intensity of the image continued to be strong even after the injection period was over (image b-4 and others). Recalling significant amounts of fuel were consumed during the premixed combustion period and finding no image captured during the same period, the images obtained under the present imaging condition are considered to be radiation of soot at high temperatures, which is far greater than that of gaseous products. In other words, under the present imaging condition having a relatively short exposure period (90µsec) and a small aperture (3mm diameter), it was very probable that the radiation from the gaseous species was insignificant during this period. It is cautioned that this may not be the case when the combustion product temperature becomes

Fig. 5. Imaging View with respect to Plume Axes.

very high, as indicated by the temperature-time (T-t) calculated by using the p-t data.

Temperature and KL Factor. Looking at the direction of fuel injection (Fig. 5), it is found that the spectral radiation measured via projected view along the axis of the plume is low. The temperature and KL factor in the combustion products calculated by the two-color method are also shown in the corresponding layout, Figs. 6-(C) and -(D). As discussed earlier, some uncertainty is involved in their computation, which is considered to occur due to an assumption of negligible radiation by the gaseous species while it may become measurable when the temperature is high. Although the exact uncertainty of the present data reduction is unknown, the main events in the combustion chamber are expected to be indicated by the processed results. Most of all, the flame temperature distribution along the axis of the plume appears to be lower than at most portions of the plume. This low temperature distribution was unexpected in view the fact that no similar finding has been found in literature. The distribution of KL factor looks different than that of temperature, that is, it was neither high along the axis where the low temperature was observed nor in other region where the temperature is found to be very high. (This remark, however, is subject to amend due to the probable effect by the radiation from the gaseous species and some assumption involved in the calculation, as mentioned above.) This is particularly obvious at the combustion period indicated by KL distributions from a-6 through b-8, which may be compared with temperature distributions calculated at the corresponding CAs.

If the above results reveal some representative nature of in-cylinder reactions in direct-injection Diesel engines, one may be able to make several remarks. The low radiation measured in the projected view along the axis of the plume was due to both low temperature and low KL
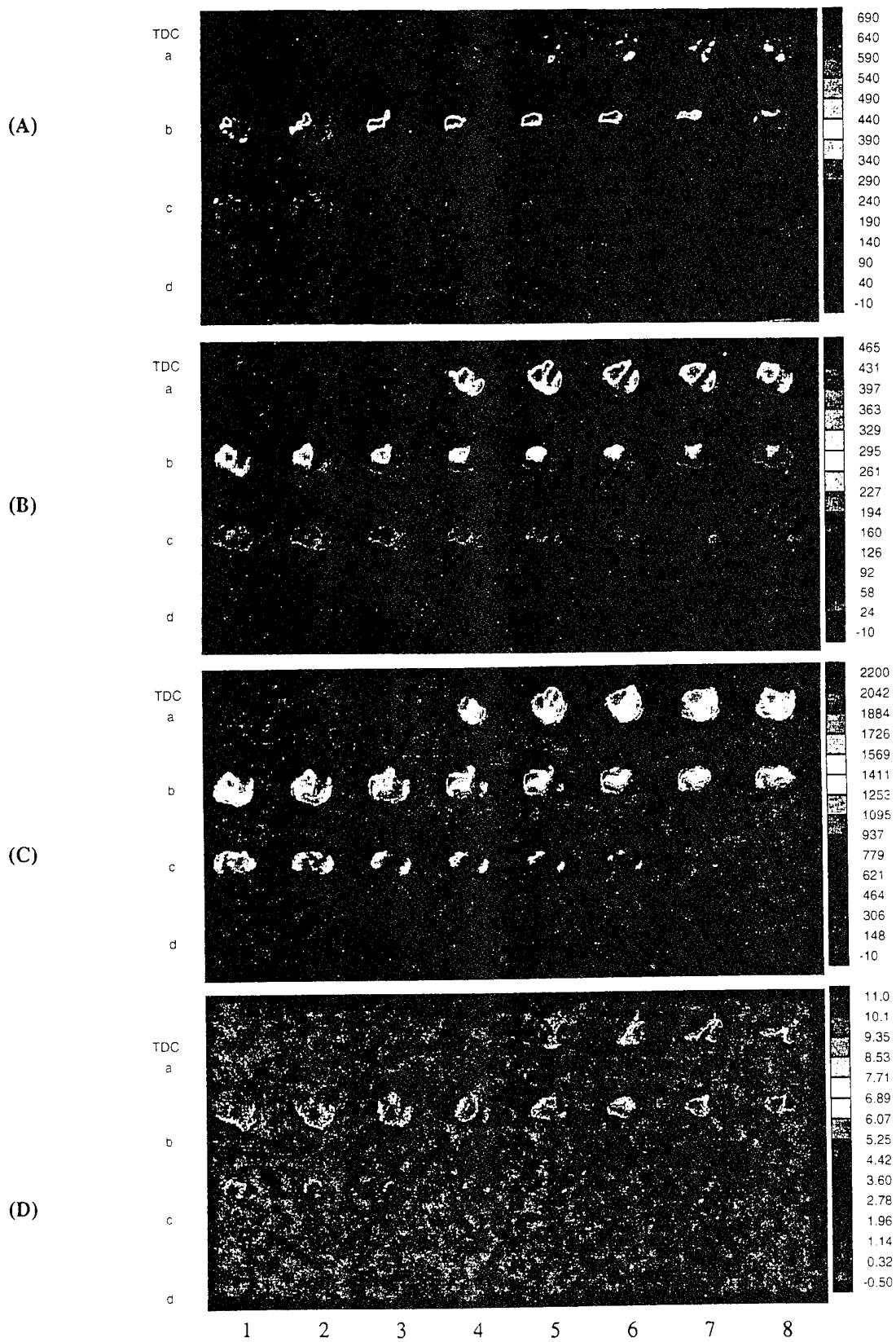
6

Fig. 6. Instantaneous IR Images Obtained in Exposure Period of 90μsec and Imagine Interval of 2.5CA from Engine Speed of 500rpm with Injection at 4dTDC. Images Obtained via Bands of (A) 2.2-2.5μm and (B) 4.5-5.5μm. Two-Color Method was Used to Calculate Distributions of (C) Temperature (K) and (D) KL Factor (in a relative scale).

7

factor distributions as found upon processing of the raw data (Fig. 6-(C) and -(D)). This should not necessarily suggest that the fuel/air in the same regions was lean because the present measurements were to capture thermal radiation by radiatively participating species: When the temperature is low, it is probable to produce weak radiations even when a mixture is fuel-rich. On the contrary, the fuel/air is expected to be rich along the axis in view that the fuel issued out of the injector hole passes through this path before being redistributed over other regions by the entrainment processes of plume formation. This, however, may not be the case at the later stage of injection as mentioned next. Again, the above statement is made in view of the relatively weak radiation from the combustion products (images a-2 through b-2) along the axis during the reaction period.

Why Low Temperature and KL Factor along the Axis of the Plume. The above discussion, then, brings about a question of what causes the temperature to be low while the fuel/air is expected to be rich in the same regions along the axis in the self-ignition environment. This presumption of a rich core has been often mentioned in literature. A brief discussion is attempted in the following in order to describe the spray structure in a DI CI engine by reviewing what has been observed in the present study and results reported by others. Two possibilities are considered:

The first possibility is discussed in terms of the air entrainment and the narrow cylinder volume (when the piston is near the TDC) where the fuel is injected. The fuel droplets produced immediately after the injector hole do not travel very far themselves into the chamber because their momentum is rapidly transferred to the high density cylinder gas. The entrained gas stream produced via the momentum transfer, which embodies the droplets, basically becomes the fuel spray plume. The fuel spray is relatively narrow and short in the beginning. In general the fuel spray tip reaches the periphery of the piston bowl within a period of a few or several crank angles from the start of the injection. (It is reminded that the injection period may range up to well over twenty CAs in most mechanically controlled fuel injectors.)

The spray plume is developed by sequentially exhibiting different geometries, namely: by starting with an appearance of a bowling pin; taking a "loaded-ice cream-cone" look later; and attaining seemingly a mushroom or bell shape near the end of injection and the combustion period. These progressively changing geometric configurations are, of course, modified by the gas (swirl) motions in the chamber. Such sequential changes of the spray plume may be seen in results obtained by various high-speed cinematographic techniques, for example the laser shadow graphic method [15]. It is reasonable to expect that after the period of the early through mid stages of injection (when the spray jet probably has a fuel-rich mixture core), the spray will become relatively "hollow." The core is expected to be lean because, even after the termination of fuel injection, some residual air entrainment will continue and produce a fuel-lean flow, which becomes the last component of the plume basically along its axis. Although no explicit description pronouncing the nature of such a hollow spray core is found in literature, it is conceivable to have such physical processes leading to a fuel-lean-core spray structure

(near the end of the injection period). This, again, seems to be supported by some of recent results, including those in the above mentioned literature and additional measurements made in our laboratory as explained later.

In the beginning, this consideration of the fuel-lean spray core did not help explain the low radiation along the projected view of the spray axis as shown in the present thermal images taken during the combustion period. This was because radiation produced by reaction zones in the (top and bottom) outskirts of the plume would not have resulted in such dramatic images. Recall however that the fuel is injected when the piston is near the TDC and the combustion chamber volume height is low. When a bell-shaped (hollow) fuel spray is introduced into such a narrow volume, it is predictable that the portions of the spray (i.e., the top and bottom outskirts) interfacing the cylinder head wall and the piston top surface would "be repelled" and pushed to both sides (as seen from the top). The repelling effect by the (top and bottom) walls would make the fuel distribution at both the ends of the spray become lean, which matches with the portions near the spray axis as observed via the optical view during the combustion period. It is reemphasized that the the spray under consideration is not at the beginning of its formation but after the onset of ignition or near the end of the injection period.

The second possibility is considered in terms of the stability and the latent heat of evaporation. Since even a shock wave is produced somewhere within the spray cone when the injection pressure is very high, it is reasonable to expect that the flow speed of air-fuel mixture along the axis is too high to attain stabilized reaction fronts. Consequently, the reaction fronts will be developed only where the mixture speed is low enough, which is basically the regions near the tip or the outer portions of the spray cone, which seems to coincide with the present IR images. At the same time, the fuel off the injector exposed to the hot cylinder gas will be rapidly vaporized and mixed with the entrained streams of gas, which effects have been widely considered by others in the past. One such effect suggests that the mixture temperature in regions near the spray axis is probably too low to get self-ignition. Although the mixtures attain marginally or even sufficiently high temperatures for self-ignition, when the above mentioned effect of flow stability for ignition is compounded together with the cooling (due to the latent heat of evaporation), it would be difficult to produce some stable reaction fronts along the regions., which might have been accordingly reflected on the present measurements.

The former possibility postulated the fuel/air ratio in regions near the axis of spray to be lean, while the latter presumes it to be probably rich. Both possibilities, nevertheless, are not inconsistent with the low KL factor measured in regions along the axis of the plume. It is simply because where there is no reaction front, there is low soot formation. It is also stated that where there is low temperature, there is low soot formation. Looking at images a-3 through b-3 in Fig. 6-(D), the regions having relatively high KL are more likely those located between the very near the spray axis and the edges of the spray plume. The regions at high temperature exhibited low KL measurements, which is considered to be attributed by rapid oxidation of soot.
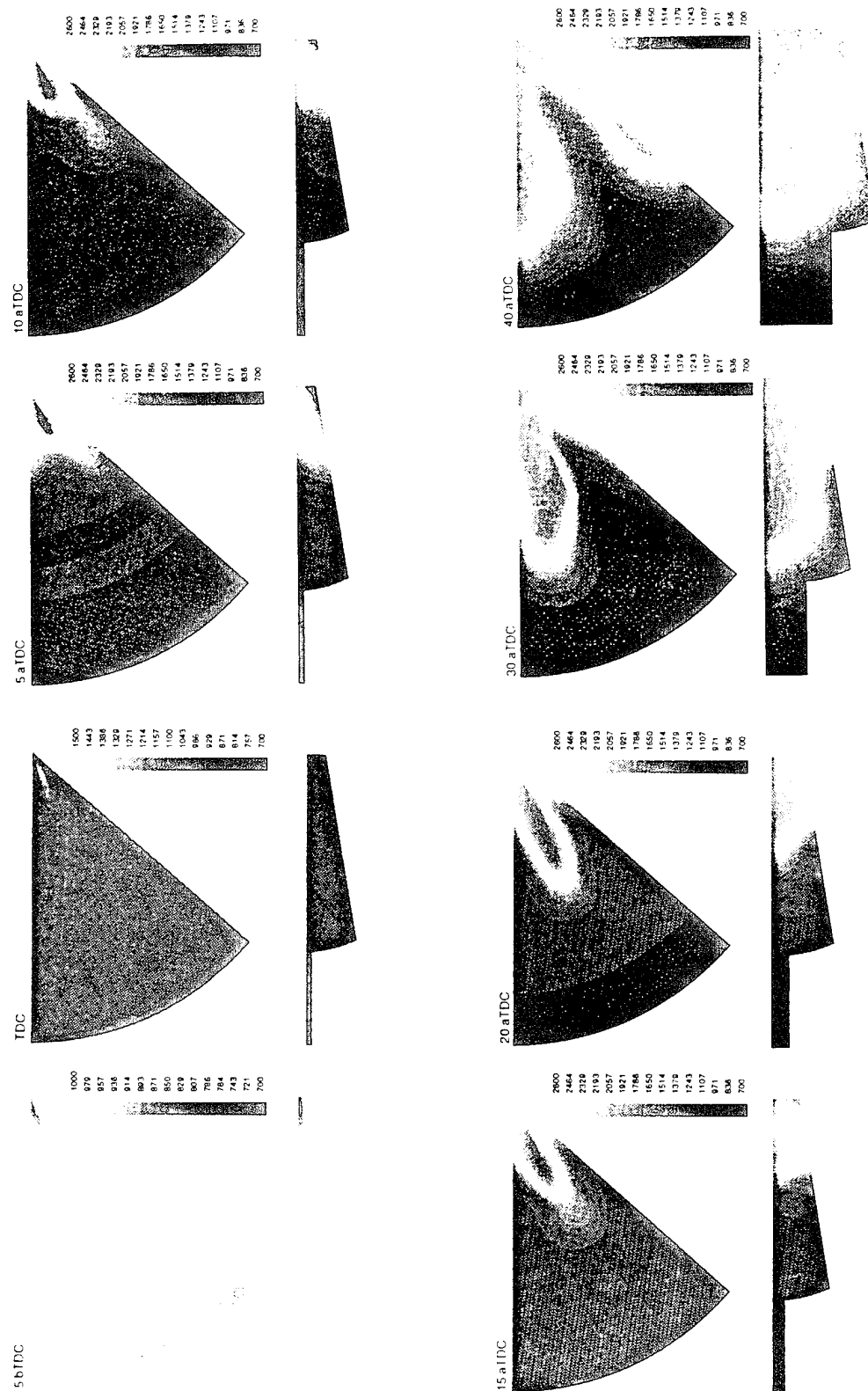
8

Fig. 7. Predicted Temperature Distribution of a Spray Flame in a DI CI Engine using KIVA II Code Performed under the Same Engine and Operating Conditions Employed for Obtaining Results Shown in Fig. 6.

9

Regardless of what causes to occur, (e.g. by either the former or the latter possibility, as mentioned above) it seems to be a fact that the combustion processes by at least some DI CI engine injectors generate low radiation from the regions along the axis of the spray plume indicating low temperature zones accordingly. This statement is supported by our additional observations obtained in separate studies, which employed a high-pressure electronic-controlled fuel injector in the same engine [5,13].

Computational Results

Several engine parameters were varied in the present computation including grid configuration, swirl ratio, number of spray parcels, and droplet diameter distribution, which were compared with the reference condition specified in Table-II. Although no predicted pressure (p-t) history obtained in this work was comparable with any measured result, further computation on the fuel spray combustion in the cylinder was performed. This was because a p-t result is the combined effect of all reaction steps, which would be difficult to accurately predict by a model.

The temperature distributions predicted for the engine condition as specified in Table-II using grid arrangement case-(2) are shown in Fig. 7. Two cross-sectional views along the axis of the spray plume are displayed for the individual instants of time (in CA): a side section and a horizontal section. Since the spray plume had six degrees in angle with respect to the head surface, this horizontal section is therefore placed by an inclined plane in the corresponding amount of angles. Note that in order to show the local variation, the temperature distribution scale was varied in the early part of combustion.

Although the fuel injection begins at 11 bTDC, the predicted temperature change in the chamber occurs around 5bTDC. The spray angle with respect to the head surface is not seen in the beginning, but it causes the spray deflection from the piston surface starting around 10aTDC, which became more obvious at 30aTDC. The swirl (in the clockwise direction) is reflected on the spray development, which effect is quite obvious around 30aTDC when the adjacent spray begins to be seen.

The seemingly low temperature zones predicted along the spray axis (particularly in distributions at 15, 20 and 30aTDC) may remind us of the similar findings in the measurements discussed earlier. Their mutual similarity, however, should not be interpreted that the present computation predicted the measurements. The low temperature distribution zones shown along the axis are due to the deflection of the spray to develop a shallow-well shape distribution (30 aTDC, Fig. 7) and the cross-section was made along the axis of the plume having an inclination of six degrees. If the distribution of (averaged) temperature were plotted by integrating along the line of sight, no such low temperature zones would be predicted along the axis of the spray plume. It might be added that no computational prediction in literature has suggested the same finding of low temperature zones along the plume axis.

It is noted again that the initial objective of the work was to compare the experimental results with those

predicted by the computational method. In spite of some reasonable amount of resources used for performing the computational part, which employed the (most advanced) computer code made available to the general technical community, our computational results failed to predict the key events shown by the measurements. Two possibilities: The computational method has limitations that the computer code will have to be made more realistic and user-friendly. Or, the present engine measurements do not represent the typical DI CI engine environment.

Summary

The in-cylinder processes were studied by two methods: Successive infrared images of combustion reactions around a spray plume were simultaneously obtained in two respective spectral bands in 2.5CA interval through an optical access in a DI Diesel engine cylinder head. Temperature distributions in the corresponding spray were predicted by using KIVA II, which was refitted with comparable engine conditions employed in the measurements. The spectral measurements were processed by using the conventional two-color method to determine the temperature distributions. We attempted to compare them with the prediction.

Among the more significant findings from the study was that the radiation is lower along the spray axis of the projected view. The temperature distribution calculated using these spectral digital images shows similar low temperature zones along the axis. These low temperature zones are interpreted to occur due to, either a possibility of the spray formation process involving a hollow spray injected into the combustion volume with a narrow height, or a possibility associated with unstable high-speed flows and the latent heat of evaporation leading to inability of permitting flames in the zones. Zones at low temperatures are not expected to produce large amounts of soot because the reactions there are simply slow while those at high temperature would consume the soot at high rates.

Under the engine and operating conditions investigated in this study, our computational results failed to predict the measurements. The reasons for the discrepancy may be due to either that the model prediction did not follow actual reactions in the cylinder or that the present measurements did not represent the typical CI combustion.

References

1. Nehmer, D.A. and Reitz, R.D., "Measurement of the Effect of Injection Rate and Split Injections on Diesel Engine Soot and NOx Emissions," SAE Paper-940668, 1994.

10

2. Kobayashi, s. et al., "Measurement of Flame Temperature Distribution in DI Diesel Engine with High Pressure Fuel Injection," SAE Paper-920692, 1992.

3. Yang, Minggao, Sorenson, S.C., "Direct Digital Control of Diesel Engines, " SAE Paper-940372, 1994.

4. Wood, M.E., Bryzik, W. and Schwarz, E., "100 Hour Endurance Testing of a High Output Adiabatic Diesel Engine," SAE Paper-940951, 1994.

5. Kajitani, S., Usisaki, H., Clasen, E., Campbell, S. and Rhee, K.T., "MTBE for Improved Diesel Combustion and Emissions?," SAE Paper-941688, 1994.

6. Desai, R.R., Gaynor, E., and Watson, H.C., "Giving Standard Diesel Fuels Premium Performance Using Oxygen-Enriched Air in Diesel Engines," SAE Paper-932806,1993.

7. Pataky, G., Baumgard, K.J., Gratz, L.D., Bagley, S.T., Leddy, D.G., Johnson, J.H., "Effect of an Oxidation Catalytic Converter on Regulated and Unregulated Diesel Emissions," SAE Paper-940243, 1994

8. Jiang, H. and Rhee, K.T., "High-Speed Imaging of Bunsen Burner Combustion Product," Paper No. 67, Proceedings of Canadian and Western States Section of the Combustion Institute, Spring Technical Meeting, Alberta, Canada, May 1990.

9. Rhee, K.T., "Spectral Infrared Imaging of Flames in Narrow Clearances," Combustion Science and Technology, 75, 4-6, 1991, p. 333.

10. Jiang, H., McComiskey, T., Qian, Y., Jeong, Y.I., Rhee, K.T., and J.C. Kent,"A New High-Speed Spectral Infrared Imaging Device Applied for Imaging Gaseous Mixtures from Combustion Devices," Combustion Science and Technology, 90, 5-6, p. 341, 1993.

11. McComiskey, T., Jiang, H., Qian, Y., Rhee, K.T., and Kent, J.C., "High-Speed Spectral Infrared Imaging of Spark Ignition Engine Combustion," SAE Paper-930865, 1993.

12. Jiang, H., Qian, Y. and Rhee, K.T., "High-Speed Dual-Spectra Infrared Imaging," Optical Engineering, 32 (6), pp. 1281-1289, 1993.

13. Clasen, E., Campbell, S., Jiang, H., Rhee, K.T., Kent, J.C., Studzinski, W., "High Speed Multispectral Infrared Imaging Applied to Engine Combustion Research," Technical Meeting, Central State Section of the Combustion Institute, University of Wisconsin-Madison, June 5-7, 1994.

14. Matsui, Y., Kamimoto, T., Matsuoka, S., "A Study on the Time- and Space-resolved Measurement of Flame Temperature and Soot Concentration in a DI Diesel Engine by the Two-Color Method," SAE Paper-790491, 1979.

15. Won, Y.H., Kamimoto, T., and Kosaka, H., "A Study on Soot Formation in Unsteady Spray Flames via 2-D Soot Imaging," SAE Paper-920114, 1992.

11

941688

MTBE for Improved Diesel Combustion and Emissions?

Shuichi Kajitani and H. Usisaki
Ibaraki Univ.

E. Clasen, S. Campbell, and K. T. Rhee
Rutgers - The State University of New Jersey

Abstract

Reduced emissions from the spark-ignition engine, when fueled by gasoline containing small amounts of MTBE, have led us to explore similar positive results in compression-ignition (CI) engine combustion by adding this oxygenate compound to Diesel fuel. This study was performed in two separate laboratories by employing the respective experimental apparatus.

When a pre-chamber type CI engine was operated by using Diesel fuel mixed with several volume portions of MTBE, including 5, 10 and 15%, several positive results were obtained, as compared with those from the baseline neat Diesel-fueled operations: (1) The engine delivers overall comparable or better performance characteristics; (2) The brake thermal efficiency is higher at the advanced and late injection times; (3) Some considerable reduction of both soot and NOx emissions is found; (4) The ignition delay increases but the combustion duration decreases.

In order to help explain the unexpected responses of CI combustion to the above fuel modifications, high-speed in-cylinder spectral infrared digital imaging was performed for the same fuel modification. Some plausible and consistent results are observed, which help explain the above findings.

Introduction

The formulation of fuels and new additives, introduced for transportation powerplants in the past, have often been made without basic knowledge of the mechanism that would lead to the end results. A typical example may be tetraethyl lead, which was a revolutionary discovery achieved after trying many hundreds of different chemicals in the laboratory. Even though this additive was widely used as an octane booster for a long time, the chemistry of how it improved the octane rating of gasoline was not understood. The 1990 Amendment to the Clean Air Act, which requires the use of fuels containing 2.0 and 2.7 weight percents of oxygen in non-attainment areas of atmospheric ozone and carbon monoxide concentrations, respectively, was based on laboratory measurements. Probably, the most widely used oxygenate fuel additive (or a gasoline extender) for this, at present, is methyl tertiary butyl ether (MTBE, $(CH_3)_3COCH_3$). Again, the exact in-cylinder chemistry is not known how this oxygenated chemical in gasoline results in low emissions from spark-ignition (SI) engines. One of the most prevailing theories on the reaction mechanism at present is that the additive eliminates hydroxyl (OH) radicals in the preflame zone to slow down the spontaneous ignition, consequently to reduce the tendency of knock [1]*.

Such a role by the oxygenate of delaying self-ignition will result in a decrease of the cetane number if blended with Diesel fuel, which is not, in general, a desirable consequence in the formulation of Diesel fuel. Nevertheless, some unpublished works in recent years were directed to finding if the same oxygenate being used in SI engines would produce some positive effects on compression-ignition (CI) combustion to result in low emissions. No concrete theoretical reason for motivating such studies was seen in the beginning. Simply, if the same role by this oxygenated additive of delaying the self-ignition, as being inferred to occur in the SI engine end gas, is also taking place in CI combustion, one could expect it to bring about a longer ignition delay period, as mentioned above. If this is the case, the premixed portion of the combustion will be increased, which in general decreases the soot formation. Without a serious analysis of flame chemistry under this condition, one may immediately recall the well-known mutual exclusivity in engine/fuel effects on soot and NOx formation in CI combustion. That is, such a measure of reducing soot would increase NOx emission. Our experimental measurements, however, indicate that this exclusivity does not seem to apply in the present case, i.e., the addition of a small amount of MTBE in Diesel fuel does reduce both soot and NOx emissions at the same time. A joint experimental study has been performed as a continuing collaboration between two university laboratories to investigate this new finding.

---

*Numbers in parentheses designate references at end of paper.

Experiment

Apparatuses and Fuels. Two separate engine setups were used in the study. Performance and emissions measurements were obtained in a single cylinder indirect injection (IDI) CI engine having bore-stroke of 95-155mm with the nominal compression ratio of 20. The experiment was carried out at an engine speed of 1,200 revolutions per minute (rpm). The mixture of Diesel fuel with MTBE was simple to prepare and easy to use in the engine, i.e., neither any phase separation nor an abnormal response by the engine was observed during the experiment. The volumetric portions of MTBE in the fuel blend investigated in the present work included 5, 10 and 15%, which were equivalent to the mass fractions of oxygen in the blend of 0.91, 1.82, and 2.72%, respectively. The mixtures with these proportions of MTBE also resulted in corresponding reductions of the heating value, the viscosity, and the theoretical air ratio by: 1, 2, 3%; 2, 4, 5%; 1, 2, 3%, respectively. For convenience, the fuels having portions of MTBE, 0, 5, 10, and 15% will be hereafter referred to, as neat (Diesel fuel), MTBE-5, MTBE-10, and MTBE-15, respectively. The fuel mixture containing MTBE will also be called, the blend. The measurement of soot and NOx was made by using the Bosch scaling method and the zinc-reduced naptylene diamin method (JIS K0104), respectively.

In order to obtain a better insight into the reaction processes in the combustion chamber, it was decided to investigate the in-cylinder reactions by capturing instantaneous spectral infrared (IR) digital images using the Rutgers IR imaging system. Since this new IR imaging system has been described earlier [2-5], no detailed system description is made here. In brief, two geometrically identical (pixel-to-pixel corresponding) digital images were simultaneously obtained in spectral bands of $2.20\mu m$ and $2.47\mu m$ at a rate of over 1,200 frames/sec. The pair of identical images were obtained as triggered by the successive corresponding engine crank angle markers. The former band was mainly to capture the radiation from the soot and the latter was intended to measure that from the water vapor produced during the combustion processes.

Since the above mentioned mutual exclusivity of engine/fuel effects on soot and NOx emissions prevails in existing CI engines, regardless of type and size, and since the in-cylinder imaging is facilitated in a direct injection (DI) type engine, a single-cylinder DI CI engine with optical access was used for imaging. In view that even constant-volume bombs are often used for investigating the spray and flame behaviors in CI engines, the use of a DI CI engine for the in-cylinder imaging in order to help explain the measurements from an IDI engine may be further justifiable.

The DI CI engine has bore-stroke, 139-117mm; connecting rod length, 201mm; compression ratio, 13.5:1; injector hole diameter, 0.15mm; and number of holes, 8. The engine was equipped with an electronically controlled fuel injection. Since the actual start of injection was not measurable when the present experiment was performed, the injection control was adjusted such that the engine delivers the best torque to obtain the imaging results. The view of the imaging is shown in a self-explanatory schematic in Fig. 1, and additional details may be found elsewhere [5].
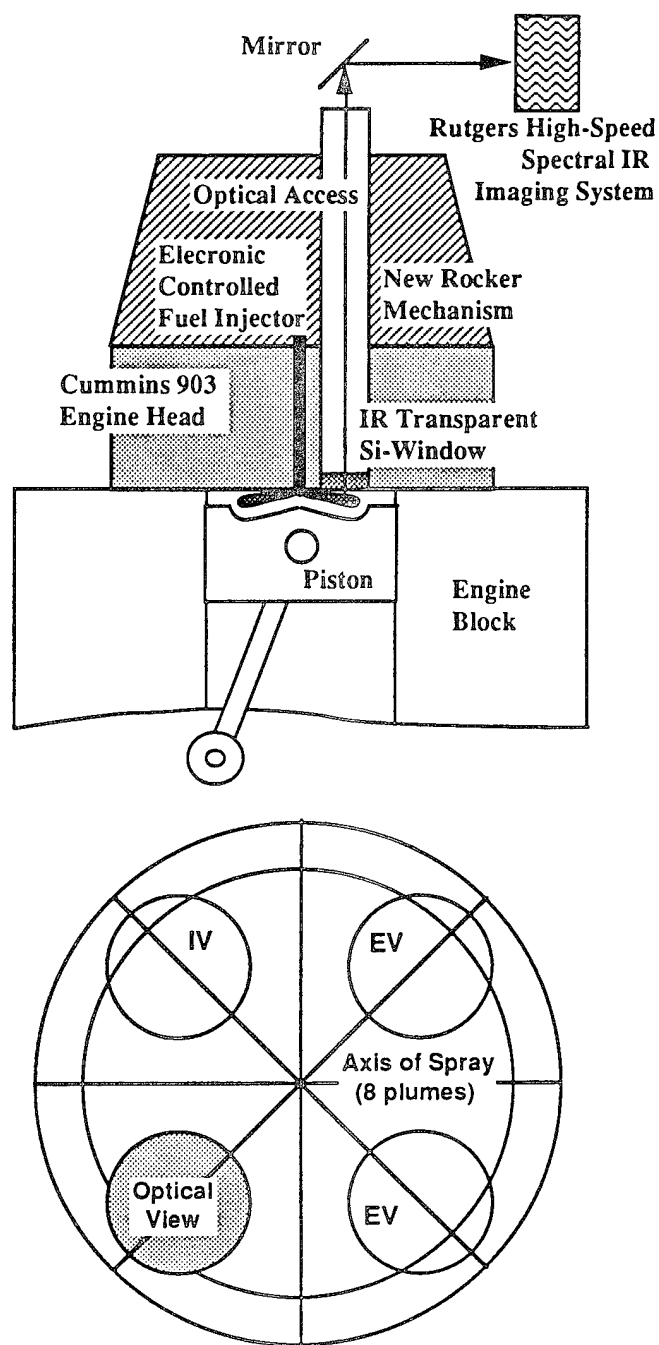

Fig. 1. Schematics of the Engine Combustion Chamber and Optical Access with respect to the Spray Axes.

Results

Engine Performance and Interpretation. When the engine at Ibaraki Laboratory was operated for the first time on the blend, almost no change in the engine response was felt from that of the baseline operation, the neat Diesel fueled engine. The undetectable difference in the peak pressures obtained at the various engine operating conditions with the blend fuels (Fig. 2) confirms this initial observation.
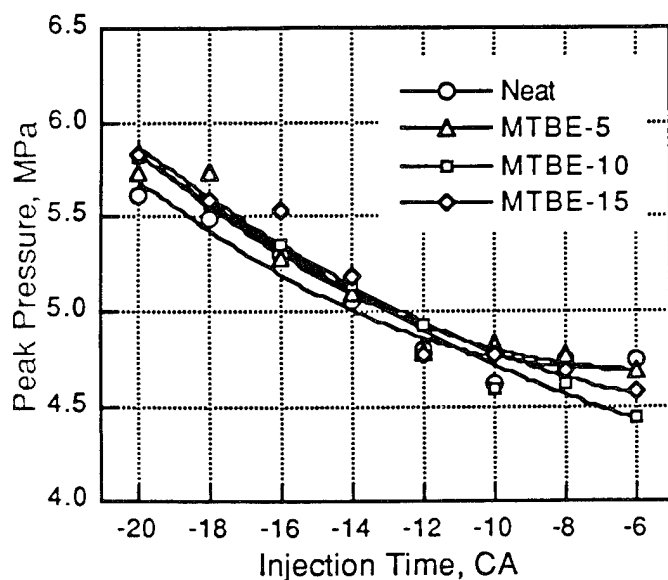
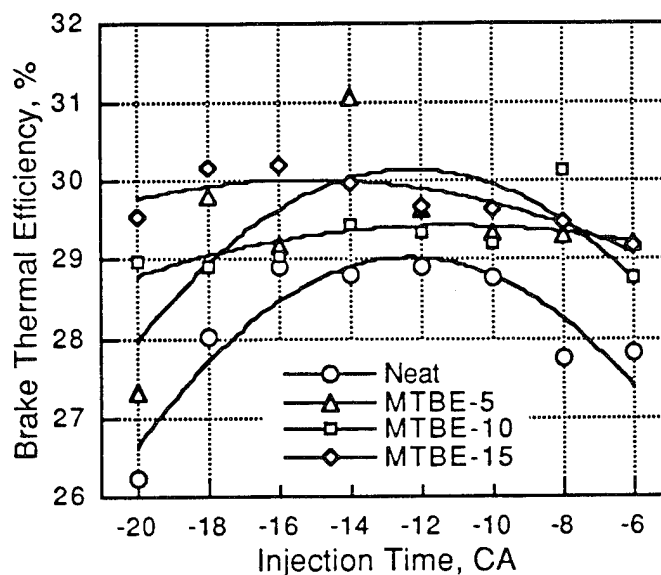Fig. 2. Peak Cylinder Pressure Obtained with Different Fuels.

Fig. 4. Brake Thermal Efficiency at Varied Injection Time for Neat and Blend Fueled Engine Operations.
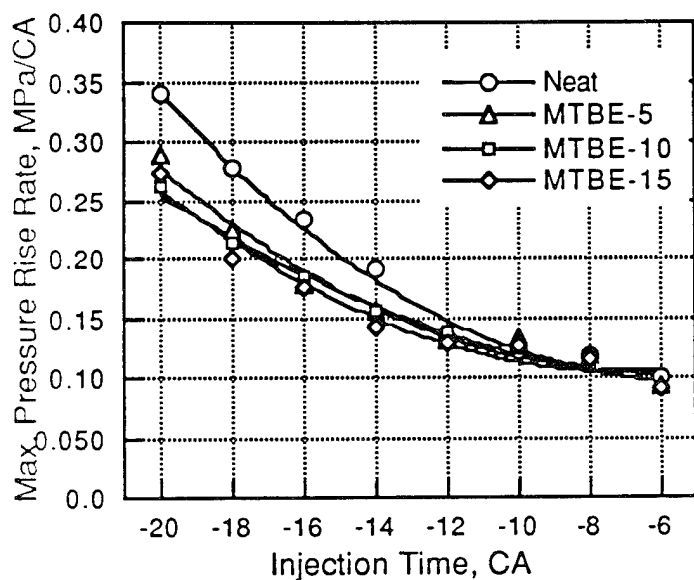

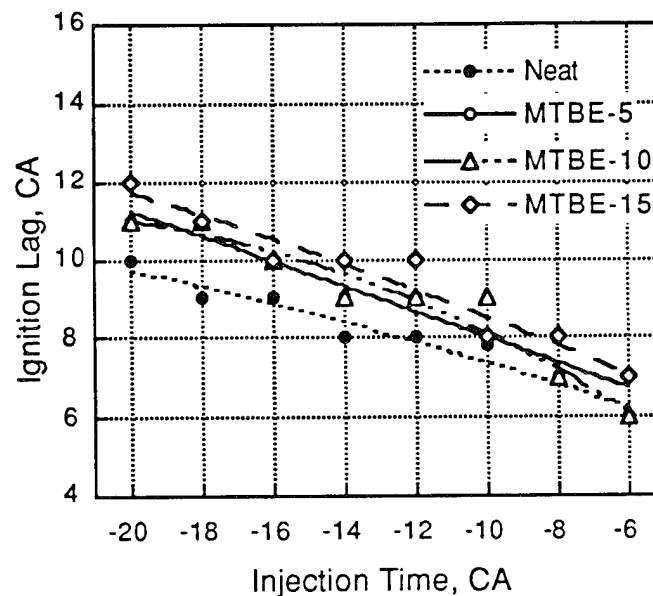Fig. 3. Maximum Pressure Rise Rate Obtained with Different Fuels.

Fig. 5. Ignition Delay Period Measured with Different Fuels.

The blend exhibited, however, a smoother operation for the advanced fuel injection times compared with the neat fuel, as reflected by the lower maximum pressure-rise rate, (dp/dt)-max, shown in Fig. 3. (Unlike such an observation with MTBE blend fueled IDI CI combustion, measurable changes in engine performance were found in the DI CI engine experiment, as mentioned later.)

While no significant adverse impact on the engine operation, such as roughness, was discovered when this engine was operated by the blend, as mentioned above, the detailed measurements of the brake thermal efficiency showed some significant difference (Fig. 4). The efficiency was higher, by as much as ten percent, in the blend operated engine compared with the neat fueled operations. This was more significant in those with the extreme advanced and late injection times, although such extreme operations are not generally employed in the actual engines. This efficiency increase is explained by correlating several findings from
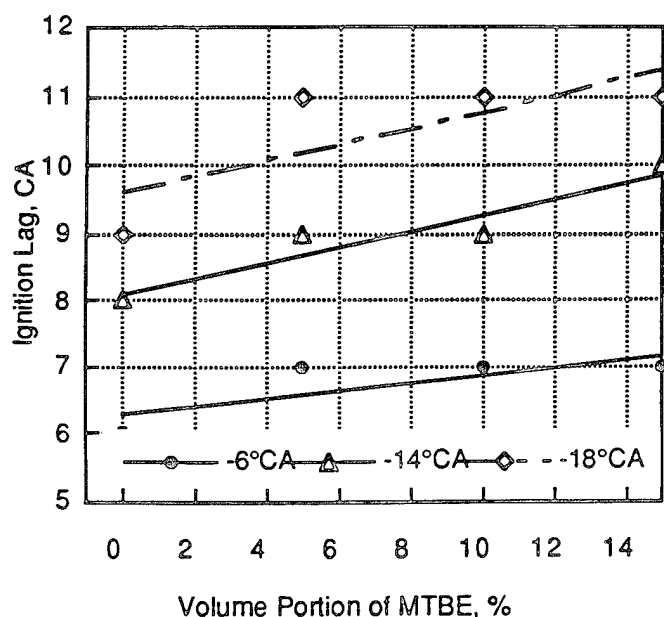
3

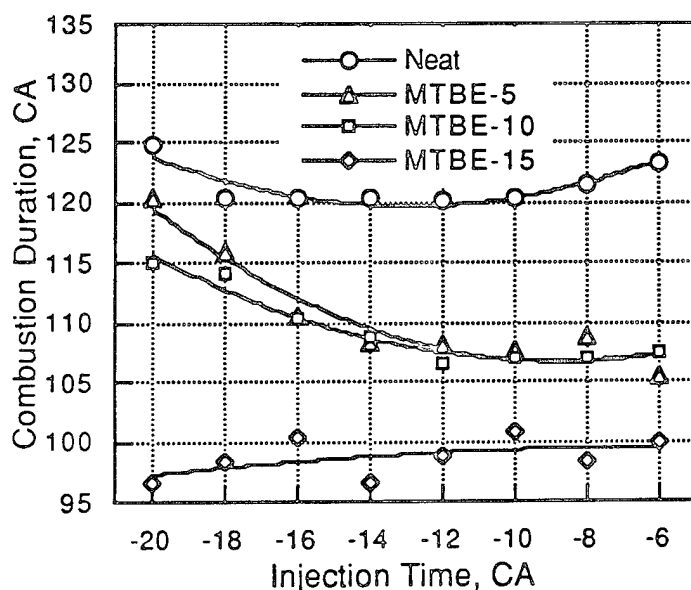Fig. 6. Ignition Delay period with respect to the Content of MTBE.

Fig. 7. The Overall Combustion Periods of Different Fueled Engine Operations.

the experiment, as included next.

The blend was expected to have a lower cetane number, which resulted in an increased ignition delay, as confirmed by the measurements shown in Fig. 5. This measurement found from pressure-time (p-t) data was consistent with the observation made from the high-speed IR

imaging, as explained later. The delay would increase the portion of heat release in the premixed combustion. Note that this heat release occurs while the piston is near top dead center (TDC), an effect of increasing the thermal efficiency. The effect of the content of MTBE on the ignition delay was predictable as shown in Fig. 6, i.e., the larger the amount of MTBE, the longer the ignition delay. In addition, the longer ignition delay was followed by shorter overall combustion periods (Fig. 7). These findings well compare with the observation made by using high-speed spectral IR images, as presented later.

Those measurements not only seem to be mutually consistent with each other but also help explain the increase in the thermal efficiency in the MTBE blend fueled engine: The increased ignition delay would result in a greater portion of the premixed combustion and a shorter overall combustion period. They would bring the combustion process to be near a constant-volume reaction resulting in an increased brake thermal efficiency.

Emissions. The effects of MTBE blended with Diesel fuel on exhaust emissions are shown in Figs. 8. The NOx emissions were consistently low when the engine was operated by the blend (Fig. 8-(A)). Although the injection timing effect on NOx emission was expected, i.e., the earlier the injection, the more the NOx emission, the effect of the portion of MTBE in the blend did not exhibit any consistent trend. According to the present measurements, the greatest reduction of NOx emission was achieved by a blend with 5% volume fraction of MTBE, the least reduction was found with a blend having 10%, and the effect of a 15%-blend was between the two. The reason for this finding is not known.

Examination of the effects of the blend on the smoke emission yields that while a small reduction was obtained in combustion with late fuel injection, some considerable decrease was measured in operation with advanced injection (Fig. 8-(B)). The effect of injection time on the exhaust soot was much more obvious with the neat fueled operation than those by the blend. In spite of the measurable effect of the portion of MTBE on the ignition delay (Fig. 6), no significant impact on the soot emission (by the variation of the MTBE portion) in the blend was realized in the measurement.

High-Speed In-Cylinder IR Imaging. Unlike the insignificant change found in the engine operations when the IDI CI engine was fueled by the blends, some measurable deterioration in the power output was observed in the (blend fueled) DI CI engine. Since this DI CI engine apparatus was used primarily for obtaining IR images, no systematic performance analysis was attempted, however.

Figure 9 shows the instantaneous in-cylinder images obtained from the above mentioned DI CI engine. The sets of successive images were obtained in three CA intervals from the engine operated at a speed of 500rpm, as indicated by the sequential CA numbers included in the look-up table. Keep in mind that the negative number represents CA before TDC (bTDC). The images were simultaneously captured in the respective spectral bands of 2.20μm and 2.47μm. The images in the former band shows the radiation from soot. Those in the latter band exhibit the emissions from both water vapor and soot, although the original intent was to investigate only the presence of the
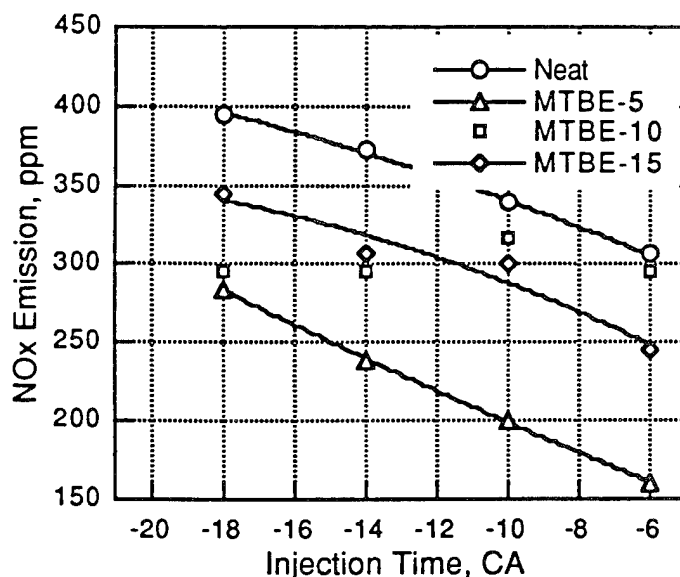
Fig. 8-(A). Exhaust NOx Emissions Obtained using Blends.

Fig. 8-(B). Exhaust Smoke Emissions Obtained using Blends.

water vapor. This was due to the strong radiation from the soot cloud over the entire wavelength range in the IR regime. The successive images are nearly instantaneous in nature, for they were captured with an exposure period of 90μsec throughout the experiment. The images of other in-cylinder events would have been captured, including the pre-flame reaction, if the exposure period was extended, as observed in separate experiments.

The images of spectral infrared radiation shown in Figs. 9-(A) and -(B) indicate the progress of the combustion reaction for engine operations by neat fuel and MTBE-5, respectively. The bright image seen around 5 after TDC (aTDC) is considered to indicate the rapid consumption of the premixed mixture at the end of the ignition delay, which is particularly violent with the neat Diesel fuel. The intensity of radiation when the engine was fueled by MTBE-5, under the exactly the same condition as the above, is much weaker in this early premixed combustion. This observation seems to compare with the weaker maximum pressure-rise-rate measurements with MTBE blends, as shown in Fig. 3. The combustion reaction preceded by this weak combustion, however, is stronger than that observed in the neat fueled engine operation, which is clearly seen by comparing corresponding images at 8, 11, and 14 aTDC in Figs. 9-(A) and -(B). Furthermore, this strong combustion with MTBE-5 is followed by an earlier completion of radiation, which represents the similar process of the combustion reaction. This observation from IR imaging results is also comparable with the shorter combustion duration inferred from the p-t data obtained in the MTBE blend fueled engine as shown in Fig. 7.

The formation of soot in the combustion chamber for these two different fuels can be viewed in the IR images.
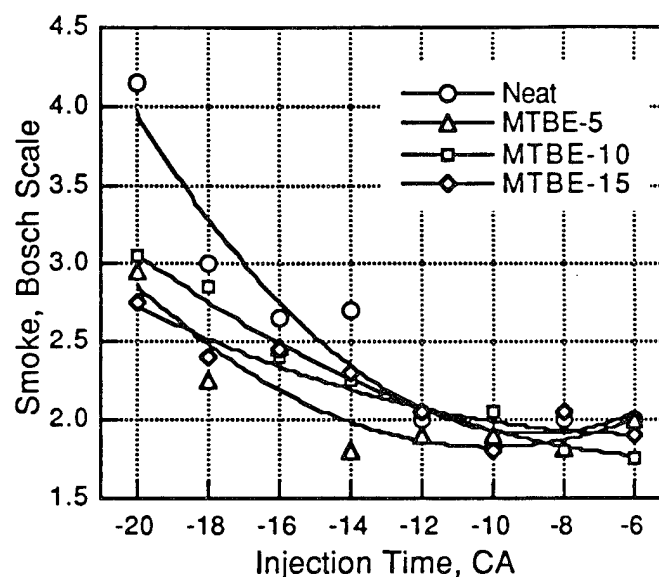
Our literature study suggests that near the waveband of 2.20μm no significant radiation emitted by other gaseous species normally contained in the hydrocarbon-air flame zone exists. Since the radiation emitted by the soot cloud is rather continuous over the wide range of wavelength in the IR regime, the images captured in this band are expected to exhibit the presence of soot. Looking at corresponding sequential images in Figs. 9-(C) and -(D), which were obtained using the neat and MTBE-5, respectively, it is quite obvious that the radiation levels are mutually comparable with each other in the early stage (see matching images at 8 and 11). The radiation, however, more rapidly disappears in the engine operation by MTBE-5. This may lead to an expectation that the oxidation of soot in the engine operation by MTBE-5 is accordingly rapid. Note that the p-t data obtained at the same time of the imaging for both fuels were similar. Thus, it is unlikely that the low radiation captured via the 2.20mm band in the MTBE-5 operated engine is caused by the low (average) in-cylinder temperature.

Although a more systematic measurement of such digital IR images is warranted, several remarks may be summarized about the present spectral IR data of the in-cylinder processes. The findings with the MTBE-5 operated engine compared with the neat fuel operated experiment include: The ignition delay is longer; The premixed combustion seems to be much weaker, which is followed by a stronger but shorter reaction period. In addition while the initial radiation from the soot in both fuel operated engines are comparable each other, it disappeared at a higher rate in the MTBE-5 combustion. These observations will be further discussed to explain the emissions and performance results in the following.
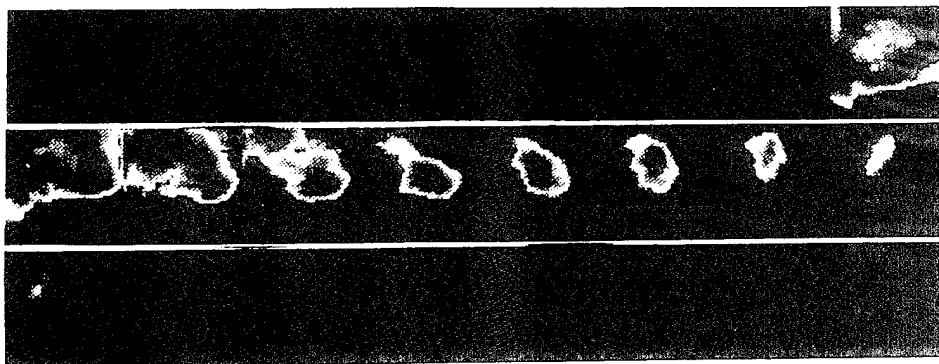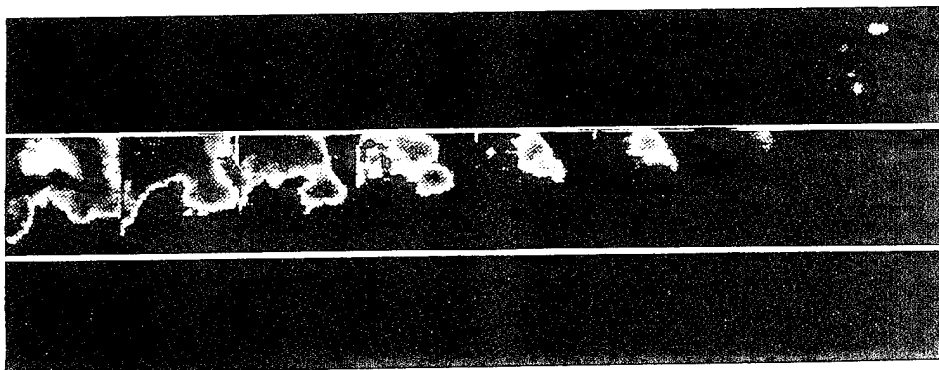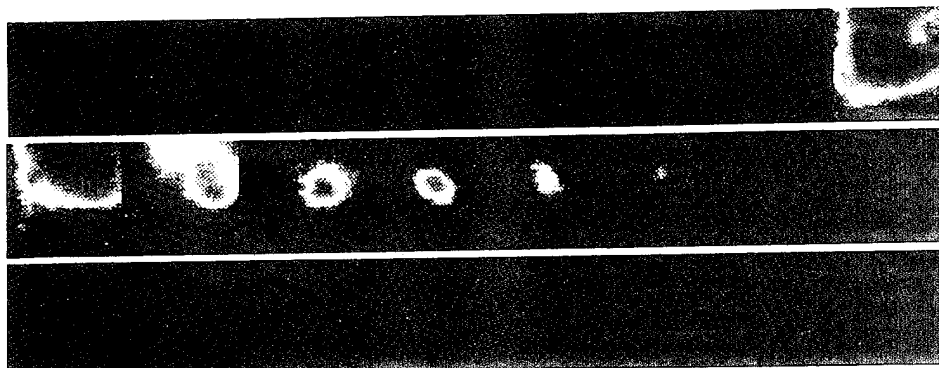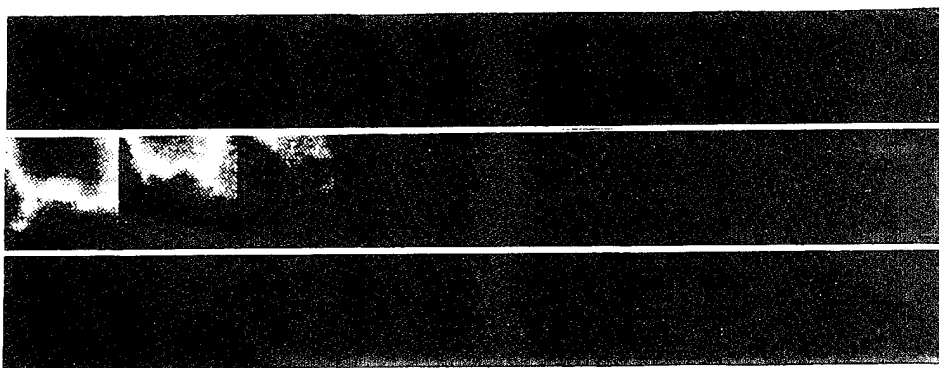
Fig. 9. High-Speed Spectral Infrared Images of In-Cylinder Reactions Obtained in (A) 2.47μm, Neat Fuel; (B) 2.47μm, MTBE-5; (C) 2.20μm, Neat Fuel; (D) 2.20μm, MTBE-5, and (E) Look-up Table.

Discussion

In explaining the reduction of both emissions, several possible reasons in physical and chemical aspects may be considered. Physically, the addition of MTBE to the Diesel fuel is expected to alter the spray geometry and its characteristics. Chemically, the elemental reactions affected by the additives via either producing or eliminating key radicals, will modify the processes leading to the self-ignition and the formation/destruction of pollutants. The in-cylinder spectral IR images seem to exhibit some of the alterations. Change of the temperature distribution by the addition of the oxygenate in the reaction zones of the spray will affect both aspects of reaction. One of the probable chemical effects by the MTBE in the blend to consider for the present discussion is the modification of the critical reaction (mechanism) steps in both the formation and oxidation of the participating species to affect the emissions.

Soot Formation. The dilution of Diesel fuel by the low viscosity-surface tension oxygenate is expected to produce an altered spray having smaller droplet diameters, which will result in enhanced mixing. The high volatility of the oxygenate in the blend will also help promote the formation of the premixed gaseous mixture. These factors all will increase amount of heat release during the premixed combustion stage, which change is generally known to reduce the soot formation. The abrupt combustion of the premixed mixture seems to be somewhat delayed in the MTBE blend operated engine, as observed from the in-cylinder images.

In addition to the physical roles of MTBE in the blend, the oxygenate itself has a low tendency of forming soot. The volumetric displacement of Diesel fuel by MTBE in the blend, therefore, is expected to produce smaller amounts of soot. If this effect is strongly prevalent, one could expect to observe proportionately decreasing soot emissions with increase of MTBE in the blend. The measurement, however, does not seem to support this expectation, namely, no effect of the volumetric portion of MTBE on the emission was observed (Fig. 8-(B)). According to the present measurement, the dilution role of MTBE may not be a significant factor on the soot formation.

The chain-branched compact-molecular structure of MTBE is considered to have a relatively greater resistance to decomposition during the ignition delay period (and in the preflame zone of SI engine combustion). This is an opposite characteristics to that of other ethers having a straight chain structure, which have a tendency of easy self-ignition, as often used for aiding the cold-start of CI engines. This tendency of hard-to-decompose and MTBE's consumption of OH radicals during the (low-temperature kinetic) reaction are expected to affect both physical and chemical aspects of soot formation. The role of removing OH radicals will provide more physical time for the other fuel species in the blend with a greater tendency of soot formation to be vaporized and mixed with air, consequently to produce overall smaller amounts of soot.

Chemically, the role of eliminating OH and/or the role of oxidation would break the chemical steps of the soot formation, which may occur via oxidation of the soot precursor radicals and/or growth species (e.g. acetylene). In addition to this potential effect at the formation stage, because of its tendency of hard-to-react, some portion of MTBE may even survive to be decomposed at the later stage of combustion. (This probability may be low if the oxygenate is mostly exposed to the high-temperature reaction zones.) If it survives by a significant portion until the later stage of combustion, which is dominated by the diffusion combustion mode and when the soot formation is expected to be most active, its late decomposition would affect the elimination of soot. That is, the role of oxidation by MTBE is expected to help oxidize the soot nuclei before coagulation. This consideration of the probable late oxidation of soot by the MTBE blend reminds us an observation made from the in-cylinder soot radiation images. That is, the radiation from the soot cloud disappeared at a higher rate in the MTBE-5 fueled engine.

Let us look into the accelerated soot oxidation in terms of the physical alteration of the spray (thus the reaction zone) in the MTBE blend operated combustion, as explained earlier. This remark is made from the comparison of images obtained using the MTBE blend and the neat (for example, see corresponding images obtained from 8 through 20 after TDC in Fig. 9-(A) and -(B), respectively. Images obtained in the MTBE-5 operated combustion indicate a greater area of inflammation in the (two-dimentional in line-of-the-sight) picture. When such a spreading (thus, fuel thinning) effect of the reaction zones is significant, the availability of oxygen for the consumption of soot would be high. Having mentioned the thinning effect, let's recall that no significant difference on the soot formation was observed when the portion of MTBE was varied in the blend, regardless of the injection timing. This may rule out the significance of its diluting role, which is considered to be a different kind of thinning effect from that mentioned above.

The consideration as to the (chemical) roles of eliminating OH, and oxidizing the key precursors and growth species affecting both the formation and oxidation processes of soot nuclei is interesting, but the details are not available for any further analysis. Such key roles expected at those stages, however, may well be achieved even by a small amount of the oxygenate in the blend, which seems to be supported by the present exhaust measurement. This discussion is made in view that the smallest soot (and NOx) emissions were measured when the engine was operated by MTBE-5 of all blend operations we investigated.

NOx Formation. The same factors mentioned above for explaining the soot emissions are expected to affect the NOx formation in one way or another. Under a given overall fuel/air ratio, a mixture would produce smaller amounts of NOx in the mode of premixed combustion than the diffusion combustion. The basic argument for this expectation is that the flame temperature in the rich pockets of a diffusion flame is higher than that in a relatively lean premixed flame. Note that this is often mentioned in predicting the low NOx emission by the uncooled CI engine, which is predicted to have a greater portion of heat release in the premixed combustion stage. This argument, however, is in conflict with other factors dictating the NOx formation. Among the basics concerning this conflict is that a greater amount of heat release in premixed combustion (which is known to produce low soot emissions) provides a longer

period of reaction time (with the after-compression) for more NOx formation.

The flame temperature is expected to be a bit lower with the blend because the heat of combustion of MTBE is slightly lower compared with neat Diesel fuel. The lowest NOx emissions obtained by the blend of 5% MTBE of all tested, however, suggest that this thermal effect on the NOx formation may be insignificant. That is, a higher portion of MTBE did not necessarily lead to lower NOx emissions. This issue of heating value of the fuel is not pronounced to be unimportant because its effects might have been offset by some significant (physical) change in the spray formation.

Regarding the NOx formation (in the chemical aspect), several routes of formation have been considered in the past, e.g. the Zeldovich scheme, the extended Zeldovich mechanism, the prompt NO formation and the fuel-bound nitrogen. In this discussion, however, the reaction involving OH radical is only mentioned because of the similar reasons discussed in the soot formation. If the OH radical population becomes low due to its consumption by MTBE, the NO formation, via the extended Zeldovich mechanism, N + OH -> NO + H, will become affected. Reviewing the basic characteristics of other elementary steps involving this reaction, the reaction constant of the forward reaction is independent of temperature, while the formation of N radical is only possible at high temperatures, and the OH consumption by MTBE is expected to occur via the low-temperature kinetic reactions. Obviously the species concentrations are mutually exclusive. Due to the insufficient information as to the reactions determining the OH population (in the MTBE blend fuel reaction) and the complexity in these elementary steps, no simple and convincing analysis of this aspect appears to be attainable.

Recalling the observation that the most significant NOx reduction was achieved by MTBE-5, even without comprehension of the chemical reaction details, one may expect that the role of MTBE on NOx formation is similar to that in soot formation. That is, some critical reaction chains seemed to have been affected by the incorporation of MTBE, which may be independent of its portion in the blend.

Mentioning the physical role of MTBE, as discussed before, the spray penetration appears to have an increased reaction volume (and mixed better) in the engine operation by the MTBE blend than the neat fuel. The probability of having pockets of high temperature is low under such a condition. Since this physical aspect helps thin out the reaction intensity and since the heating value of the MTBE blend is slightly lower than the neat, it is reasonable to expect that the reduced high-temperature zones would produce low NOx emissions. This again is consistent with such exhaust NOx measurements as explained earlier using Fig. 8-(A).

A brief review of the present results reminds us low emissions of both soot and NOx from spark-ignition Diesel engines fueled by methyl alcohol. It is noted that the present approach does not require a major modification in the engine. The favorable emission and performance results obtained from both approaches of using oxygenated fuels suggest their potential of reducing the emissions from Diesel engines. That is, when the in-cylinder reaction is properly controlled by either modifying the engine (e.g. by using an electric ignition device) or formulating new fuels The latter approach includes oxygenated fuels having a high cetane number that facilitates the self-ignition. The present experiment was to study one of such fuel formulations.

Summary

The engine performance and emission characteristics were investigated when an indirect-injection CI engine was operated by Diesel fuel containing small amounts of MTBE. The blends included portions of MTBE by 5, 10, and 15% in volume. The results were compared with those obtained using the neat Diesel fuel. In order to explain the findings from this measurement, instantaneous spectral images were obtained from a direct-injection type CI engine using the Rutgers high-speed infrared imaging system.

The effects of MTBE blend on the engine operation were investigated to find several new results, including: the longer ignition delay; the shorter combustion period, seemingly a increased size of the reaction zone. In spite of these change, the engine performance was quite comparable each other in the ID CI engine experiment (but some deterioration in the DI CI engine operation), and the brake thermal efficiency with MTBE blends was remarkably higher. The performance measurements are consistent with most results obtained in the IR imaging.

The MTBE blend produced low emissions of both soot and NOx. The low soot emission is consistent with the longer ignition delay period observed with the MTBE blends. While its chemical role in the soot formation is not known at the present, some physical aspects, that is, an increased size of the reaction zone, appears to be a plausible reason for the observation. This would reduce the tendency of producing high-temperature pockets. In addition, the weaker premixed combustion stage is expected to reduce the NOx emission. The low soot emission may also be explained by the thinly populated soot being rapidly oxidized in the MTBE blend operated engine. The in-cylinder imaging results seem to back up this consideration by revealing that (although the formation of soot in the early stage of combustion looks mutually comparable in both the neat and blend fueled operations) the soot image became thin more rapidly in the blend fueled engine.

There is no question that an additional study of the issue is needed, for some of the findings are highly intriguing, such as the observation of the lowest NOx and soot emissions when the engine was fueled by MTBE-5. Although the chemical roles of MTBE may be important to affect the in-cylinder reactions as reflected in the present findings, no in-depth discussion is attempted here because simply they are not known well.

References

1. Li, H., Prabhu, S. K., Miller, D., and Cernansky, N., "The Effects of Octane Enhancing Ethers on the Reactivity of a Primary Reference Fuel Blend in a Motored Engine," SAE Paper-940478, 1994

2. Jiang, H., McComiskey, T., Qian, Y., Jeong, Y.I., Rhee, K.T., and J.C. Kent,"A New High-Speed Spectral Infrared Imaging Device Applied for Imaging Gaseous Mixtures from Combustion Devices," Combustion Science and Technology, 90, 5-6, p. 341, 1993.

3. McComiskey, T., Jiang, H., Qian, Y., Rhee, K.T., and Kent, J.C., "High-Speed Spectral Infrared Imaging of Spark Ignition Engine Combustion," SAE Paper-930865, 1993 and also in the 1993 SAE Transactions.

4. Jiang, H., Qian, Y. and Rhee, K.T., "High-Speed Dual-Spectra Infrared Imaging," Optical Engineering, 32 (6), pp. 1281-1289, 1993.

5. Jeong, Y.I., Qian, Y., Campbell, S. and Rhee, K.T., "Investigation of a Direct Injection Diesel Engine by High-Speed Spectral IR Imaging and KIVA-II," SAE Paper 941732, 1994.

Spectral IR Images of Direct-Injection Diesel Combustion by High-pressure Fuel Injection

E. Clasen, S. Campbell, and K. T. Rhee
Department of Mechanical and Aerospace Engineering
Rutgers, The State University of New Jersey
Piscataway, NJ 08855

Abstract

Instantaneous successive spectral infrared (IR) images were obtained from a spray plume in a direct injection (DI) type compression-ignition (CI) engine during the compression and combustion periods. The engine equipped with a high pressure electronic-controlled fuel injector system was operated by using D-2 Diesel fuel.

In the new imaging system used for the present study, four high-speed IR cameras (with respective band filters in front) were lined up to a single optical arrangement containing three spectral beam splitters to obtain four spectral images at once. Two band filters were used for imaging the water vapor distribution and another two band filters were placed for capturing images of combustion chamber wall or soot formation.

The simultaneous imaging was successively triggered by signals from an encoder connected to the engine. The fuel injection parameters were precisely controlled and the pressure-time (p-t) history was obtained for individual sets of images. The start of fuel injection was varied through four different crank angle positions.

Mentioning some results from the study, the spectral IR images had no resemblance with the ones obtained using a visible-range camera from a comparable engine system as reported by others. In general, the present spectral images taken at the same crank angle were not mutually comparable.

A highly unexpected phenomenon was observed in the study, i.e., the images recorded during the ignition delay period exhibit some strong preflame reactions over the fuel spray plume. The preflame reactions appear to have started *immediately after* the fuel injection. This newly observed phenomenon is interpreted to represent strong chemiluminescence seemingly followed by exothermic reactions. The heat release during the ignition delay period is expected to be offset by the latent heat of evaporation to cause no measurable change in p-t history compared with the same measured from a hot-motoring condition.

Introduction

A direct injection (DI) compression ignition (CI) engine has advantages over an indirect injection (IDI) engine, including higher efficiency and power density. The engine's simple induction system and open chamber for rapid heat release, however, produce low gas motions. This requires a greater role by the fuel injection unit for improved mixing, particularly if a high smoke-limited power output is to be obtained. A "better" injector is also desired for increasing the engine speed and induction pressure, both of which are typical design practices employed for achieving a higher power density.

Any measure of improving the engine performance, however, is only useful when the new engine meets the regulatory emission standards and other desirable characteristics, e.g. low noise and easy starting. In developing an improved DI-CI engine that delivers those desirable engine characteristics, some of which are mutually exclusive with each other, many unconventional changes in the engine-fuel system are implemented, such as: very high pressure fuel injection (HPI); multiple fuel injections per cycle; pilot injection; new fuel additives; fuel reformulation (e.g. oxygenated fuels having high cetane number), and even oxygen-enrichment of the intake air. In view of the ever growing demand for an improved engine by the law as well as engine-users, such radical changes in both the engine and fuels will continue to be explored in the future.

Note that some of those methods have already offered promising improvement: For example, a tailored-double fuel-injection (achieved by an electronic-controlled injector) produced low emissions of both NOx and particulates. The HPI, a similar methodology of tailored-injection, also appears to be an attractive strategy for advancement of Diesel engine technology. It is to complete the fuel injection within a short period of time by starting it relatively late but delivering fuel at a high rate. The method is expected to result in smaller droplets more uniformly spread over a large volume of fuel spray plume, which gives rise to a short ignition delay. The uniform distribution is

expected to reduce excessively fuel-rich (high-temperature) pockets. These all would help produce more rapid heat release occurring at a somewhat delayed time, which is expected to improve thermal efficiency and to produce low emissions of NOx and also particulates.

While those developmental measures are incorporated with the system basics of existing DI-CI engines, there is no doubt that the development can be much better facilitated (e.g. design of a new matching combustion chamber) if the in-cylinder reaction processes are better understood when such engine-fuel changes are made. Probably one of the more important pieces of information missing at present are those about thermo-chemical behaviors as fuel and air are mixed during the period of early fuel injection or ignition delay, particularly when the injector parameters are greatly changed. (It is noted that the same is not well known for the existing engine either.) It is reasonable to predict that the preflame reactions altered by the HPI highly dictate the subsequent in-cylinder processes.

In spite of their usefulness in other aspects, the images of very high-temperature reaction zones (during the post flame period), obtained by using conventional high-speed photography (or a visible-range light sensor), do not directly indicate what is happening during the preflame period. In addition to helping study invisible (low-temperature thermal) as well as visible in-cylinder processes, a new engine/flame diagnostic system has been developed during last several years [1-4]*. The system simultaneously captures four identical infrared (IR) images in respective spectral bands at high rates for quantitative analysis. For convenience of discussion, this system is hereafter called as Rutgers system, or super imaging system (SIS) as referred to by others. This prototype system, made operational in early 1994, has continuously been improved and new data-processing methods have also been developed for its enhanced applications to engine/flame studies. The present paper reports some of results obtained using the methods for investigating in-cylinder processes of a DI-CI engine equipped with an HPI system.

Experimental

The engine apparatus having an IR optical access equipped with an HPI injector is briefly explained, which is followed by a description of the Rutgers system or SIS. The advantages of obtaining multispectral IR images from the engine are also discussed.

Engine. A new single-cylinder DI-CI engine was constructed in collaboration with Power Energy International (Madison, WI) and BKM, Inc. (San Diego, CA), under a sponsorship of the U.S. Department of Defense University Research Initiative. The engine body was constructed to accommodate components from a Cummins 903 engine. It is pointed out that in this new single-cylinder arrangement, the engine (Fig. 1) uses a section of the 903 cylinder head to obtain representative characteristics of the DI-CI engine

*Numbers in parentheses designate references at end of paper.

population. In order to facilitate future investigation of other combustion problems, the new engine design-construction incorporated several flexible design considerations, such as separate control of both coolant and oil flows in the cylinder head and the block, respectively; reserving a large amount of space in the crankcase (e.g. for easy installation of a linkage system that retains thermocouple wires from the piston-crown to the data system outside the engine crankcase).

Some modifications were made on the Cummins engine cylinder head for installing an IR optical window: conversion of one of the intake valves to the optical access; a new rocker-arm mechanism, which provided a cylindrical space for the optical passage; a pressure transducer installed flush with the chamber wall; a measure to use either a Cummins (mechanical) PT unit injector or BKM's Servojet electronic-controlled HPI injector. In addition, since the installation of the IR window was to be made leak-proof, while permitting frequent cleaning of the soot deposit over the surface, an installation method was newly introduced by using an o-ring [4]. (The typical time required to complete the window cleaning was about three minutes.) The optical access (with viewing area of 37mm diameter) was made barely big enough to cover the projected view of a spray plume out of an eight-hole (0.15mm diameter) nozzle, which assumes all spray plumes to be identical. Figure 2 shows the axes of plumes with respect to the (imaging) optical access, which will be referred to when the in-cylinder spectral IR images are discussed later.

High-Pressure Injection. The electronically controlled HPI system which replaced the Cummins PT type injector in our 903 engine for the present study was basically a Servojet unit injector of the accumulator type [6]. Because of the crowded engine cylinder head due to new installation of an optical access and a pressure transducer (in addition to the existing components such as the valve train), the relatively bulky Servojet unit was not usable in the apparatus. Keeping the original system design features, an entirely new injector unit was fabricated in our laboratory: Among the key considerations taken into account for this was to use original injector tips of the Cummins PT nozzle, which was to provide technical and economic flexibility in choosing different injector tip geometries. The operation of the injector was performed by using the same electronic package given with the original Servojet unit.

An extensive bench-top characterization of this new injector package was performed prior to in-cylinder measurement. This was necessary to determine several important pieces of information about the new HPI, including the relationships of the actual start of fuel injection and the amount of fuel injected per cycle to the input control by the electronic signals, i.e., the pulse width and timing, and the accumulator pressure, respectively. It is pointed out that the start of injection was defined as the time when the fuel plume tip reached a sensor located about 10mm away from the injector nozzle hole. The injection (sac) pressure-time history was not measured in the present characterization, but is inferred to be the same as the original unit [6], which resembles a spike-shape that collapses rapidly to have a very short residual period of low injection pressure.
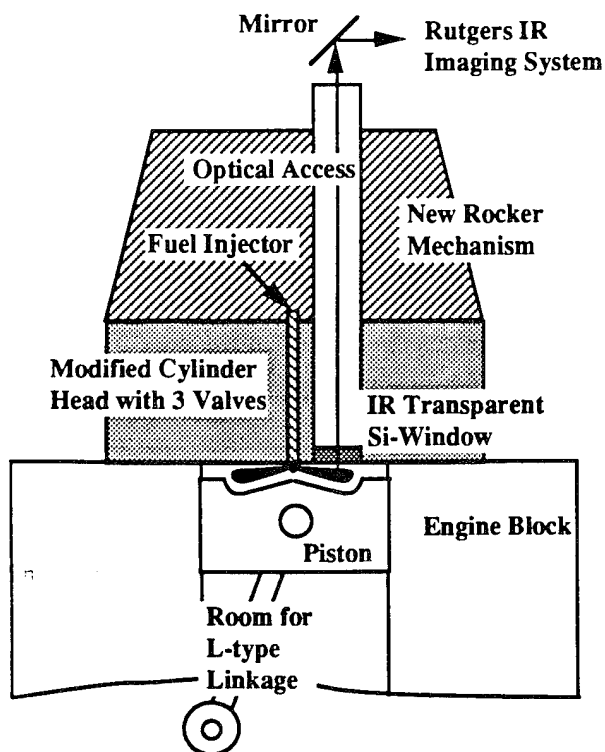
2

Fig. 1. Schematic Presentation of the Single Cylinder
Engine Mounted by a Cummins 903 Cylinder Head
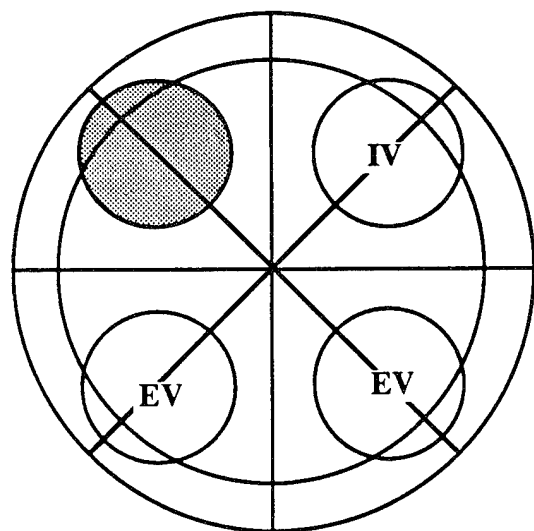with Optical Access for the SIS or Rutgers IR System.

Fig. 2. Optical Access (shaded area) with respect to
Spray Plume Axes.

**High-Speed Multispectral Infrared Imaging
System.** The "fingerprint" of (both low and high
temperature) thermo-chemical molecular characteristics
(such as distributions of temperature, reaction fronts and
species population) can be found more in the IR domain than
the visible range. This fact motivated us to develop a new
high-speed spectral IR digital imaging system several years
ago. The development of our IR system at Rutgers has been
a progressive course of work. The first generation of this
research tool captured successive flame images at high rates
using only a single camera head [1]. The next system
employed two camera heads in order to capture two
geometrically (pixel-to-pixel) identical IR images in
respective spectral bands, i.e., a two-color system [2,3],
which permitted determination of temperature and water
vapor distributions in flames [3]. Its prototype electronic
systems were all fabricated via hand-wiring directly using
many transistor-transistor-logic (TTL) components. One of
the main functions of the camera circuits was to generate the
timing signals required to operate the charge-coupled-device
(CCD). This two-color system was redesigned (using Protel
and Orcad design systems) and constructed in printed
boards, which included several programmable logic gate
arrays (using Max-Plus, Altera Corp.) that replaced most
TTL components to take IR images having minimum noise.

In the new system, four separate high-speed IR
cameras are lined up to a single optical unit, and are
simultaneously triggered at successive instants of time by
using signals generated from the engine being investigated,
which permits capturing a set of four geometrically identical
images at each moment. In order to maximize the radiation
energy incident on the imagers housed in the liquid-nitrogen
cooled Dewars, a large reflective optical head (152mm
diameter) was employed which was followed by three pieces
of new spectral beam splitters. This divides the IR domain
into four ranges for respective imagers. Narrow band filters
were installed in front of respective cameras. Among the
filters with central wavelengths employed to date are 2.2μm,
2.47μm, 3.43μm, and 3.8μm. In spite of a small amount of
radiation passing through those band filters, cryogenically
cooled PtSi imagers have sufficiently high sensitivity.
Unlike in most high-speed visible-range imaging, no separate
(IR) light source was needed.

Since the development of our IR imaging system
was an unconventional attempt using IR imagers (64x128
PtSi Schottky-barrier detector) other peripheral units were
newly designed/fabricated in our laboratory. Figure 3 shows
a block diagram of this four-color system, or SIS. Those
printed in an outlined font in the figure were newly
developed at Rutgers because no ready-made substitute was
available at reasonable costs on the market. The imaging rate
is changeable to obtain over 4 x 1,800 frames/sec and the
exposure period can be adjusted at the same time to have as
short as 10μsec. The imaging system was integrated with a
new package of electronic circuits to independently vary: (1)
the start of imaging; (2) the interval of imaging (as
individually triggered by the corresponding engine CA
markers); and (3) the number of images to be captured per
cycle of the engine. As mentioned before, this prototype
four-color system which was made operational earlier had
many things to be improved upon, which include several
modifications in the imager-driving circuits for increased
sensitivity, disposal of video signal prior to digitization, and
elimination of unwanted charge generated during the off-data
acquisition periods. A parametric study of the new imaging
system for characterizing its performance was an important
precondition in order to obtain predictable and consistent
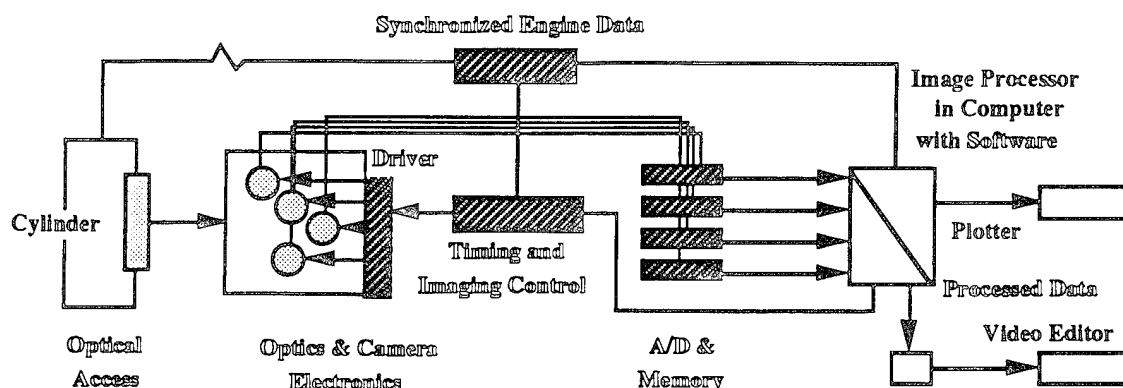digital images under various imaging conditions.

3

Fig. 3. High-Speed Multispectral IR Imaging System with Data Acquisition-Processing Units.
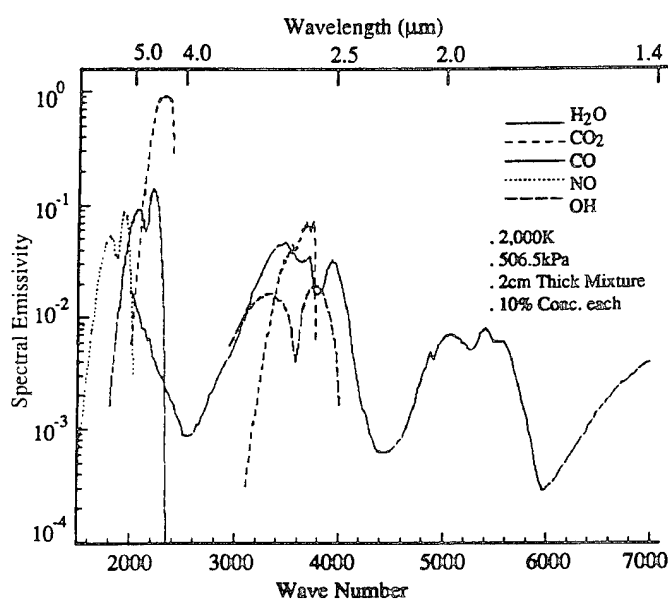

Fig. 4. Spectral Emissivity of a Gaseous Mixture having thickness of two centimeters at a uniform temperature of 2,000K and five atmospheric pressure.

Quantitative Imaging. The digital data from individual pixels of spectral images are obtained in a 12-bit dynamic resolution, which are then processed for "quantitative imaging." In order to discuss the method of processing digital data from four spectral images, Fig. 4 is included. This diagram was constructed by using our data-based computer program that employs the single-line-group model by Ludwig, et al. [5]. The spectral emissivity was calculated for the condition indicated in the diagram, which suggests that images captured in wavebands of 2.47μm and 3.43μm indicate radiation emitted from water vapor contained in the combustion product and those obtained in wavebands of 2.2μm and 3.8μm represent radiation from the combustion chamber surface having minimum (radiative) participation by the product in front.

Our new dual-band method previously applied [3] for determining temperature and water concentration distributions in a simple hydrogen-air flame is extended for hydrocarbon-fueled engine applications, which may use the former pair of bands. Because of strong radiation from soot in diffusion flames, however, an application of this method in a CI engine is deferred. Instead, those obtained in the latter pair of bands are expected to show the radiation from the soot cloud with minimum interference from other gaseous combustion products and from the background wall surface when the engine is relatively cold. (In fact, the wall radiation was insignificant compared with those from combustion products, even when the engine was warm.) Thus, determination of spatial and temporal distributions of temperature and soot cloud in the plume is being performed: The technique for this quantitative imaging was extensively explained elsewhere [4]. The multispectral images, therefore, were expected to allow us to observe the formation of soot and combustion reactions.

This original objective of determining the in-cylinder temperature distributions has been temporally put aside upon finding a new phenomenon, which indeed became the main topic of the present discussion. It might be added that images simultaneously taken in those IR filter bands have been quite unpredictable and offered new opportunities of freshly thinking about in-cylinder processes.

Results and Discussion

Again, although the *thermal nature* of high-speed spectral IR images obtained using the SIS was kept in mind, those captured from the present DI-CI engine exhibited a highly unexpected feature. When an early exploratory study of in-cylinder reaction processes was performed by using the present SIS, something never reported in the past was observed. High-speed images obtained in the 3.43μm (with 200nm width) band exhibited measurable and strong signatures of preflame reactions during the ignition delay period, which appeared to have started *almost immediately after* the fuel injection. That is, they preceded those indicating the first presence of final combustion products,

4

e.g. water vapor and soot, as obtained in other spectral bands. In addition, no direct similarity was found between the present results and those obtained by visible-ray high-speed photography [6].

In order to concentrate on investigation of the "preflame reaction" mentioned above, the optical train was slightly modified to capture two spectral images at the same time, i.e., one was in a spectral band of 2.2-2.5μm and other was in the 3.43μm. This change was made in order to capture the presence of not only soot but also water vapor using the former band (see spectral diagram in Fig. 4), and the new preflame image in the latter band.

Engine and Imaging Conditions. In this study on the new phenomenon as well as the subsequent processes, the injection time was varied, but the intake manifold pressure was maintained at 15.6kPa (gage pressure) and the engine was operated at approximately 500rpm throughout the experiment. Although the exact injection pressure at the sac volume is not known, according to the line pressure, which is intensified by factor of sixteen times in our new injector, it was expected to be around 165 MPa.

The imaging was performed with the object cassagrain at about 100cm away from the mirror mounted on the cylinder head (Fig. 1), which approximates the imaging via parallel rays. Although images can be captured in an (electronically controlled) exposure period as short as 10μsec (using a wide band filter), in order to obtain all of the spectral images in comparable intensity, apertures were placed in the optical path where needed. The exposure period employed for the present work, therefore, was increased to 190μsec. As briefly mentioned earlier, images in the band ranges were simultaneously obtained as triggered by corresponding signals generated from the encoder connected to the test engine. The interval between successive sets of images was three crank angles.

After the engine was warmed up, the IR window was cleaned for each experiment. The imaging was performed within several cycles from the start of the engine. During these early periods of running, the window (in the engine with the present HIP) did not have a significant amount of soot deposit affecting the image quality. Note that the IR imaging is far less affected by the window deposit than visible-ray photography.

Injection Time and Pressure-time Diagrams. Imaging was performed with the engine operated by starting the injection at four different crank angle positions: (1) 25 before TDC (i.e., bTDC); (2) 18bTDC; (3) 12bTDC; and (4) 4bTDC. Figure 5 shows the pressure-time (p-t) diagrams obtained from each of these conditions together with the same recorded under a hot-motoring condition. In spite of the injection time variation, when the amount of fuel injection was maintained the same throughout the experiment, the torque outputs were mutually comparable with each other. Generally speaking, according to the p-t history, the CI combustion engine with the present HIP appears to be quite comparable with the typical results expected from the counter parts equipped with a mechanical PT type injector unit [4].
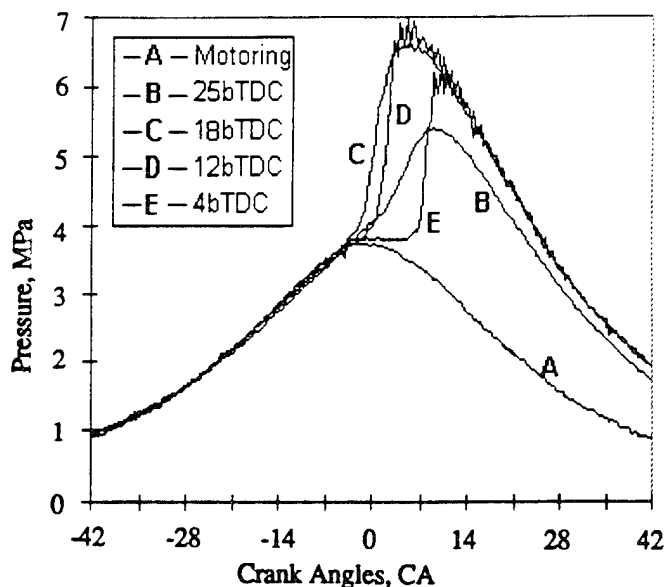

Fig. 5. Pressure-time Diagrams for Varied Injection Times and Hot-motoring Condition.
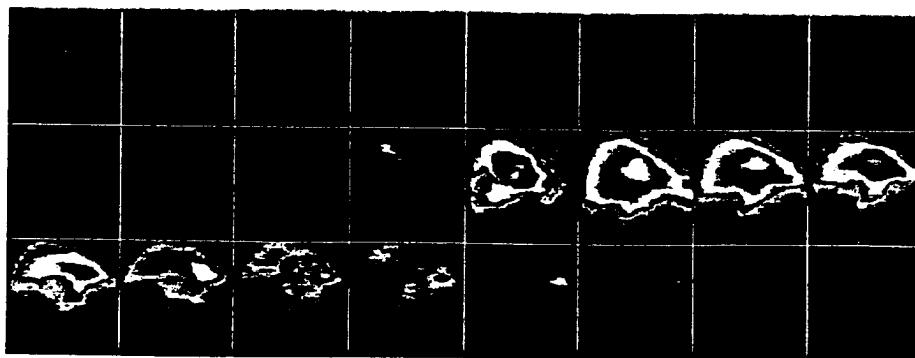
Spectral IR Images. Sets of spectral IR images captured in the band of 2.2-2.5μm and 3.43μm, are shown in Figs. 6 and 7, respectively. They were obtained by varying the start of injection, as mentioned above. The sequence of the images goes from the left to right and continues from the top to bottom, which may be referred to a corresponding look-up table (LUT) included in Table-I. (Note the minus sign indicates crank angle position before TDC.) Explaining the LUT and corresponding images, the imaging started at -34 in all of the experiments. But, since the images obtained with injection time at 4bTDC had some residual signatures even after 35 aTDC, eight additional frames were included in both Figs. 6-(4) and 7-(4) as well as in Table-I, which covers images over a period from 38 through 59 degrees in crank angle position.

The sets of images obtained in two spectral bands (i.e., one band of 2.2-2.5μm showing only the final combustion products, and other of 3.43μm exhibiting the preflame reactions as well as the subsequent combustion products) are plotted in pseudo-color. The relative strength of radiation was normalized within individual sets of images. Therefore, the colors do not represent a direct comparison between these two groups of spectral images.

Ignition Delay and Preflame Reactions. Reviewing results shown in Figs. 6 and 7, and referring to the p-t diagrams, Table-II was prepared. A few remarks are in order prior to discussion of the table: As indicated earlier, the injection time was defined as the moment when the fuel plume tip reaches about 10mm away from the nozzle hole. In addition, since the successive imaging was performed in a three-crank-angle interval, the exact time of the "first" image listed in the table has a maximum error of two crank angle degrees.
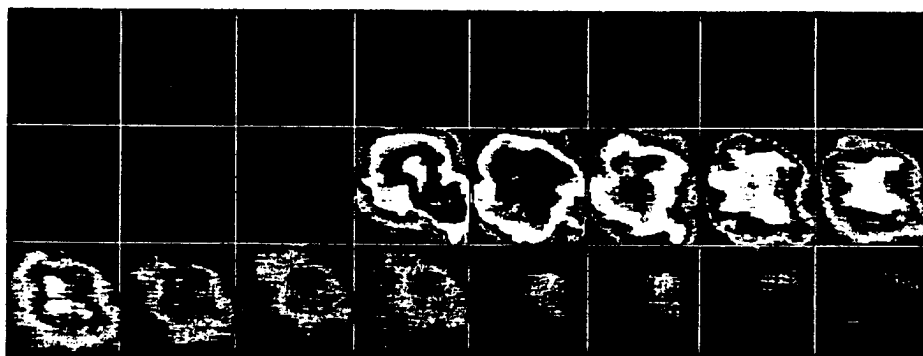
5
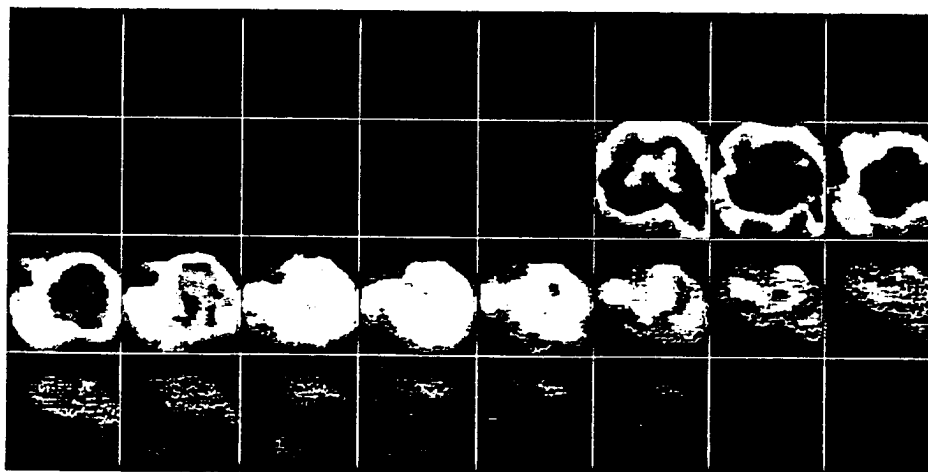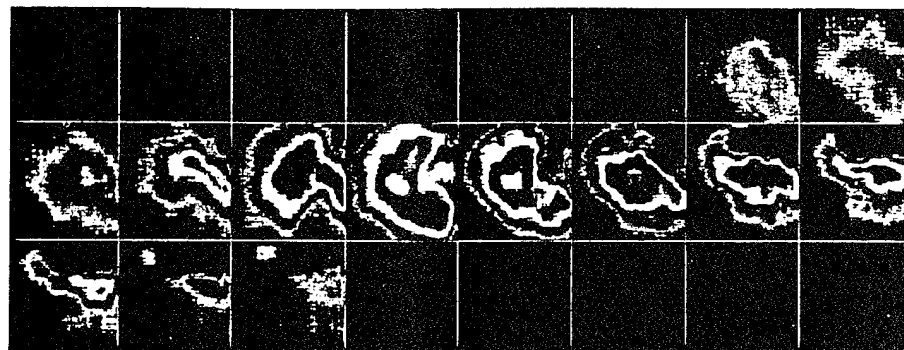
Fig. 6. High-speed Spectral IR Images of a Plume in CI-DI Engine Combustion Chamber
in Band of 2.2-2.5μm for Injection started at
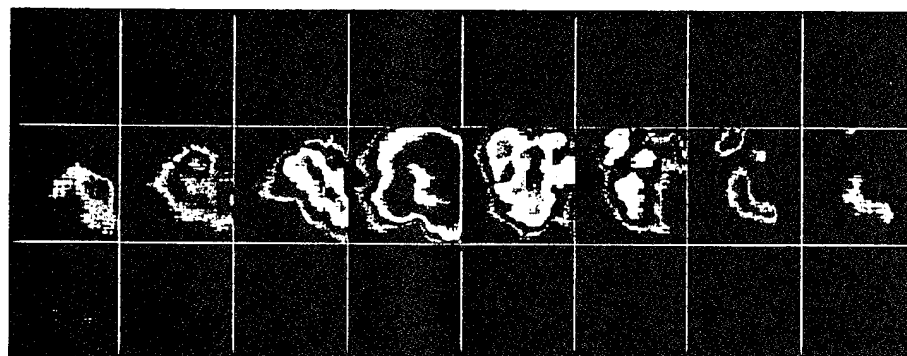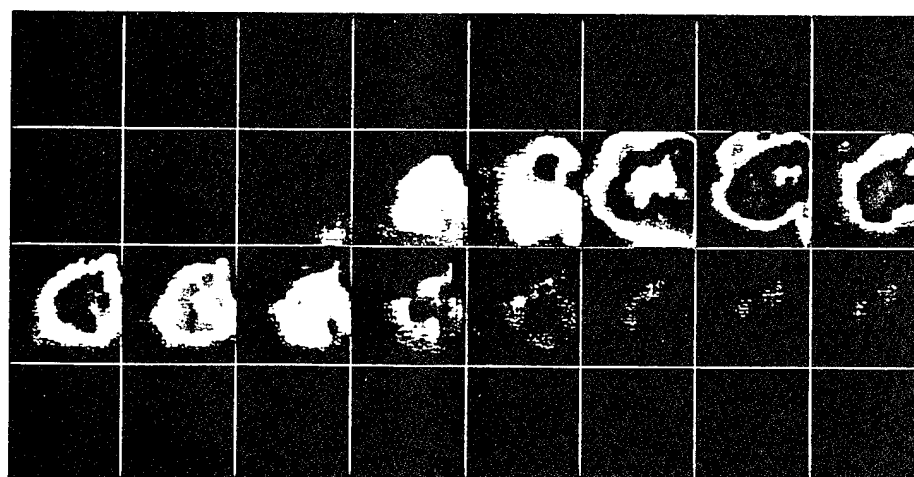(1) 25bTDC); (2) 18bTDC; (3) 12bTDC and (4) 4bTDC.

6

Fig. 7. High-speed Spectral IR Images of a Plume in CI-DI Engine Combustion Chamber
in Band Filter with Central Wavelength of 3.43μm for Injection started at
(1) 25bTDC); (2) 18bTDC; (3) 12bTDC and (4) 4bTDC.

1	-34	-31	-28	-25	-22	-18	-15	-13
2	-10	-7	-4	-1	2	5	8	11
3	14	17	20	23	26	29	32	35
4	38	41	44	47	50	53	56	59
	a	b	c	d	e	f	g	h

Table-I. Look-up Table for Figs. 6 and 7.

In general, results in the table seem to be consistent with each other. The ignition delay periods inferred from p-t diagrams are longer than those determined by the time of first combustion product image (in 2.2-2.5μm band). This was observed to have a difference of two crank angles throughout the results, which may be actually of up to four crank angles due to the error, as mentioned above. The difference is not considered to occur due to a slow response of pressure measurement instrumentation but the phenomenon itself. Possibly, the latent heat for fuel evaporation would delay the pressure rise. (This, however, assumes that there are zones at high temperatures as reflected by strong thermal images of combustion products in 2.2-2.5μm band, and zones at relatively low temperature due to the latent heat of evaporation offsetting the energy released by the exothermic reaction.) The most intriguing finding is that the first image in 3.43μm band was captured *almost exactly the same time* of the fuel injection, which was an unexpected new observation.

Injection Time	-25	-18	-12	-4
Start of Rapid Pressure Rise	1	-2	1	7
First 2.2-2.5μm Image	-1	-4	-1	5
First 3.43μm Image	-25	-18	-10	-4

Table-II. Crank Angle Positions of Various Events.

The first response to this finding was to look at the spectral diagram such as shown in Fig. 4. According to this diagram, the only significant species radiating via 3.43μm band include the OH radical and water vapor. The role of water vapor (or soot), however, was ruled because no image in 2.2-2.5μm band was found at the same crank angle positions.

Since the water vapor was not expected to be produced during the ignition delay period, as a logical consequence, it was decided to obtain images in a new spectral band that would reveal the presence of OH radicals: For this, simultaneous spectral imaging was performed via a band with central wavelength of 3.25μm and the band of 2.2-2.5μm (refer to Fig. 4 again). At this time, it was not a surprise to obtain a similar finding, that is, preflame images were also captured through 3.25μm band as in 3.43μm band.

Without excluding a possibility that some other unknown species in the plume radiated to result in such early images (during the ignition delay period), for now it does not seem too unreasonable to consider that they are likely OH-radical images. If this is the case, one can expect that fuel droplets exposed to high-temperature cylinder air immediately start to undergo active chemical reactions, which is not what has been known in the past. Also, it is not known at present if such an early reaction is only a unique phenomena in a HIP operated CI combustion (compared with a counter part with a relatively low pressure fuel injection unit), which warrants further study.

Two possibilities are considered in identifying causes for the instant preflame images, i.e., thermal or chemiluminescent effect. Suppose the reaction centers were at sufficiently high temperatures due to heat release to put out such amounts of measurable radiation energy. This, then, assumes that, during the period, the latent energy for fuel evaporation would have to be high enough to offset the amount by the exothermic reaction resulting in no measurable pressure rise compared with p-t data obtained in a hot-motoring condition. This seems to be consistent with other consideration: Recall that the role of the latent heat of evaporation, which was expected to cause the delayed pressure rise after the first strong image of combustion products was observed earlier by as much as an interval of 2-4 crank angles. It is pointed out again that this discussion is made on an important assumption that within the same spray plume, hot mixture pockets (as assumed to have been captured in 3.43μm images, if it is a thermal effect) coexist with (cold) fuel-air volumes where vaporization is active enough to balance out the energy release from the exothermic reaction. Although it is not an impossible phenomenon, it seems difficult to imagine that within a plume two zones in quite different temperature ranges coexist: This consideration is particularly relevent to images obtained in the earlier portion of the ignition dealy period. Note that the role of a nonequilibruim condition between the photonic and thermal energy states possibly attributing to such an observation is not entirely ruled out.

On the other hand, the early images in 3.43μm may be mainly due to chemiluminescent radiations. By definition, chemiluminescence is referred to a chemical reaction leading to the formation of an atom or a molecule in an electronically excited state to radiate "a light emission out of all proportion to that to be expected from thermal emission" [7]. When the electronically excited species in such a reaction, i.e., C^* in a reaction like, $A + B + C = AB + C^*$, is in high concentration, it liberates radiation generally under a relatively low temperature environment. An additional possibility is that indirect chemiluminescence, which is referred to excited molecules formed in a chemical reaction, by collision, to pass on their excitation to other species, produces some unusually excited metastable species having more than a fair share of vibrational energy. Species

8

in such metastable states often mentioned in hydrocarbon flames include aldehydes, CH, C_2 and notably OH. Those radicals infesting the low-temperature reaction environment will be rapidly consumed, however, once the high-temperature processes take over the reaction.

Facts about Preflame Images? Now, we are faced with a question as to whether the preflame radiation occurred due to either a high thermal energy state of the injected fuel, or due to chemiluminescent reaction, or a combined effect of both. Mentioning the combined effect, as discussed above, it is more probable that the early portion of ignition delay is dominantly controlled by chemiluminescence reaction and the later portion of the period is dictated by exothermic thermal reaction.

In order to help find an answer, the following is summarized as observed from the experiment (not in an order of importance). A brief note is included, as much as deemed reasonable, in order to explain if the respective finding is consistent with either of the two processes or a combined effect, as considered above.

(a) Two sets of spectral image (i.e., 2.2-2.5μm and 3.43μm bands) obtained at corresponding crank angle positions do not seem to have strong resemblance each other. (Concerning resemblance, an additional observation is mentioned later.) This supports more the possibility of a chemiluminescence reaction process than a thermal one because if it was a thermally dictated process, the signature of two spectral images of combustion products would have been similar to each other.

(b) These IR images were not comparable with those obtained by using visible-ray high-speed photography [6]. This fact does not reject either reaction scheme.

(c) For engine operations with early injection time, almost no discontinuity was found in the successiveness of 3.43μm images even when the abrupt premixed combustion (observed in 2.2-2.5μm images) occurred (compare images 2-c with 2-d in Fig. 7-1; and 2-b with 2-c in Fig. 7-2 each other), but some significant discontinuity was realized for those with late injection (compare images 2-c and 2-d in Fig. 7-3; and 2-e and 2-f in Fig. 7-4 each other). The earlier the fuel injection, the more it mixes with air at lower temperature. The mixture would, therefore, produce more radical species as dictated by low-temperature chemistry. When the injection is made near TDC, the fuel is mixed with air at high temperature, which will produce radicals but they will be rapidly consumed leading to exothermic reactions. The transition from early stage to premixed combustion would be relatively less dramatic with early opposed to late injections.

(d) The earlier the injection time, the longer the preflame period but with relatively weak radiation intensity, and vice versa.

(e) Images in the 3.43μm band were also found even after the occurrence of the premixed flame combustion, which look similar to those obtained before the onset of the premixed combustion flame (for example, there are some similarity between the images 1-e through 1-h and those 3-a through 3-d in Fig. 7-1). Since no chemiluminecent radiation will be liberated after the premixed combustion

Observation	Consistent with effects by		
	Chemilu.	Thermal	Combnd.
(a) No resemblance	xx		xx
(b) No comparison w/ photos	xx	x	xx
(c) Discontinuity vs. inj. time	xx	x	xx
(d) Inj. time vs. preflame	xx	xx	xx
(e) Late preflame-like image		xx	xx
(f) No pressure rise	xx	x	xx
(g) Delayed pressure rise	x	xx	xx
(h) Preflame image at injectn.	xx		xx
(i) Likely OH images	xx		xx

Table-III. Summary of Observation and Consistency with Probable Causes.

flame, the images in 3.43μm are *not all* from chemiluminescence.

(f) No pressure rise was observed during the preflame reactions. This more supports an expectation that chemiluminecent rather than thermal effects cause the preflame images.

(g) There was some time delay in the pressure rise after the premixed combustion. This seems to support a consideration of the thermal effect to produce the unusual images.

(h) The preflame images were captured immediately after fuel injection. It is hardly possible for the liquid fuel jet to immediately commence exothermic reaction.

(i) The images revealing preflame reactions seem to be those of OH radicals.

Due to the conflicting nature of these observations, it is difficult to clarify the causes for the preflame images. In order to sort out the observations to see if they are a result of either chemiluminescence or thermal reactions or a combined effect as mentioned above, Table-III was constructed. The number of x-marks indicates the degree of correlationship and no mark suggests low possibility. Although the table may be incomplete and has room for correction, this summary generally suggests that no single reaction mechanism is likely to explain all the observations, but a sequential combined effect is most consistent with the findings.

This suggestion is not unusual in nature by recalling the cool flame reaction followed by rapid thermal reaction observed in some hydrocarbon-air mixtures when they are suddenly exposed to a relatively low temperature reaction environment. The big difference between such two-stage combustion and the present observation is that (unlike the relatively long τ_1 period in a two-stage combustion) No 2 Diesel fuel injected into the DI-CI engine *immediately starts chemical reactions* to liberate radiations, as captured in 3.43μm (also in 3.25μm) band.

9

Onset of Flame Kernel and Flame Propagation.
The reaction processes involved in the ignition delay would greatly affect the subsequent (heat releasing) combustion processes, which dictates important engine behaviors, including noise, emission formation, and thermal efficiency. In addition, the location of the "very first" flame kernel formation is of great importance under varied operating conditions, because first of all it will help find the "most favorable self-ignition" zone (to be ignited earlier than others) within the plume.

The 3.43μm images obtained using the SIS appear to facilitate identification of the zone where the first (visible) reaction center starts. In spite of the fact that almost no resemblance being found between the two spectral images obtained at the same crank angle position, the ones in 3.43μm band captured during the early ignition period have some similarity with the very first (premixed combustion flame) image obtained in 2.2-2.5μm band. In general, the ones found (in 3.43μm) right before the premixed flame image (in 2.2-2.5μm) and the very first image of the premixed flame seem to have most similarity each other. For example, compare respectively, images 2-b in Fig. 7-2 vs. 2-c in Fig. 6-2; and images 2-c in Fig. 7-3 vs. 2-d in Fig. 6-3. If such a correlationship is further extrapolated, despite that CI in-cylinder processes are a rapidly changing transient flow reaction, it seems most probable that some localized reaction centers (in 3.43μm) identified in earlier crank positions are expected to be the spot for the first kernel formation.

The crank angle position when the first flame kernel occurred (with respect to the piston location) is also an important piece of information, because it triggers the consumption of fuel accumulated in the cylinder, which controls the temperature distribution and the pressure. In general, the earlier the injection, the smaller the amount of radiation from the first (premixed) flame, which can be seen by comparing images 2-c in Fig. 6-2; 2-d in Fig. 6-3; 2-f in Fig. 6-4. It is also noted that the earlier the injection time, the stronger the radiation from the combustion product and the longer the period of exhibiting flame images as seen in images in 2.2-2.5μm.

In order to evaluate in more detail the impact of the preflame reaction, the distributions of temperature and soot formation were determined by employing the techniques explained earlier. Results from this work, however, will be further studied for reporting in the future, mainly because of some uncertainty in their accuracy and inability to orrelate them with those reported here.

Summary

Upon performing an exploratory investigation of in-cylinder combustion processes of a DI-CI engine equipped with a HIP injector by using a new high-speed spectral IR imaging system, images in 2.2-2.5μm band and 3.43μm band were extensively obtained for investigation of a new discovery. The former band was to obtain images of combustion products (e.g. water vapor and soot) and the latter was to capture those of preflame reaction as well as subsequent combustion products.

What is new in the present result is that the fuel introduced into the combustion chamber (by the present HIP) undergoes active (preflame) chemical reactions immediately after the injection. In other words, we captured images of progressively changing preflame reaction zones throughout the entire ignition delay period until the very occurrence of the premixed flame. This finding is unusual because a conventional term, the physical delay, as deemed in the past, excludes the possibility of such chemical reactions taking place during this period.

Realizing that possible effects for liberating radiation as indicated in 3.43μm band images are either thermal, or chemiluminesecent or combined reaction processes, a summary of several new observations are listed before an interpretation for the discovery is offered:

(1) Successive images obtained in 2-2-2.5μm and 3.43μm bands at the corresponding crank angle positions do not have discernable resemblance to each other.

(2) Any of spectral IR images was not comparable with those obtained using the visible-ray high-speed photography from a comparable engine system.

(3) When injection was started early, there was almost no discontinuity between the succession of preflame reactions to the sudden (thermal) premixed flame, which was opposite otherwise.

(4) The earlier the injection time, the longer the preflame reaction period but with weaker radiation intensity, and vice versa.

(5) No pressure rise was observed during the preflame reaction period compared with the same from a hot-motoring condition.

(6) The ignition delay inferred from p-t diagrams were longer than that defined from the presence of the very first image of premixed (thermal) combustion flame.

(7) The reaction center where the first flame kernel initiates seems to be reasonably identifiable from the progressive images of preflame reactions obtained using the present new SIS.

(8) It seems very probable that the radiation from preflame reaction as seen in the images is from OH radicals.

An analysis of these observation suggests that no single effect can explain everything but sequential combined reaction steps would. That is, the images obtained in the early part of preflame reaction are considered to stem from chemiluminescence reactions and those in the later part of the period reflects more of thermal radiations. This interpretation is not unusual in view of the two-stage combustion phenomenon revealed by some hydrocarbon-air mixtures suddenly subject to a (moderately) high temperature environment. What is new here is that the D-2 fuel injected into a DI-CI engine via a HPI exhibits preflame reactions as soon as it is injected into the engine cylinder.

10

References

1. Jiang, H., McComiskey, T., Qian, Y., Jeong, Y.I., Rhee, K.T., and J.C. Kent,"A New High-Speed Spectral Infrared Imaging Device Applied for Imaging Gaseous Mixtures from Combustion Devices," Combustion Science and Technology, 90, 5-6, p. 341, 1993.
2. McComiskey, T., Jiang, H., Qian, Y., Rhee, K.T., and Kent, J.C., "High-Speed Spectral Infrared Imaging of Spark Ignition Engine Combustion," SAE Paper-930865, 1993.
3. Jiang, H., Qian, Y. and Rhee, K.T., "High-Speed Dual-Spectra Infrared Imaging," Optical Engineering, 32 (6), pp. 1281-1289, 1993.
4. Jeong, Y.I., Qian, Y., Campbell, S. and Rhee, K.T., "Investigation of a Direct Injection Diesel Engine by High-Speed Spectral IR Imaging and KIVA-II," SAE Paper-941732, 1994.
5. Ludwig, C.B., Malkmus, W., Reardon, J.E., and Thomson, J.A.L., Handbook of Infrared Radiation from Combustion Gases, NASA SP-3080, 1973.
6. Abata, D., Stroia, B.J., Beck, N.J., and Roach, A.R., "Diesel Engine Flame Photographs with High Pressure Injection," SAE Paper-880298, 1988.
7. Gaydon, A.G. and Wolfhard, H.D., Flames, *Their structure, radiation and temperature*, Chapman and Hall, Ltd., London, 1970.

11

Post-flame Oxidation and Unburned Hydrocarbon in a Spark-ignition Engine

Song, K., Clasen, E., Chang, C., Campbell, S. and Rhee, K.T.
Department of Mechanical and Aerospace Engineering
Rutgers, The State University of New Jersey
Piscataway, NJ 08855

Abstract

Many recent publications indicate that spark ignition (SI) engines equipped with the conventional port-injection fuel system (PIF) seem to have serious fuel-maldistribution problems, including the formation of liquid layers over the combustion chamber surfaces. It is reasonable to expect that such a maldistribution is an unfavorable condition for the flame propagation in the cylinder.

The in-cylinder flame behaviors of a PIF-SI engine as fueled with gasoline are investigated by using the Rutgers high-speed spectral infrared imaging system. These results are then compared with those obtained from the same engine operated by gaseous fuels and other simple fuels.

The results from the engine operated by gasoline reveal slowly burning fuel-rich local pockets under both fully warmed and room-temperature conditions. The local pockets seem to stem from the liquid layers formed over the surfaces during the intake period. The (invisible) post-flame oxidation of the rich pockets is observed to continue even after the exhaust valve opens. On the contrary, the same engine run with a gaseous fuel exhibits some predictable and "clean" flame propagations.

The new results obtained from the present study suggest that such a late oxidation of locally fuel-rich liquid pockets may be a significant cause for the emission of the engine-out unburned hydrocarbon (UHC). The sluggish consumption of the fuel there may also be a factor for reducing the thermal efficiency of the engine. A parametric study of this observation is performed to obtain a better understanding of the findings.

Introduction

According to an estimate, even after the entire combustion chamber is fully enflamed in a spark-ignition (SI) engine, some 25 percent of the fuel by mass still has to burn [1]*. If this is the case, a large amount of this fuel is consumed via invisible reactions, namely in-cylinder post-flame oxidation (PFO). Since in a typical SI engine no significant luminous flame front is observable beyond about 30 crank angle (CA) after the top-dead-center (TDC), the in-cylinder PFO commences thereafter to continue for a period of over 100CA, i.e., until the exhaust valve opens. The completeness of the invisible PFO reaction during this period will obviously dictate the amount of the engine-out unburned hydrocarbon (UHC). If the exhaust UHC is to be further reduced, whatever engine or fuel variables affecting the PFO will have to be identified for improvement. It may be also pointed out that the late burning of this fuel will reduce the thermal efficiency of the engine.

Several explanations of the physical processes that cause incomplete PFO have been considered during the past decades, which include the quenched boundary layer, the crevice volume and the oil film. The fuel in the quenched boundary layer, although considered earlier to become exhaust UHC, was suggested to be unimportant for the reason that it would be rapidly diffused out and be oxidized by high-temperature combustion products. The fuel-air mixture (of course with some residual gas) squeezed into the crevice volume during the compression and combustion periods may not be directly burned by the flame propagation, but the fuel portion issued out of this volume, as the piston expands, would be oxidized in a similar fate of the fuel molecules diffused out from the quenched boundary layer. One may expect that UHC coming out late from the crevice volume, that is, after the exhaust valve opens, remains unreacted by a greater portion. The amount of the crevice-origin mixture coming out after the blowdown, however, may not fully account for the engine-out UHC. The fact that such processes for UHC generation and its incomplete PFO have been proposed, renewed and amended in the past may indicate that much is still unknown about the causes for the UHC emission. Nevertheless, in this paper, an additional physical process is considered in an attempt to help explain the incomplete PFO in an SI engine.

---

*Numbers in parentheses designate references at end of paper.

1

In order to facilitate the present discussion, let's consider the processes of fuel-air mixture preparation in the modern auto SI engine. The port-injection fuel system (PIF) in the engines, which is employed to prepare mixtures to be within a narrow band near the stoichiometric ratio for achieving a high catalytic converter efficiency, is operated in a rather "unusual" manner. That is, fuel is injected at the intake port, in general, with the intake valve closed, which means that the delivered fuel waits there for a while before subsequently entering the combustion chamber. Basically because there is too small a volume in the intake port to accommodate the fuel jet, the injected fuel impinges against the wall and some of the fuel starts to form a liquid layer or puddle around the port [2]. This liquid as well as atomized/vaporized portions of fuel at the port are drawn into the combustion chamber when the valve opens. Between these two-stage fuel deliveries, the (high-temperature) backflow plays an important role to "reprocess" the fuel staying near the port, which includes laminating the fuel layer and puddle, atomization, and heating. In spite of such contribution made by the backflow, there is ample evidence as reported in recent literature that the fuel-to-air ratio (F/A) of mixtures in the cylinder has a great spatial variation [3]. The variation involves differences in both the fuel concentration and the phase of fuel. Such a fuel maldistribution, particularly when liquid layers are present, is expected to increase the probability of having a large amount of UHC in the exhaust as well as to greatly slow down the heat release to decrease the energy conversion efficiency.

In spite of the need for a better understanding of the PFO in PIF-SI engines, no serious report describing the phenomena associated with the fuel maldistribution is found in the literature. The reason for this may be due to the fact that the PFO is invisible, which starts as early as around 30CA after TDC (hereafter denoted by 30CA) and continues until the exhaust valve opens (around 135CA), as mentioned earlier. (The visibility of the reaction, of course, depends on the sensitivity limitation of the existing tools.) Again, although some information is available for the processes in both the intake port and the exhaust manifold, those for the cylinder are missing.

Recent results obtained from a Diesel engine in the authors' laboratory by using a new infrared (IR) diagnostic device [4], which reports the chemiluminescent radiation captured throughout the ignition delay period, offered a promising possibility of improving our understanding of the in-cylinder reactions in an SI engine. Therefore, the same device was employed for the present study in an SI engine with optical access.

Apparatus

Multispectral IR Imaging System. As pointed out above, a new diagnostic device, called the Rutgers System or Super Imaging System (SIS) as referred to by others, was the key component permitting us to perform the present investigation of PFO in an SI engine. The system has four units of high-speed IR digital imaging cameras which are lined up to a single optical train. The basic idea of this SIS
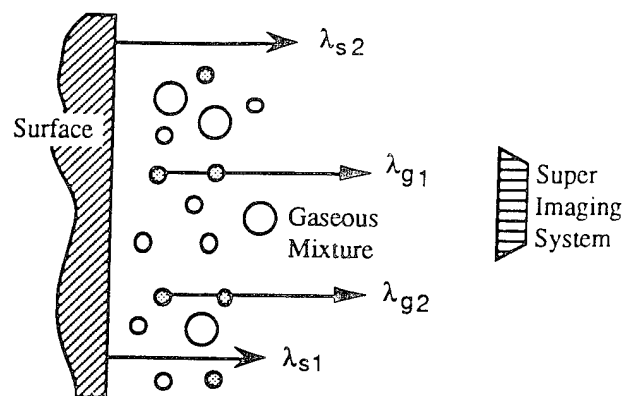

Fig. 1. Multispectral Imaging from a Combustion Chamber.

is to simultaneously obtain four geometrically identical images in respective spectral bands of the in-cylinder events at successive instants of time.

This device, which was made operational about a year ago, is a result of the progressive system development undertaken at the Internal Combustion Engines Laboratory of Rutgers University. Since the events in many thermal systems occur rapidly and some important processes are invisible, at first a single-camera digital IR imaging system was developed having an imaging rate of as high as over 1,800 frames/sec and with an independently variable exposure period as short as 20μsec [5]. The experience gained from this work led us to the next development of a two-camera system, which was applied to the determination of temperature and water vapor distributions in a hydrogen flame [6]. An entirely new four-camera system was designed at the same time, which resulted in the present SIS.

The reason for simultaneously capturing four spectral images by the SIS is only briefly explained next. It is basically to achieve quantitative imaging, i.e., determining distributions of temperature and species concentration in a combustion chamber.

Figure 1 is introduced here for describing the purpose of multispectral imaging. It represents a typical combustion chamber having a wall surface and combustion products in front. When the spectral bands are properly chosen, two sets of spectral images of a designated species are obtained (via λ_{g1} and λ_{g2}) and the same from the surface may be captured (via λ_{s1} and λ_{s2}) with a minimum mutual interference.

According to a spectral diagram generated by using our new data-base computer program, which employs the single-line-group model [4,7], as shown in Fig. 2, it seemed possible to attain a goal of spectrometric analysis. The analysis may be performed by either or both the conventional two-color method for characterizing the wall surface and our new dual-band method for studying the combustion product mixture [6].

In spite of this seemingly promising concept, contrary to previous reports suggesting otherwise [8,9], we discovered that there are measurable amounts of interference by radiation from some unknown species in the cylinder, particularly over those in 2.2μm band. (A new imaging data correction method is presently being explored for
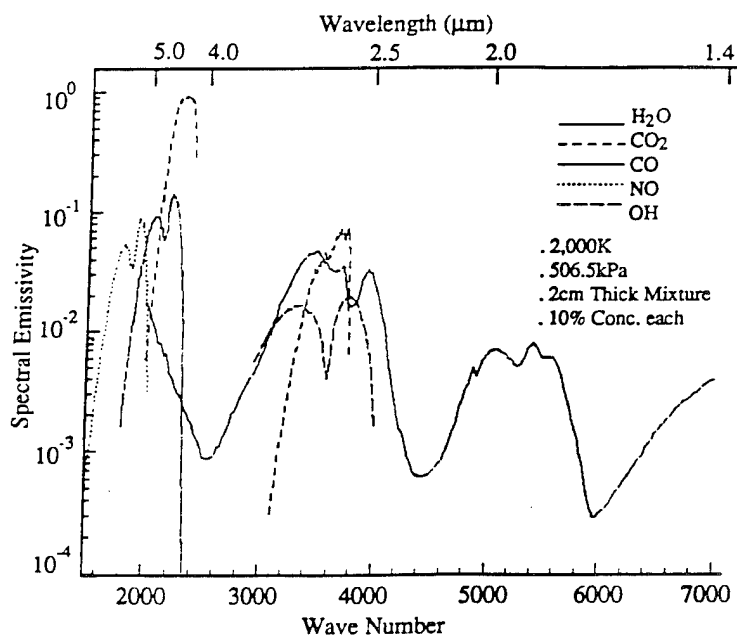
2

Fig. 2. Spectral Emissivity of a Gaseous Mixture having thickness of two centimeters at a uniform temperature of 2,000K and five atmospheric pressure.

eliminating the interference.) It is also noted that our laboratory propane-air flame exhibited interference by a similar radiation in the same band. While such interference delays our implementation of quantitative imaging, our exploratory study of the multispectral images from the SIS provided us with a new potential for investigating the in-cylinder processes, such as preflame reactions [4] and the PFO. Thanks to its spectral discriminating ability, the SIS enables us to simultaneously capture (at least qualitatively for now) images of a specific gaseous species, and even soot formation, at successive instants of time as discussed below.

Figure 3 shows a new optical train of the SIS permitting the simultaneous multiple imaging in four spectral bands. The radiation coming through an IR optical access in the engine (Fig. 4) is collected by the cassegrain unit. Then, it is relayed to respective IR cameras after passing through three (custom-designed) spectral beam splitters. This manipulation of light rays results in four images in separate broad bands placed over the respective 64x128 PtSi imagers housed in cryogenically cooled Dewars. A narrow band filter assigned to each Dewar finally leads to achieving the spectral digital image per camera (in 12-bit dynamic resolution). Since the present system was an application of existing components in an unconventional way, the entire electronic circuits boards that drive the imagers and retrieve the output were newly designed and fabricated in our laboratory.
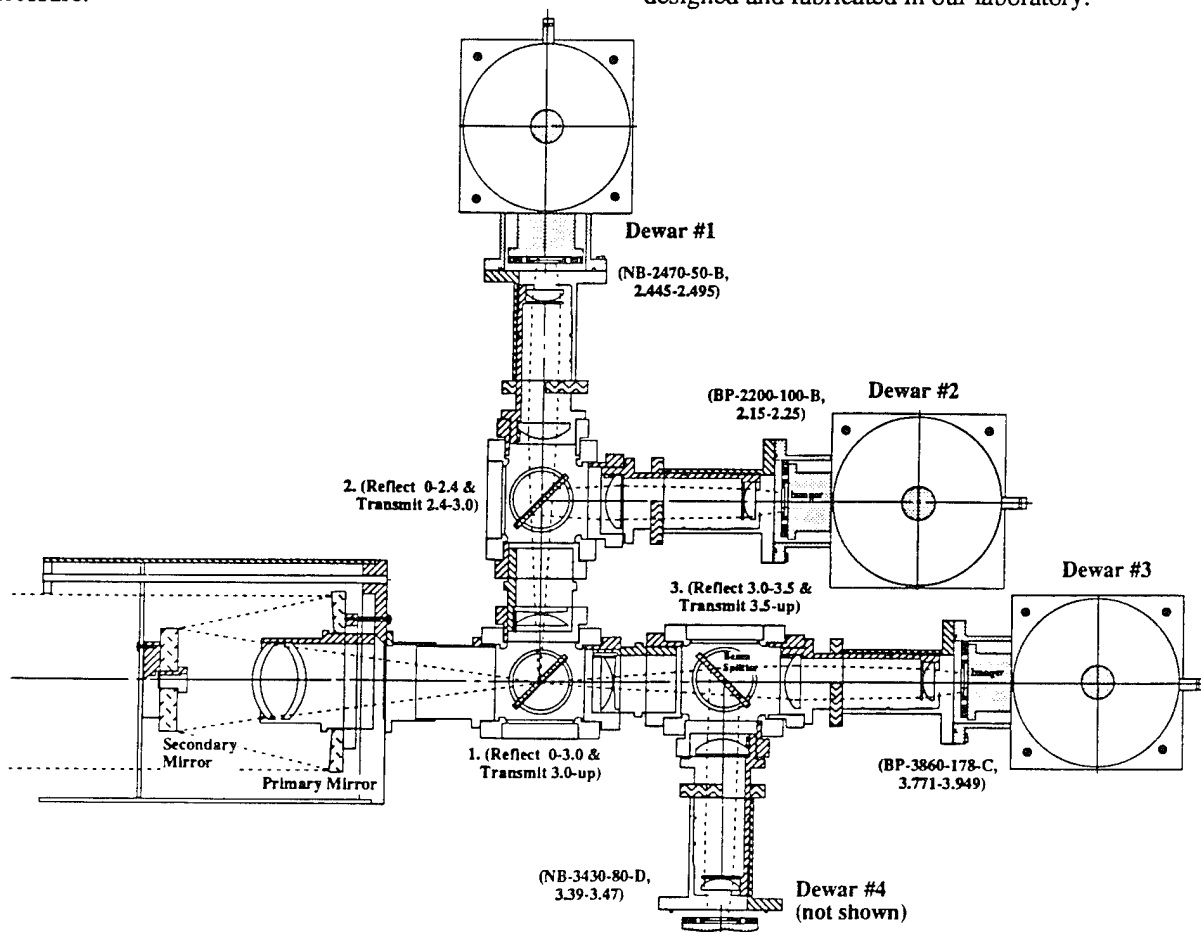

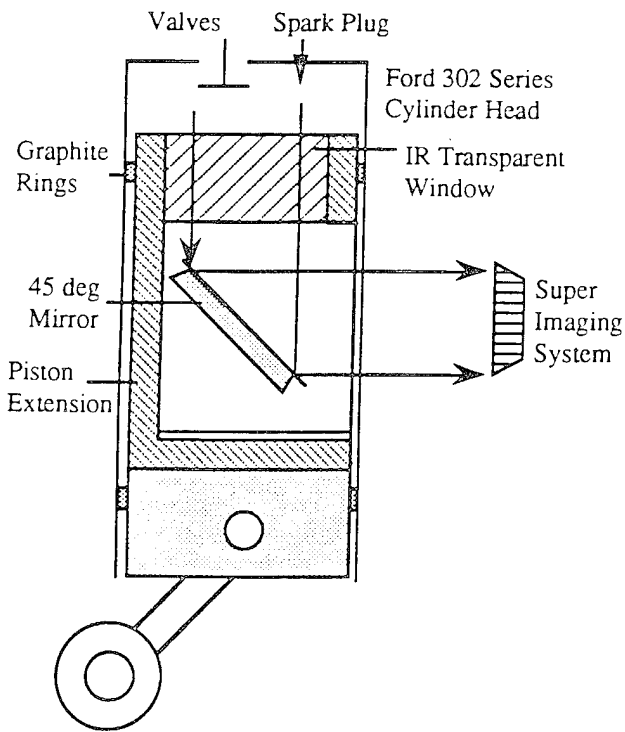Fig. 3. Optical Arrangement of the Rutgers Super Imaging System.

3

Fig. 4. The Spark-Igniton Engine with Optical Access.

Fig. 5. A Visible-Ray Photograph of the Cylinder Head Exhibiting the Imaging View.

Due to the absence of high-speed memory in such a high dynamic resolution on the market, a new memory board and its control circuits were also fabricated. An additional description of the total system may be found elsewhere [4,6]. Note that the numbers in the figure respectively represent the central wavelength of the band and the bandwidth (in nanometer) employed in the present work. The mutual compromise among the bandwidth, the aperture size of each camera, and the exposure period was experimentally determined.

The imaging by the SIS can be performed by using either the internal clock or the external signal, which is, here, the CA marker. Several control features for determining the imaging condition can be independently preset in order to capture the most informative results. They are: (1) the exposure period; (2) the start of imaging with respect to a reference signal, e.g. the TDC marker; (3) the interval between successive images in terms of CA; and (4) the number of images to be obtained per cycle. Since a total of 264 images can be stored for each camera, an observation of many successive cycles may be made at once. This is repeated by refreshing its memory upon transferring the data to a separate data storage.

Engine Apparatus. The basic configuration of the engine apparatus (Fig. 4) used in the present study is the same as that used in the previous experiments [5], but some improvements were made. In order to preserve the representative characteristics of the real-world SI engines, the apparatus was mated with a new Ford 302 cylinder head and a matching PIF. In order to increase the radiation energy captured by the SIS, the cylinder block was extensively
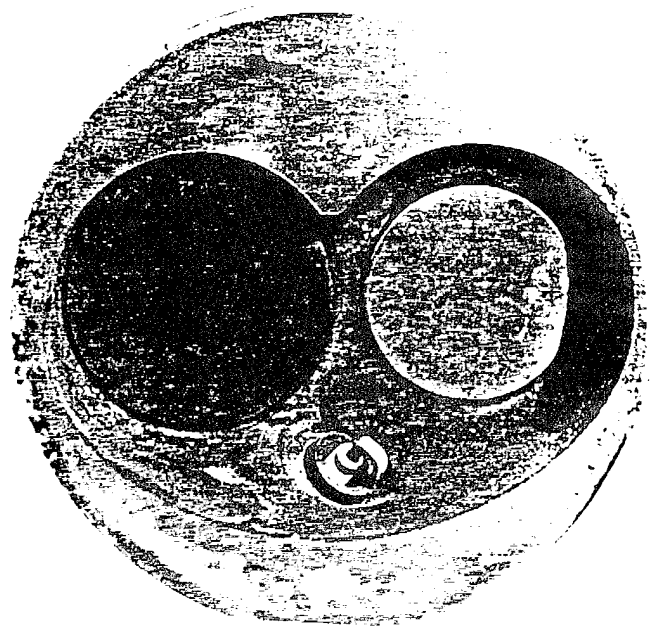
modified for the present work so that the location of mirror was raised toward the piston as much as possible. The imaging view can be seen in Fig. 5 which shows the intake valve on the left, the exhaust valve on the right and the spark plug in between. This figure will be referred to when the instantaneous spectral images are presented later. Some relevent engine information is summarized in Table-I.

Table-I. Engine Dimensions

Bore x Stroke (mm),	101.6 x 101.6
Compression Ratio,	9:1
Spark Ignition,	6 bTDC
Valve Timing:	
EVO	135 aTDC
EVC	10 aTDC
IVO	10 bTDC
IVC	135 bTDC

The engine apparatus was sufficiently instrumented in order to obtain consistent results from the experiment. For example, since the thermal condition of the cylinder head was considered to be an important factor affecting the mixture preparation, sensors were planted where deemed appropriate for close monitoring and control. In addition, the cylinder pressure-time (p-t) history was recorded to compare it with the corresponding sequential instantaneous images. This was done by using the same CA markers generated from an encoder in both the imaging and p-t data acquisition systems.

4

Results and Discussion

This paper reports a new observation obtained during the course of our exploratory study of in-cylinder processes of an SI engine by using our new SIS. A parametric study was performed in order to help explain the finding. The experiment was performed using the engine after it had warmed up to have a coolant temperature of around 75 deg C. The engine was operated by: (1) propane; (2) gasoline; (3) gasoline with 15% methyl tertiary butyl ether (MTBE); (4) isooctane; (5) a mixture of isooctane and n-heptane (in 87/13 ratio); and (6) natural gas. The knock effects were studied by seasoning a little bit of n-heptane when the engine was operated by gasoline. In addition, with the coolant at room-temperature, the same was performed using either propane or gasoline during the very first few cycles. Reasons for these parametric variation are explained when the individual results are presented.

Propane-Air. Mainly because of its simplicity and clean flame without fouling the optical window, the engine was operated by using a propane-air mixture during the warming period. Note that in order to minimize this warming period, a heated coolant was circulated through the water jacket prior to operating the engine for the warm-up.

The sequential images of the flame propagation captured with a mixture having F/A near the stoichiometric are shown in Fig. 6. Two sets of images taken simultaneously in respective spectral bands are included: (A) 2.47μm and (B) 3.43μm. In order to help explain the results, a look-up table (LUT) (Table-II) is offered by identifying the time of each image in CA. The minus sign in the LUT represents CA before TDC. Referring to the LUT, the sequence of the images in Fig. 6 (and all others included in this paper) starts from the left and goes to the right, then continues downwards. With the spark ignition given at -6CA in the present experiment, as mentioned earlier, any significantly visible flame in a typical SI engine can be seen only during the shaded portion of period in the LUT.

Discussing the spectral images in 2.47μm (Fig. 6-(A)), the flame propagation seems to be relatively predictable, i.e., it exhibits progressive steps of the combustion product formation. Referring to Fig. 2, these spectral images were expected to mainly indicate the radiation from water vapor in the product, although it is probable to include those from some unknown species. For example, the radiation from soot, if it is formed, would have been included together.

The flame propagation occurs counter clockwise and rapidly enflames the mixture trapped within the deep cavity in the cylinder head (Fig. 5), and it continues over the squish area, which is about the 1/4 upper portion of the image. The flame almost disappears after 33.5CA, as is the case in a typical SI engine. The radiation considered to be from high-temperature water vapor is overlapped with some strong radiation from the exhaust valve on the right, which becomes obvious as early as 3.5CA. Note that due to the limitations of the graphic presentation, the entire digital image are not indicated in the present pseudo-color images. For example, the present digital data reflecting the activities after 100CA are not well displayed here.

### Table-II. Look-up Table for High-Speed IR Images.

	a	b	c	d	e	f	g	h
1	-11.5	-9	-6.5	-4.0	-1.5	1	3.5	6
2	8.5	11	13.5	16	18.5	21	23.5	26
3	28.5	31	33.5	36	38.5	41	43.5	46
4	48.5	51	53.5	56	58.5	61	63.5	66
5	68.5	71	73.5	76	78.5	81	83.5	86
6	88.5	91	93.5	96	98.5	101	103.5	106
7	108.5	111	113.5	116	118.5	121	123.5	126

As the piston descends away from the TDC, such as after 61CA, the images become somewhat fuzzy, which seems to suggest that they are getting out of focus as the radiating volume increases. A relatively strong radiation seen near the intake valve at the later stage of expansion stroke may indicate the presence of high-temperature gaseous mixture, which becomes weaker as the piston further expands. This consideration seems to be supported by the observation of residual gas made in another band as explained next.

In Fig. 6-(B), spectral images of the 3.43μm band are displayed. In this result, sequentially changing images of a volume of seemingly high-temperature mixture can be seen during the period from -11.5CA through -1.5CA. This is considered to be the radiation from residual gas similar to that observed on the same region seen in Fig. 6-(A) during the expansion period. (One may also notice some radiation from the spark plug, which suggests it be one of the hottest objects in the cylinder. Notice that the radiation from the exhaust valve is relatively weak at this time.) The radiation from this volume becomes stronger when the flame propagation grows, which is expected because the temperature and species concentration increase in the volume due to compression by the expanding reaction front.

By comparing these two sets of spectral images (A and B) to each other, something new can be identified, i.e., an indication of the preflame reaction in the end gas as captured in 3.43μm band, particularly in the images from -1.5CA through 11CA. For example, let's look at the spectral images obtained at 6CA. The one in 2.47μm shows an end gas volume before the flame front without any measurable radiation (from water vapor) while the counter part in 3.43μm reveals some active signatures of reaction by issuing a remarkable amount of radiation. The occurrence of such preflame reactions in the compressed fuel-mixture, however, may not be surprising although the details of its chemistry are not clearly known. Looking at the spectrogram shown in Fig. 2, it seems to be probable that the signature of the preflame reaction indicates the presence of
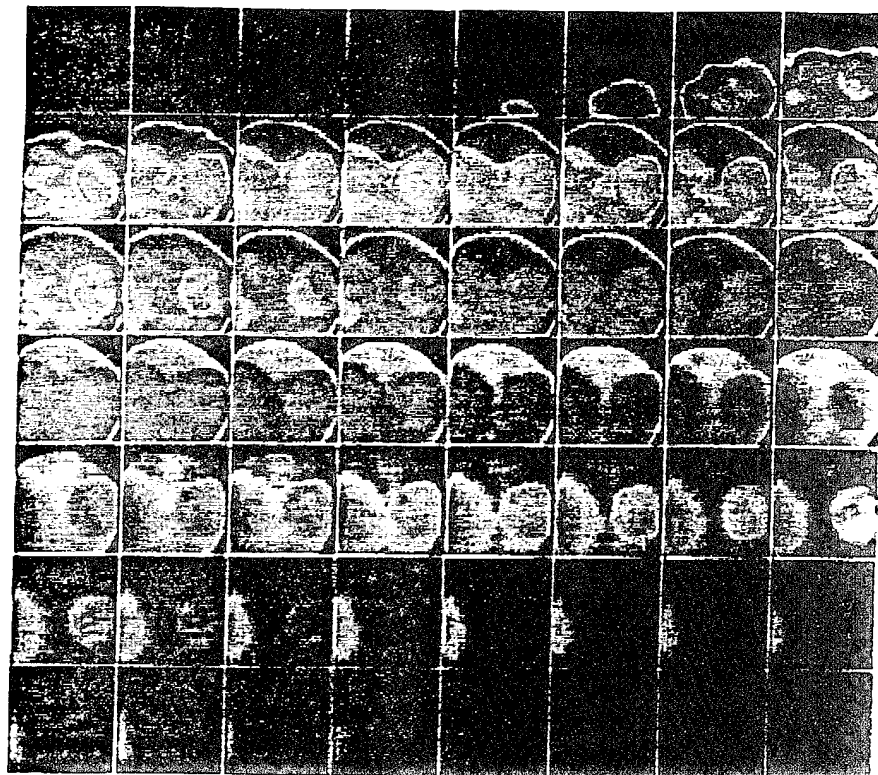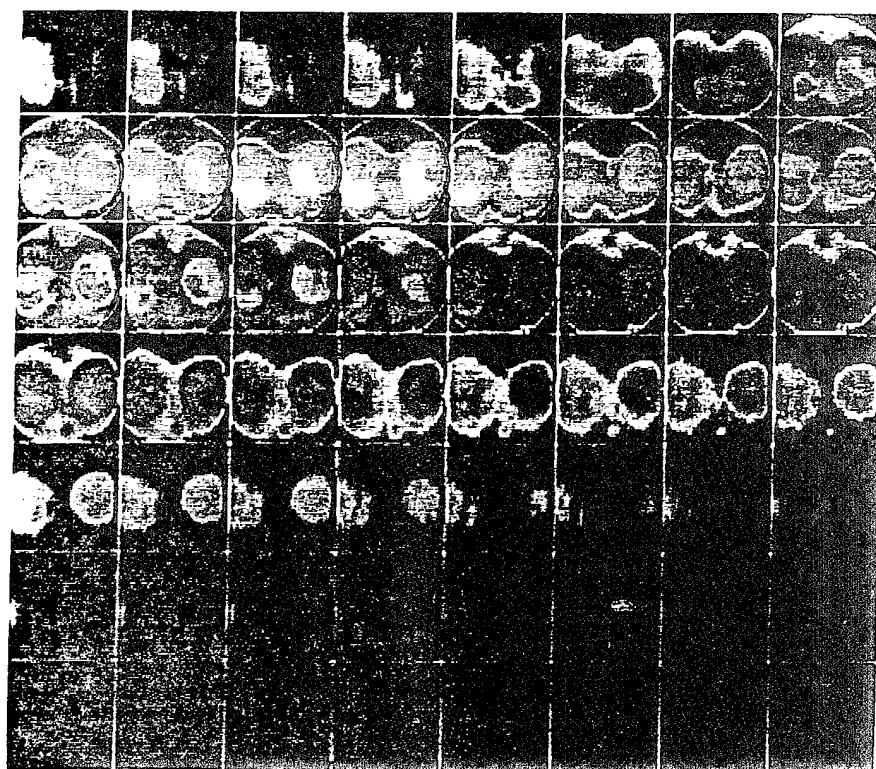
Fig. 6. High-speed Spectral IR Images of In-cylinder Events with a Propane-air Mixture near the Stoichiometric (Warm Engine): (A) 2.47mm and (B) 3.43mm.
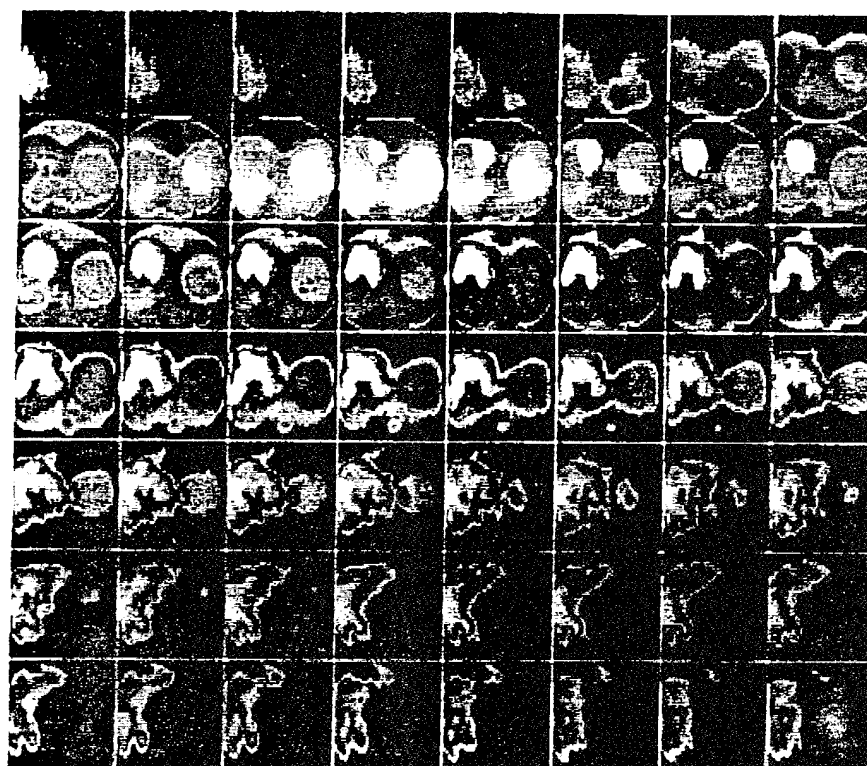
Fig. 7. High-speed Spectral IR Images of In-cylinder Events with a Gasoline-air Mixture near the Stoichiometric (Warm Engine): (A) 2.47μm and (B) 3.43μm.

OH radicals in the end gas. Without excluding a possibility of other species to cause the preflame images, this consideration seems to be reasonable by recalling that the measurements of OH radicals in the end gas has often been mentioned in the past [10]. An additional discussion on this finding is included later.

As pointed out above, whatever reactions occurring after about 30CA are regarded to be postflame reactions. According to the present observation from the SI engine operated by a propane-air mixture, the PFO reactions do not appear to be remarkable suggesting that no significant amount of fuel remains to be consumed thereafter. If the completion of PFO is an indication of a small amount of UHC in the exhaust, the following discussion is expected to offer a new insight into the formation of UHC from the current gasoline-fueled SI engines.

Gasoline-Air. Right after the above imaging was performed, the same engine equipped with a PIF was operated by a near stoichiometric gasoline-air mixture. Figure 7 shows the corresponding spectral images to those taken from the propane-engine (Fig. 6). That is, the only difference between the two was fuel. Looking at Fig. 7-(A), with spark ignition at -6CA, the first flame image and its propagation during the early stage of combustion are found to be comparable with those in Fig. 6-(A). A preflame reaction is also observed here similar to that found from the propane-air operated engine (Fig. 7-(B)). Images of the seemingly residual gas can be seen in the same location as well. It is noted that the exposure period of the imaging for both fuels mentioned above was the same (190μsec) and that the engine produced a comparable torque (at 500rpm).

What is quite unusual in this new set of images is that a bright spot is found at 13.5CA, and that it grows to become a local reaction center. The location of the reaction on the cylinder head may be identified from Fig. 5, which corresponds to the upper portion of the intake valve. The progressive change occurs only around this confined area, which continues until 71CA as *a local (surface) phenomenon*. Then, the pocket starts to move around in the counter clockwise direction finally becoming *a volume event*. Since there is no additional fuel flow into the combustion chamber (with the valves closed), the most probable explanation for this bright reaction center is a locally burning rich pocket from a liquid fuel layer (or puddle) produced during the intake stroke. In fact, there is strong evidence in literature suggesting such existence of liquid fuel in the cylinder head [2,3].

Let's consider again the reaction environment prior to the onset of the local burning. During the period from the spark ignition to around 11CA, the progressively changing flame propagation is predictable when the engine was operated by gasoline as well as propane. Such flame behaviors are expected when a flame front propagates in a premixed combustion reactor. Upon completion of this (premixed combustion) period, the new local reaction center starts to emerge, that is, the reaction center is covered by high-temperature oxygen-deficient combustion products. This burning center slowly puts out new combustion products making the local radiation very high. As the piston expands beyond 26CA, the in-cylinder radiation starts to

fade except for that from this local reaction center, which becomes even stronger. That is, the fading portion seems to represent the combustion products from the premixed mixture, while the strong radiation area appears to be from a burning liquid layer.

Other Hydrocarbon Fuels and Experiment. In an attempt to better understand the new findings, in-cylinder processes for several additional fuels were investigated. Since the liquid layer burning would be related to the distillation characteristics of the fuel, a single component hydrocarbon fuel (i.e., isooctane), and a mixture of isooctane and n-heptane (in 87/13 ratio) were employed. The absence of the less volatile components of the fuel was expected to make some difference on the liquid fuel burning. Regarding the preflame reaction, because the reaction in the end gas will be basically controlled by the low-temperature chemical kinetics, which would involve the two-stage combustion revealing chemiluminescent radiation, natural gas (mainly composed of methane) and gasoline with 15% MTBE were studied. Since methane-air mixtures produce neither two-stage combustion nor chemiluminescent radiation, it was expected to have a direct consequence on its (preflame) reaction behavior. The gasoline with MTBE was used because the MTBE is known to consume OH radicals in the self-ignition environment [11], which was also expected to make a difference in the preflame reaction.

Without showing the details of the above experiment, the following observations made under a limited operating condition are listed: (1) Isooctane and isooctane/n-heptane mixture produce significantly smaller amounts of local burning areas; (2) The natural gas experiment reveal almost no measurable preflame reaction in the end gas; (3) Gasoline with MTBE has much weaker preflame reactions compared with the regular unleaded gasoline. This fuel also revealed a weak local burning center. These results will have to be more extensively investigated, but they are all consistent with other findings and discussions offered above. According to the present results, the less volatile portion of the fuel appears to be a factor affecting the locally burning reaction center, which may be, then, expected to significantly increase the UHC in the exhaust. What is rather puzzling at present is that the preflame reactions for both isooctane and isooctane/n-heptane mixture seem to be mutually comparable, which obviously needs more study.

In addition, the knock effects on the liquid fuel burning were investigated by adding a small amount of n-heptane when the engine was run by gasoline. The preliminary observation indicates that the locally burning liquid fuel becomes a volume phenomenon sooner (to move around with the swirling gas motion) compared with that under a no knock condition. The rich burning cloud, however, seems to liberate a relatively strong radiation. These observations suggest a possibility that the knock-generated vibratory effects of the combustion chamber gas tend to help remove the liquid layer off the cylinder head surface.

Liquid Fuel and Its Impacts. The consideration of a liquid fuel layer is further supported by several facts, including: (1) The intake valve surface, where the local

8

reaction occurs, is expected to attain the lowest temperature in the cylinder head surface (upon cooling by fresh mixture containing some liquid fuel). (2) The growth of the local center is a slow process (seemingly caused by a sluggish physical process, namely the evaporation of a liquid layer) which takes a long period ranging from 11 to 71CA, and (3) Its radiation is very high, something expected from a diffusion flame. Even if the liquid layers are formed at random locations over the cylinder head surface, those formed over high temperature surfaces, such as the exhaust valve, will be rapidly vaporized. On the other hand, the liquid layer produced over the intake valve, which is cooled by the incoming mixture, would be slowly vaporized. Therefore, the layer over a cold surface will most likely be eliminated by the surface evaporation via heat transfer from high-temperature combustion products. Here, the fuel's latent heat of evaporation is expected to play a role in the process by delaying further the PFO reactions. When such a liquid layer puts out fresh fuel vapor, while it is covered by combustion products (from the premixed combustion), the fuel chemistry would be modified including its coking, dehydrogenation and recombination, as commonly considered to occur in a Diesel combustion environment. The radiation under such a condition would be very high, as observed in the present study.

At present, it is difficult to quantify the amount of fuel being consumed off the liquid layer. If the above discussion is reasonable, however, the slow burning liquid layer suggests some important implications: (1) It is (if not the most) a significant source of UHC in the exhaust and (2) It reduces the thermal efficiency of the engine. Further elaborating the role of the slowly burning zones to result in a high UHC emission, the locally strong radiation, which does not fade out (unlike that from the premixed combustion product) with the piston expansion, is an indication of continuing reaction. That is, there remains unreacted fuel and incomplete combustion products in the volume. Since this radiating volume is observed even after the blowdown, whatever incomplete product included in the volume will become the engine-out UHC.

In addition, recall the fact that the UHC emission from a typical SI engine operated by a gaseous fuel, e.g. propane, is much lower than that from a gasoline fueled counter part, often lower by several times. It would be useful if one could identify what causes the difference. According to the present results, the most obvious difference between the two seems to be the sluggishly burning rich pocket in the gasoline fueled engine, which is absent in the propane-operated engine. Let's consider the crevice volume effect on the UHC emission. Suppose that the role of the crevice volume affecting the UHC occurs roughly the same for the engine operated by either propane or gasoline. And suppose that the UHC from the propane-fueled engine is mostly from the crevice volume. Would it not be reasonable, then, to infer that the difference in the UHC emission (between gasoline and propane uses) is caused by the late burning liquid layer? Granted that the present experiment has been unable to identify the PFO reaction of the crevice-originated fuel, the slow reaction of an unusually rich fuel pocket has been discovered by using the SIS. Would it be too unreasonable to assume that what has been measurable is more important than that otherwise?

Concerning the impacts of the late burning on the engine thermal efficiency, if the estimate mentioned in the very beginning of this paper is valid, some 25% of fuel trapped in the cylinder would be consumed in a great portion after 31CA. The only significant reaction observable thereafter seem to be the locally burning rich pocket. This fuel consumption is obviously slow according to the present observation. (Recall the local surface phenomenon, which becomes a volume event quite late.) The remaining fuel seems to be reacted while the piston is far away from the TDC, which would lower the cyclic efficiency. If this observation of late burning liquid layer does represent the in-cylinder reactions in the major population of the modern SI engines, although the current PIF may satisfy the need for the catalytic convertor, it most likely would not help improve their thermal efficiency.

The impacts of the liquid layer formation on the deposit formation and removal processes may be also considered. Unlike the relatively clean surface of the cylinder head shown in Fig. 5, the actual deposit formation over the cylinder surface, when stabilized after running the engine by gasoline over one hundred hours, appeared like a black wax or varnish layer. Among the source-mechanisms of the deposit formation are those involving fuel and oil. The liquid layer, when slowly consumed while being covered by the oxygen-deficient combustion product, is expected to play a role in the formation. The liquid fuel layer will affect the removal of the deposit layer also. The deposit layer removal, which occurs along with continuous new formation, is considered to include several processes, such as: the burn-up, flaking and water-vapor absorption. In addition to those, the fresh liquid fuel flow bombarding and soaking an existing deposit layer is expected to have some effect, e.g. washing it off. Later, when the soaked fuel is vaporized out of the porous deposit layer, it may tear it off. In the process of fuel vaporization from the wet deposit layer, however, the low-volatility fuel portion is expected to be the last to come out of the layer (which would affect the engine out UHC). Or, some portion may never come out of the layer as fuel vapor.

Cold Start. Basically because of the poor combustion of overly rich mixtures and the low temperature in the catalytic converter, the emission of near 75% of the total UHC from a typical (gasoline fueled) SI engine automobile takes place during the warm-up period. Whatever processes that are unique in the cylinder of a cold engine, which produces such massive amounts of UHC, may help understand the source of the emission in a warm engine as well. The same imaging method was applied to the engine as it was started from the room-temperature. Fig. 8 shows the results obtained in the same spectral bands as displayed in Figs. 6 and 7. There are a couple of differences in this imaging, however. The F/A of the mixture was not measured, but it was barely rich enough to produce a sufficient amount of vapor for ignition. (According to other reports, it ranges from two to five times the fuel amount in the stoichiometric. So, our F/A is expected to fall somewhere within the range) Because of the excess amount
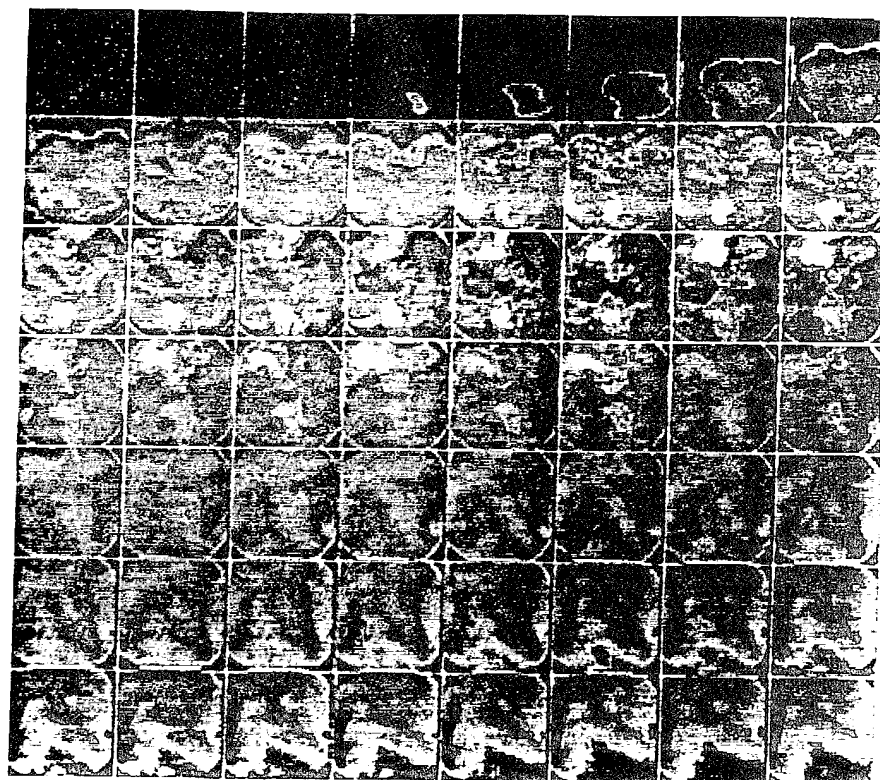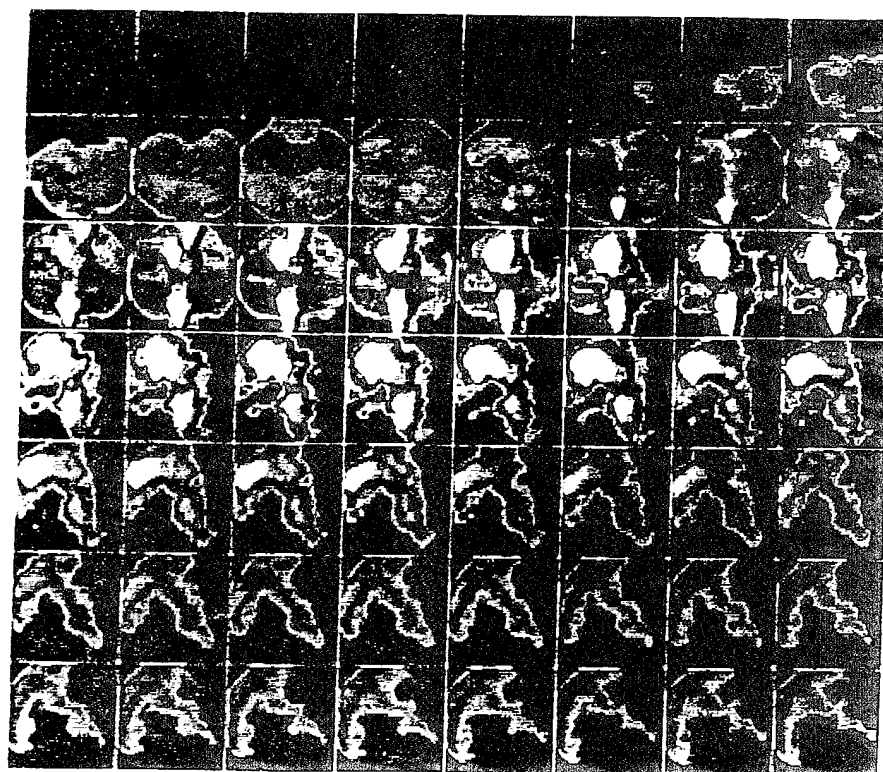
Fig. 8. High-speed Spectral IR Images of In-cylinder Events with a A Gasoline-air Mixture near the Stoichiometric (Room-Temperature Engine): (A) 2.47μm and (B) 3.43μm.

10

of fuel at this time, the radiation from the combustion chamber was very high, and so it was necessary to reduce the exposure period of imaging, which was 130μsec as opposed to 190μsec employed for obtaining Figs. 6 and 7.

A few noticeable differences are observable between these new images and those obtained from the warm PIF-engine (Fig. 7). There is no radiation from the residual gas captured from the cold start engine. Also, no preflame reaction is found in the results. The main finding in this experiment is the considerable amount of diffusion-flame-like reaction zones similar to those observed in the warm engine when operated by gasoline via the PIF. The first locally rich pockets where the growth starts are found about the same piston position as in the warm engine, i.e., around 11CA. At this time the formation of the burning center appears multiple, including zones at the intake valve, near the spark plug, over the squish area, and even around the exhaust valve. The locally rich burning centers put out new combustion products making the overall radiation very high, as similarly seen in the warm engine. Also, as the piston expands beyond 26CA, the in-cylinder radiation starts to fade except for the local reaction centers, which become even stronger. That is, the fading portion seems to represent the combustion products from the premixed mixture. The local diffusion-flame-like reaction zones are considered to occur due to, again, the liquid fuel layer, which is expected to be even more in a cold start engine [12].

Returning again to the issue of the engine-out UHC by the liquid layer, if the locally strong radiation, unlike that from the premixed combustion product being faded with the piston expansion, indicates a continuing reaction, the volume would contain some incomplete combustion products and leave the exhaust valve. The liquid burning occurs to a much greater extent in the cold engine than the warm engine, which seems to explain the UHC emissions from both. That is, the larger the amount of the liquid fuel burning, the more the engine-out UHC emissions.

Summary

A new high-speed multispectral infrared imaging system, called the Rutgers System or Super Imaging System (SIS), is used for investigating the events occurring in the combustion chamber of a spark-ignition (SI) engine equipped with the conventional port injection fuel system (PIF). Four geometrically identical images in respective spectral infrared (IR) bands are obtained at the successive instants of time, which is identified over the pressure-time history.

This investigation of in-cylinder events is performed during the almost entire cycle period of the engine, including compression, combustion and expansion strokes. A parametric study is performed involving various fuels. Several new observations are obtained in the present study. They include:

(1) Images of residual gas are obtained during the compression period.

(2) Some remarkable radiation emitted by the end gas is captured, which seems to indicate the occurrence of preflame reactions. Unlike in an engine operated by either propane or gasoline, no remarkable signature of such preflame radiation is found when it is fueled by natural gas. Some measurably weaker signatures are found when gasoline contains MTBE (15%). No such preflame signature is observed in a cold-start engine.

(3) Strongly radiating local reaction centers are observed over the surface of the cylinder head when the engine is operated by gasoline, which is not observed when it is run by gaseous fuels, e.g. propane and natural gas.

(4) The local centers are considered to occur due to the liquid fuel layer formed during the intake period upon delivery of fuel by the PIF, which produces fuel puddles or layers in the intake-port before the opening of the valve.

(5) A great portion of the local reaction occurs after the visible flame front fades away, the post flame oxidation (PFO), which is observed to be sluggish and incomplete.

(6) The reacting liquid layer is found seemingly only over the intake valve surface in a warmed engine, but when the engine is cold it is found at other areas including the spark plug, squish area and even the exhaust valve.

(7) The diffusion-flame-like reaction occurring at those areas appear to be a local surface phenomena, which become a volume phenomenon in the later stages of combustion. The strong lasting radiation from the local centers are in contrast with that from the premixed combustion product, which becomes weak as the piston expands.

(8) The PFO reactions in those volumes seem to continue even after the exhaust valve opens, which further suggests that some unreacted hydrocarbon (UHC) still exists there at that time.

(9) The continuing reaction volume leaving the exhaust valve, an aftereffect of the liquid fuel layers, is considered to be a (if not the most) significant source of the engine-out UHC.

(10) The liquid fuel pocket, which sluggishly burns with the piston far away from the top-dead-center, may be a factor lowering the thermal efficiency of the engine.

(11) The distillation characteristics of the liquid fuel seem to be a factor affecting the liquid fuel layer and its depletion. For example, the engine introduced by either isooctane or a mixture of isooctane/n-heptane (87/13 ratio) produced remarkably smaller amounts of the locally burning centers. The gasoline containing MTBE also seems to have reduced local reactions.

(12) The local liquid layer formation and its slow burning in an SI engine with the PIF may also affect the formation and removal processes of the in-cylinder deposit layer.

Acknowledgement

11

References

1. Heywood, J.B., Internal Combustion Engine Fundamentals, p372, 1988, McGraw-Hill, Inc.

2. Zhao, F-Q, Lai, M-C, and Harrington, D.L., "The Spray Characteristics of Automotive Port Fuel Injection-A Critical Review," SAE Paper-950506, 1995.

3. Takeda, K., Yaegashi, T., Sekiguchi, K., Saito, K. and Imatake, N., "Mixture Preparation and HC Emissions of a 4-Valve Engine with Port Fuel Injection during Cold Starting and Warm-up," SAE Paper-950074, 1995.

4. Clasen, E., Campbell, S., and Rhee, K.T., "Spectral IR Images of Direct Injection Diesel Engine Combustion with High Pressure Fuel Injection," SAE Paper-950605, 1995.

5. McComiskey, T., Jiang, H., Qian, Y., Rhee, K.T., and Kent, J.C., "High-Speed Spectral Infrared Imaging of Spark Ignition Engine Combustion," SAE Paper-930865, 1993.

6. Jiang, H., Qian, Y. and Rhee, K.T., "High-Speed Dual-Spectra Infrared Imaging," Optical Engineering, 32 (6), pp. 1281-1289, 1993.

7. Ludwig, C.B., Malkmus, W., Reardon, J.E., and Thomson, J.A.L., Handbook of Infrared Radiation from Combustion Gases, NASA SP-3080, 1973.

8. Matsui, Y., Kamimoto, T. and Matsuoka, S., "A Study on the Application of the Two-color Method to the Measurement of Flame Temperature and Soot Concentration in Diesel Engines, " SAE Paper-800970, 1980.

9. Ferriso, C.C., Ludwif, C.B. and Boynton, F.P., "A Band-Ratio Technique for Determining Temperatures and Concentrations of Hot Combustion Gases from Infrared-Emission Spectra," 10th Symposium (Int'l) on Combustion, pp161-175, 1965.

10. Lee, K-W, Miyake, S., Tabuchi, T., Kawai, T., Tsukamoto, T., Senda, J. and Fujimoto, H., "Analysis of Knocking Mechanism Applying the Chemiluminescence Method," SAE Paper-951005, 1995.

11. Kajitani, S., Usisaki, H., Clasen, E., Campbell, S. and Rhee, K.T., "MTBE for Improved Diesel Combustion and Emissions?," SAE Paper-941688, 1994.

12. Shin, Y., Cheng, W.K., Heywood, J.B., : Liquid Gasoline Behavior in the Cylinder of an SI Engine," SAE Paper 941872, 1994.